LINEWIDTH OF SHORT EXTERNAL CAVITY SEMICONDUCTOR LASERS

LINEWIDTH OF SHORT EXTERNAL CAVITY SEMICONDUCTOR LASERS

by

SHANE HEATH WOODSIDE, B.Sc., P. Eng.

A Thesis

Submitted to the School of Graduate Studies

in Partial Fulfilment of the Requirements

for the Degree

Master of Engineering

McMaster University

May, 1992

MASTER OF ENGINEERING McMASTER UNIVERSITY

(Engineering Physics) Hamilton, Ontario

TITLE: LINEWIDTH OF SHORT EXTERNAL CAVITY SEMICONDUCTOR LASERS

AUTHOR: Shane H. Woodside, B. Sc. (Mount Allison University)
P. Eng. (Technical University of Nova Scotia)

SUPERVISOR: Professor D.T. Cassidy

NUMBER OF PAGES: xii, 141

ABSTRACT

This thesis describes the development of a technique for measuring frequency noise of semiconductor lasers. Equivalent laser linewidths were calculated from frequency noise measurements on several InGaAsP lasers with short external cavities to give single mode operation. Conventional 250 μm lasers demonstrated linewidths of about 125 MHz-mW, compressively strained quantum well lasers of commensurate length had linewidth of 37 MHz-mW, and 500 μm strained quantum well lasers had linewidth of 18 to 28 MHz-mW with an apparent strain dependence. The short external configuration allowed selection of a number of laser modes. Measurement of linewidth variation with laser mode showed a 20% to 40% change over six to eight modes.

The system was adapted to make measurements of the optical frequency tuning with fine external cavity length change. This measurement provided a novel means to estimate the linewidth enhancement factor and the reflectivity of the external cavity element. The estimated values of the linewidth enhancement factor for 250 μm conventional and quantum well lasers were found to be in the correct ratio to account for the measured difference in linewidth.

ACKNOWLEDGEMENTS

I would like to express my appreciation to Dr. Cassidy for helpful support and accomodation, and to my friends and co-workers for their tolerance and good will.

Appreciation is extended to John (Jack) Evans who supplied the quantum well lasers used in this thesis.

Financial support from the Natural Sciences and Engineering Research Council is gratefully acknowledged.

Most of all I wish to thank Val, who provided all the incentive one could possibly require.

TABLE OF CONTENTS

LIST OF FIGURES

CHAPTER 1 INTRODUCTION

Lasers emit light in a very narrow wavelength band. This spectral purity is one of the most interesting and useful properties of lasers. Lasers which oscillate in several longitudinal modes simultaneously are referred to as multimode lasers. In multimode lasers the spectral width is governed by the number of lasing modes and the mode spacing. Multimode semiconductor lasers exhibit spectral widths of 100 to 1000 GHz.

Single mode lasers are lasers with almost all optical energy contained in a single longitudinal mode. The spectral shape of laser emission in this case is given solely by the line shape of the lasing mode. The width of emission is usually evaluated by measuring the linewidth, which is defined as the full width at half maximum (FWHM) of the line shape. The linewidth varies inversely with optical power and for a conventional InGaAsP laser is about 10 to 100 MHz. Obviously single mode lasers are preferred in applications critically requiring narrow emission spectra. Unless expressly stated otherwise, this thesis is concerned with single mode

semiconductor lasers.

Most other types of lasers, for example gas and solid state lasers, have linewidths which are dominated by external perturbations such as temperature fluctuations and vibrations. In semiconductor lasers, the linewidth is due to intrinsic noise [1]. As discussed in Chapter 2, spontaneous emission is the dominant noise mechanism. The type of noise which contributes to the linewidth is alternately called phase noise, frequency noise, or FM noise.

Frequency noise of semiconductor lasers is important for several reasons. Semiconductor lasers have increasingly found application in spectroscopy [2,3]. For nonlinear spectroscopy applications where natural, sub-Doppler linewidths must be determined, the laser must have a linewidth smaller than the natural width of the transition being investigated. Interferometric sensors, particularly optical fibre sensors, typically employ semiconductor lasers as optical sources. The ultimate sensitivity of these sensors is limited by laser noise [4], which has motivated semiconductor laser phase noise measurements [5].

However, the principal impetus toward understanding, characterizing, and minimizing FM noise and linewidth comes from the fibre optic telecommunications industry. Current telecommunications systems commonly use direct detection of an intensity modulated optical wave. The signal to noise ratio

at the receiver is ultimately limited by receiver thermal noise. Multiplexing has been limited to far below the intrinsic bandwidth limitations of optical fibre due to the unavailability of practical demultiplexing schemes with high wavelength selectivity.

Next generation optical telecommunications systems are expected to employ coherent detection [6]. Coherent detection involves mixing the received signal with a coherent signal from a local oscillator, in this case a laser, prior to detection. Coherent systems offer increased signal to noise ratio over direct detection systems. The improvement can be as high as 20 dB [6]. In addition, the wavelength selectivity of coherent detection is inherently very high, allowing a high degree of multiplexing. Heterodyne linewidth measurement is essentially an example of coherent detection.

A chief impediment in the development of coherent optical systems is FM noise in the transmitter and local oscillator lasers. The tolerable FM noise level is a complicated function of the type of the modulation format, the detection method (balanced/unbalanced, heterodyne/homodyne) and the data rate [6]. An FM noise level corresponding to 1 MHz linewidth is considered suitable for a typical coherent communications system [7]. This is about an order of magnitude less than the minimum linewidth typical of a conventional InGaAsP laser.

Early measurements on AlGaAs semiconductor lasers revealed linewidths about fifty times greater than that predicted by the modified Schawlow-Townes formula [8]. It was demonstrated that the discrepancy was due to instrinsic coupling between gain fluctuations and frequency fluctuations within semiconductor lasers [1]. The magnitude of linewidth broadening from this effect is characterized by the linewidth enhancement factor, usually denoted α. The linewidth enhancement factor had previously been identified with gain induced antiguiding effects [9] and with multistability and hysteresis in external cavity lasers [10]. With the identification of the effect of α on laser linewidth [1], it has become a widely investigated parameter. Despite the considerable efforts expended in measurement of α, there are still large discrepancies in reported values, which are probably more indicative of differences between measurement techniques than differences in α between devices [11].

Linewidth reduction in semiconductor lasers has been widely reported. The linewidth can be reduced to some extent by adjustment of certain laser parameters, as discussed in Chapter 2. Quantum well and especially strained layer quantum well lasers offer considerable improvements over bulk devices [12]. Feedback techniques can give large supression of FM noise and reduced linewidth. Optical feedback using simple planar reflectors [13], gratings [14], and resonant

reflectors [15,16] have demonstrated linewidth reduction by several orders of magnitude. Negative electrical feedback has also been used [17,18]. FM noise supression is achieved by interferometrically sensing frequency fluctuations in the laser output and feeding back a correction, usually by current tuning of the laser frequency. The linewidths achieved using negative electrical feedback are comparable to those obtained using optical feedback.

Despite the large volume of work completed to date, there remain many unanswered questions. The discrepancy between linewidth enhancement factor measurements obtained using different techniques remains unexplained. Excess FM noise with a 1/f spectrum has been identified [7] and correlated with a departure of measured linewidth from theoretically predicted behaviour. A strong dependence of linewidth on strain in quantum structures has been predicted theoretically [19], but results to date indicate some confusion as to the effects and relative merits of compressive and tensile type strain.

Semiconductor laser linewidth is typically measured with self-heterodyne [20] or self-homodyne [21] techniques. However, it has been pointed out [7,22] that frequency noise generally provides information more directly applicable to calculation of signal to noise ratio in coherent communications. Although there have been a few published

results of frequency noise measurement, few details have been given regarding calibration. Direct FM noise measurement is usually avoided because it is more difficult to calibrate than direct linewidth measurements.

This thesis describes the development of instrumentation for measuring FM noise in semiconductor lasers. A significant portion of the work was devoted to demonstrating a suitable calibration technique and to investigating inherent limitations in the technique. The instrument was then used to study FM noise and linewidth in short external cavity (SXC) InGaAsP lasers.

There were several motivations for this study. SXC lasers have been used within this research group at McMaster for spectroscopy [2] and as a means for studying laser device physics. Knowledge of noise properties will augment the SXC laser's utility as a research tool. Most linewidth work with InGaAsP lasers has been restricted to distributed feedback and distributed Bragg reflector lasers due to the multimode nature of Fabry-Perot InGaAsP lasers. Introduction of a SXC to Fabry-Perot InGaAsP laser allows study of single mode behaviour without a complicated laser structure. In [23] a SXC was used to determine the dependence of linewidth of the main mode on the strength of side modes. Most previous linewidth measurements on external cavity lasers have been with long cavity configurations designed for linewidth

reduction. A SXC may be introduced without significantly affecting the intrinsic frequency noise properties, allowing the natural noise and linewidth of the solitary laser to be measured. The SXC allows oscillation on a number of longitudinal modes of the Fabry Perot laser, and so changes in noise properties and linewidth with longitudinal mode may be investigated.

Adjustment of the external cavity length causes frequency shifts in the laser emission **[24,25]**. The instrumentation developed for frequency noise measurement was adapted to record laser frequency versus SXC length, hereafter referred to as frequency tuning. This measurement provides complementary information to the frequency noise measurements by enabling an independent estimate of the linewidth enhancement factor α.

This thesis is divided into 6 chapters. Chapter 2 provides the theoretical background for studying FM noise and linewidth of semiconductor lasers. Chapter 3 decribes the instrumentation in detail in the context of frequency noise measurement. Chapter 4 presents measurements of FM noise and linewidth from several InGaAsP SXC lasers. Frequency tuning theory and experimental results are given in Chapter 5. A thesis summary is given in Chapter 6, along with recommendations for future work.

CHAPTER 2 THEORY OF LINEWIDTH AND FM NOISE

2.1 Introduction

This chapter deals with the theoretical description of frequency noise and linewidth in semiconductor lasers. Section 2.2 provides a brief description of semiconductor lasers. The rate equations for a single mode laser including noise terms are introduced in Section 2.3. The solution of these equations gives the frequency noise spectrum. The relationship between frequency noise and spectral lineshape is given in Section 2.4. Section 2.5 decribes how the laser operation is affected by weak optical feedback. Section 2.6 summarizes the major points of this chapter.

2.2 Semiconductor Laser Background

Lasers are examples of gain saturated oscillators [26]. The oscillator output grows from noise by regenerative feedback. In lasers the feedback mechanism and gain are frequency dependent, which results in a narrow spectral output. The noise which seeds laser oscillation is

spontaneous emission. For semiconductor lasers, spontaneous emission is the primary origin of output noise and linewidth.

Two basic requirements for laser operation are a medium which exhibits optical gain, and a means for optical feedback. Semiconductor lasers are composed of III-IV compounds such as AlGaAs and InGaAsP. Optical gain is provided by current injection through a pn junction. The injected current creates electron-hole pairs in the semiconductor energy bands. At sufficiently high levels of injection, a population inversion is obtained and the material exhibits net optical gain. With increasing current the optical gain increases until it almost matches waveguide and output coupling losses, the difference being made up by spontaneous emission. This level of current is referred to as threshold. Above threshold stimulated emission dominates over absorption and spontaneous emission, giving a dramatic increase in power output and decrease in spectral width.

A schematic diagram of a Fabry Perot laser is given in Figure 2.1. The active semiconductor region is assumed to fill the volume between the two mirrors with reflectivities R_1, R_2. The mirrors are facets, usually formed by cleaving the laser chip along a crystal plane. The index step at the facet causes the reflection that provides the optical feedback. No transverse laser structure is shown, but the laser is assumed to operate in the fundamental transverse waveguide mode. This

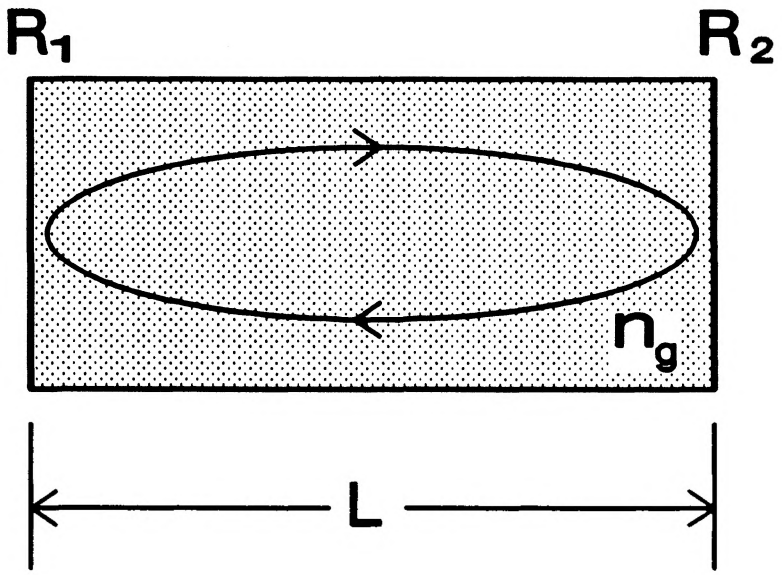

Figure 2.1 Schematic of a Fabry-Perot laser

is achieved by using a narrow stripe contact to laterally confine recombination to a small region in gain-guided lasers. Index-guided lasers have a built-in waveguide structure [27].

Longitudinal modes are centred at frequencies where a half-integral number of wavelengths equals the cavity length. The frequency separation of the longitudinal modes is given by the free spectral range of the Fabry Perot cavity

$$FSR_{FP} = \frac{c}{2n_g L} \qquad (2.1)$$

where n_g is the group refractive index.

By considering propagation of a wave through an infinitessimal section of gain medium, a relationship between the complex refractive index and gain is obtained **[28, p22]**

$$n'' = -\frac{g\lambda}{4\pi} \qquad (2.2)$$

where n′-in″ defines the complex refractive index, g is the electric field gain per unit length, and λ is the free space wavelength. The real and imaginary parts of the refractive index are interdependent according to the Kramers-Kroenig relations **[29]**. Changes in the real and imaginary parts at the laser emission wavelength define the linewidth enhancement factor

$$\alpha = \frac{\Delta n'}{\Delta n''} \qquad (2.3)$$

Equations (2.2) and (2.3) indicate that for $\alpha \neq 0$ changes in gain are accompanied by changes in the real part of the refractive index. This result significantly affects the FM noise and linewidth of semiconductor lasers.

2.3 Langevin Rate Equations

A rigorous treatment of noise in semiconductor lasers requires use of quantum theory since the noise origins lie in the creation and annihilation of photons and carriers, random processes which are inherently quantum mechanical in nature. However, it has been shown **[30]** that a macroscopic rate equation approach yields equivalent results when appropriate Langevin forcing terms are included.

Semiconductor laser devices occupy a finite volume, with stimulated emission, spontaneous emission and absorption being distributed over this volume. Usually these processes are assumed to occur uniformly throughout the active volume, which greatly reduces the complexity involved with modelling the laser. The rate equation approach also treats output coupling loss (facet loss) as if it were distributed uniformly throughout the laser. The laser equations are thus reduced to temporal dependence only. The validity of these assumptions is discussed in **[31]**.

The following treatment loosely follows **[32]**. Single mode operation of the laser is assumed. The laser field is written as

$$E(t) = \sqrt{I(t)}\, e^{-j(\omega_o t + \phi(t))} \qquad \textbf{(2.4)}$$

The normalization of E is such that I(t) is the number of

photons in the laser mode. For the purposes of analysis (2.4) can be decomposed into a fully coherent sinusoidal wave plus random fluctuations, or noise. In this representation the noise is broken into amplitude and phase components. The amplitude fluctuations are implicit in the time dependence of I(t). This noise is usually referred to as amplitude noise, AM (amplitude modulation) noise, IM (intensity modulation) noise, or RIN (relative intensity noise). The term $\phi(t)$ is referred to as phase noise, frequency noise, or FM (frequency modulation) noise.

The effect of noise on the laser field is given a phasor representation in Figure 2.2. The noise phasor can be interpreted as a spontaneously emitted photon. The phasor at A represents the laser field before the spontaneous emission. Immediately after the spontaneous emission, the field sums to point B. The in phase component of the noise phasor generates AM noise, while the quadrature component contributes FM noise. This represents the noise directly due to spontaneous emission.

The gain saturation inherent in a laser operating above threshold causes a suppression of the intensity noise, returning the field to steady state at point C. The gain change necessary to achieve this generates an additional phase change.

The effects of AM and FM noise are quite different, as

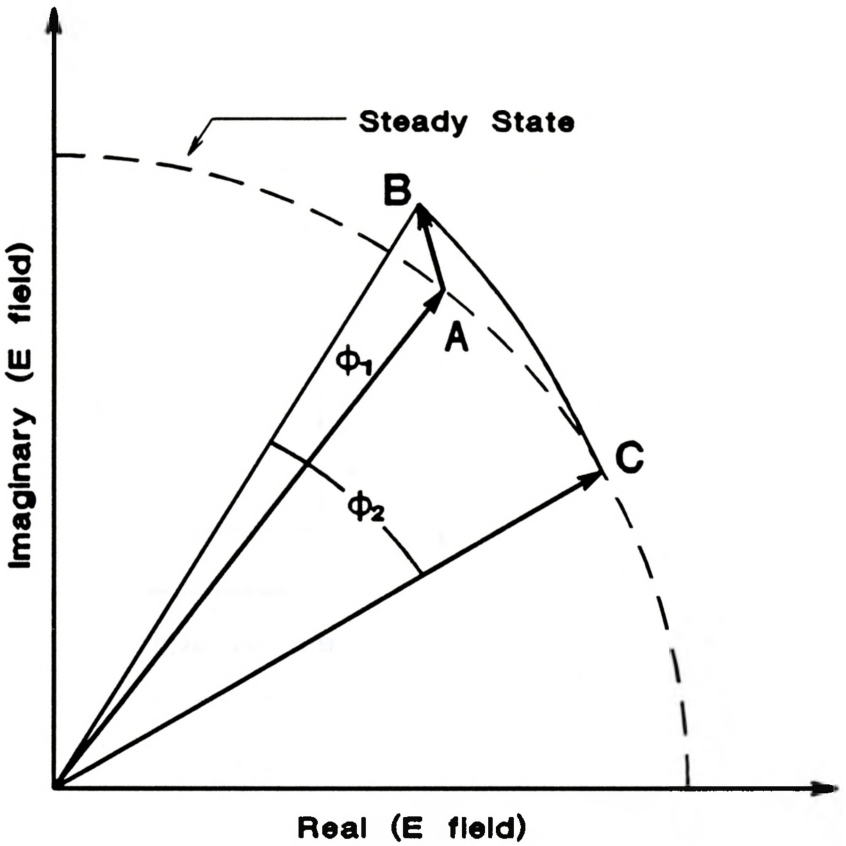

Figure 2.2 Phasor representation of noise in a laser.

shown by Figure 2.3. A coherent field is represented by the delta function power spectrum. The AM noise of a semiconductor laser is spread over a frequency range > 100 GHz and can be considered white. AM noise is additive in the sense that in the presence of AM noise only, the laser power spectrum consists of the noise spectrum plus the coherent spectrum. AM noise thus results in a noise floor of the laser

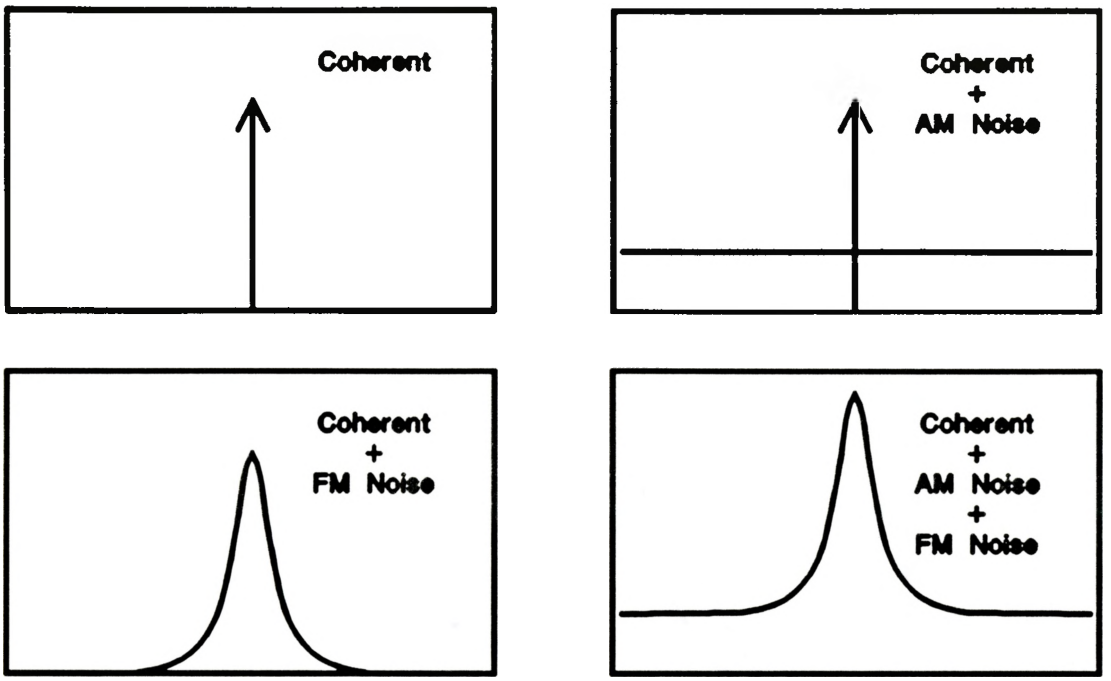

Figure 2.3 Comparison of the effect of adding white AM and FM noise to a coherent signal

field spectrum, and does not contribute directly to the line shape of the longitudinal laser modes.

FM noise is also spread over a wide frequency span. However, FM noise effectively makes laser frequency a random variable, broadening the coherent spectrum into a finite laser linewidth.

Description of noise in semiconductor lasers begins by considering the internal noise sources of the laser such as spontaneous emission and nonradiative recombination. The response of the laser must be considered to obtain the output noise of the laser. To illustrate, consider the laser

response to intensity fluctuations. Above threshold, intensity fluctuations are quickly compensated due to the gain saturation feedback mechanism. In this way, the laser tends to suppress intensity noise. I(t) may be written

$$I(t) = I + i(t) \quad ; \; i(t) \ll I \tag{2.5}$$

where I represents an average value and i(t) the fluctuations.

Laser noise can be derived from the Langevin rate equations, which are standard rate equations with additional forcing terms representative of internal noise processes. The Langevin equations describing the time evolution of the optical field phase, the photon number, and the carrier number are [32]

$$\frac{d\phi}{dt} = \frac{\alpha\,(G(t) - \Gamma)}{2} + \frac{\alpha R}{2I} + F_{\phi}(t) \tag{2.4}$$

$$\frac{dI}{dt} = (G(t) - \Gamma)\, I(t) + R + F_I(t) \tag{2.5}$$

$$\frac{dN}{dt} = C - G(t)\, I(t) - S(t) + F_N(t) \tag{2.6}$$

where

ϕ ≡ phase of the optical field
I ≡ number of photons in the mode
N ≡ number of carriers
G ≡ photon gain (per unit time)
Γ ≡ photon loss (per unit time)
R ≡ average rate of spontaneous emission into the mode
C ≡ injection current (carriers per unit time)

$S \equiv$ total spontaneous + nonradiative recombination rate
$F_\phi \equiv$ Langevin forcing term for ϕ
$F_I \equiv$ Langevin forcing term for I
$F_N \equiv$ Langevin forcing term for N

The time dependent terms are labelled so explicitly. F_N represents random fluctuations which occur in carrier recombination. The random nature of spontaneous emission has been accounted for in (2.5) by including a time independent rate R and the Langevin force $F_I(t)$, which represents random deviations of the instantaneous spontaneous emission rate from R.

F_ϕ is also related to the spontaneous emission. Spontaneous emission is phase uncorrelated with the laser field, so each spontaneous emission event alters the phase of the total field as shown in Figure 2.2. The relative phase angle of spontaneous emission is uniformly distributed over 2π radians, giving a time-averaged net phase contribution of zero. However, there is no feedback mechanism to return ϕ to a steady state value as in the case of I and N, and so ϕ undergoes a form of Brownian motion [1]. These fluctuations in phase imply changes in instantaneous optical frequency

$$\nu(t) = \nu_o + \frac{1}{2\pi}\frac{d\phi}{dt} = \nu_o + f_d(t) \qquad (2.7)$$

ν_o is the average optical frequency, and $f_d(t)$ is termed the

instantaneous frequency deviation.

A full analytic solution of these rate equations can be obtained by linearizing (2.5,2.6) in terms of small fluctuations about mean values **[32]**. This approach has the advantage of including line broadening due to carrier noise, and describes FM noise at frequencies near the relaxation oscillation. Although not difficult, this approach is relatively lengthy and tends to obscure a clear physical picture of the major sources of line broadening. A more intuitive solution is available by considering only the low frequency behaviour.

The full solution for I(t) and N(t) is characterized by damped oscillations typically occurring at frequencies above 1 GHz. At frequencies lower than this the laser adiabatically follows the Langevin forces by continually adjusting the gain to return to steady state photon number. In this approximation dI/dt can be neglected and (2.4,2.5) combined to yield a single rate equation describing the phase evolution

$$\frac{d\phi}{dt} = F_{\phi}(t) - \frac{\alpha F_I(t)}{2I} \qquad \textbf{(2.8)}$$

Figure 2.2 illustrates how a single spontaneous emission event can cause phase change in the total laser field. The initial operating point of the laser is labelled A. After a spontaneous emission event the total field sums to

point B, giving an immediate phase shift ϕ_1. After the spontaneous emission the total field is no longer at a steady state value and undergoes relaxation oscillations, eventually decaying to point C. The associated gain change causes a change in refractive index as discussed in the previous section, which results in the secondary phase shift ϕ_2. The first and second terms in (2.8) generate ϕ_1 and ϕ_2 respectively. It should be noted that the laser responds to many spontaneous photons at any given time, since the time required for the field to decay from B to C (~1 nanosecond) is much larger than the average time between spontaneous emission events coupling into the laser mode (~1-10 picoseconds). In this sense steady state is never realized, and should only be pictured as an average state for the laser.

Equation 2.8 can be rewritten in terms of instantaneous frequency deviation†

$$f_d(t) = \frac{F_\phi(t)}{2\pi} - \frac{\alpha F_I(t)}{4\pi I} \qquad (2.11)$$

The frequency deviation is obviously still a random variable. Experimentally it is more convenient to measure the spectral

---

† Due to the nature of the experimental technique, it is more useful to consider frequency noise rather than phase noise. The spectral densities are simply related by

$$S_\phi(f) = \frac{S_{f_d}(f)}{f^2}$$

density of $f_d(t)$. By the Wiener-Khintchine theorem **[33, p112]** it is given by the Fourier tranform of the autocorrelation of $f_d(t)$. In order to calculate this, the autocorrelations and cross correlations of $F_I(t)$ and $F_\phi(t)$ are required. They are given by **[32]**†

$$\left\langle F_\phi(t)\, F_\phi^*(t-\tau)\right\rangle = \frac{R}{2I}\delta(\tau) \qquad \textbf{(2.12)}$$

$$\left\langle F_I(t)\, F_I^*(t-\tau)\right\rangle = 2RI\delta(\tau) \qquad \textbf{(2.13)}$$

$$\left\langle F_\phi(t)\, F_I^*(t-\tau)\right\rangle = \left\langle F_I(t)\, F_\phi^*(t-\tau)\right\rangle = 0 \qquad \textbf{(2.14)}$$

Thus the FM noise spectrum is††

$$S_{f_d}(f) = \frac{R(1+\alpha^2)}{8\pi^2 I} \qquad \textbf{(2.15)}$$

This treatment has given a flat FM noise spectrum, valid for frequencies below about 1 GHz. At frequencies near the relaxation oscillation peak, the gain fluctuations are enhanced, giving increased FM noise. At frequencies far above the relaxation oscillation the gain fluctuations are not in effect. This results in a second region of flat, but lower FM noise. This behavior may be quantified by full solution of the Langevin rate equations **[32]**.

---

† The fact that $F_I(t)$ and $F_\phi(t)$ are real valued functions has been used.

†† This is a theoretical two-sided (positive and negative frequency) spectral density. The experimentally determined FM noise spectrum is one-sided, and hence twice as large.

This analysis has not considered thermal effects. The refractive index of the active region is temperature dependent, while temperature of the active region is expected to depend to some extent on the carrier density and/or photon density. Since the carrier density and photon density are fluctuating, at frequencies below the thermal response cut off of the active region, the temperature will be similarly modulated and give temperature induced frequency shifts. This behavior is discussed briefly in [3] and is consistent with data recorded in Chapter 4. Inclusion of thermal effects requires an accurate decription of the processes contributing to heating in the laser and is beyond the scope of this thesis.

Experimental FM noise spectra have demonstrated a component with a 1/f dependence which dominates over the white component at frequecies below about 100 kHz [7]. The origin of this 1/f noise has not been determined. One possible explanation for 1/f FM and AM noise relies on spatially dependent temperature and carrier fluctuations [34].

Figure 2.4 gives a pictorial representation of the anticipated FM noise spectrum of a semiconductor laser, based on the various contributions discussed above. The dashed line indicates the FM noise predicted by solution of equations (2.4-2.6), using the parameters given in [35]. 1/f noise has been included with a magnitude such that it is significant

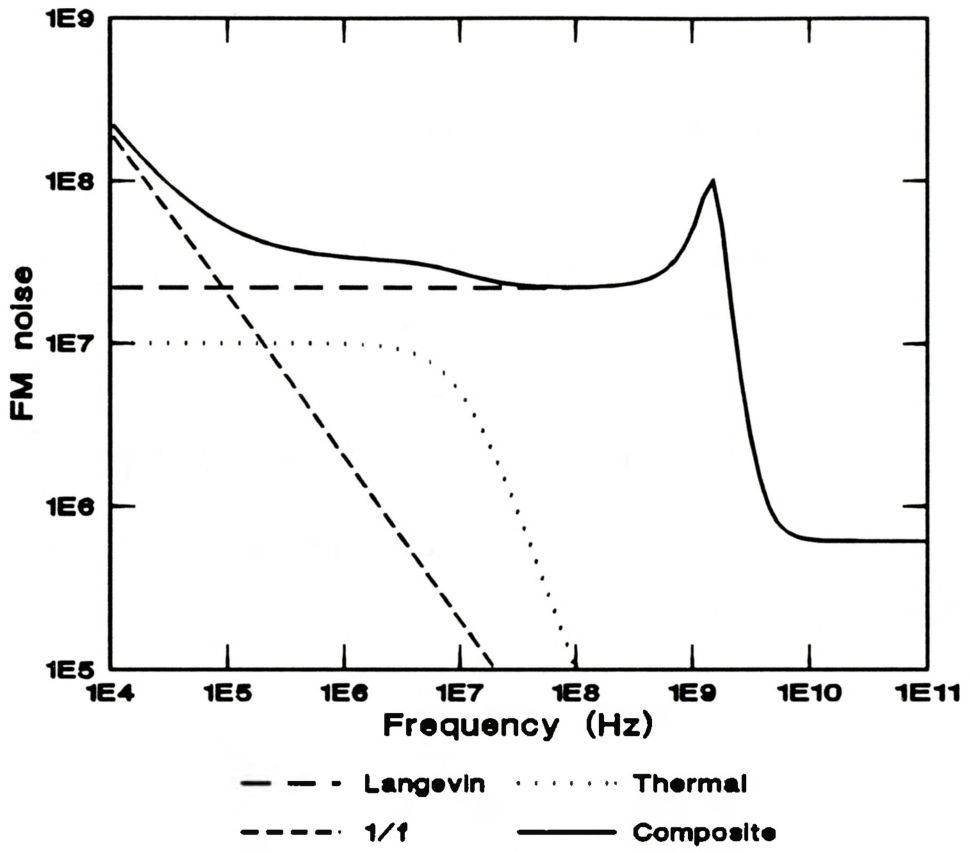

Figure 2.4 Representation of a realistic FM noise spectrum demonstrating various contributions

for f ≤ 100 kHz [7]. The thermal noise was approximated by assuming thermal fluctuations caused by intensity fluctuations, with a thermal cutoff of about 5 MHz. The amplitude was arbitrarily chosen to agree roughly with typical results from Chapter 4. The solid curve represents the

composite FM noise, assuming the individual terms add as uncorrelated sources. Figure 2.4 should be considered as representative only. A similar figure is given in **[3]**.

2.4 Linewidth from FM Noise Spectra

The spectral density of the laser field is related to the FM noise spectral density by **[36,37]**

$$S_E(\nu) = \mathcal{F}\left(\exp\left(-2\pi^2\tau^2\int_{-\infty}^{+\infty} S_{f_d}(f)\left(\frac{\sin(\pi f\tau)}{\pi f\tau}\right)^2 df\right)\right) \qquad \textbf{(2.16)}$$

Using (2.15,2.16) gives a theoretical expression for the laser line shape (normalized)

$$S_E(\nu) = \frac{\Delta\nu^2}{\Delta\nu^2+4\nu^2} \qquad \textbf{(2.17)}$$

where the FWHM linewidth is given by

$$\Delta\nu = 2\pi S_{f_d}(0) = \frac{R(1+\alpha^2)}{4\pi I} \qquad \textbf{(2.18)}$$

The actual laser power spectrum is centred at ν_0. The laser lineshape is a Lorentzian with a half width inversely proportional to the number of photons in the laser mode. By approximating R and I in terms of commonly used laser parameters, the linewidth of a Fabry-Perot laser can be expressed in a more convenient form **[1]**

$$\Delta\nu = \frac{\gamma_m(\gamma+\gamma_m)\, v_g^2\, n_{sp} \hbar\nu\,(1+\alpha^2)}{8\pi P_o} \qquad (2.19)$$

A discussion of the parameters in (2.20) is given in [32]. The linewidth varies inversely with the single facet power P_o, thus the linewidth characteristics of a laser are usually expressed as a linewidth-power (MHz-mW) product. The distributed facet loss γ_m is given by

$$\gamma_m = \frac{1}{L}\ln\frac{1}{\sqrt{R_1 R_2}} \qquad (2.20)$$

from which the dependence on length and facet reflectivity comes. The factor n_{sp} accounts for incomplete inversion of carriers in the laser, and is approximately 2 for bulk lasers. The waveguide loss γ is dominated by scattering loss and intraband absorption. Intraband absorption can be reduced in quantum well lasers [32], whereas scattering in semiconductor lasers has been correlated with device structure [38]. The linewidth enhancement factor α is approximately 6 in bulk lasers [11], 3.5 in quantum well lasers [39], and 2 in strained layer quantum well lasers [40]. The reduction of α from 6 to 2 implies linewidth reduction by a factor of about 7, assuming other parameters to remain constant.

Equation (2.17) is valid only in as much as the FM

noise can be considered white. A relaxation oscillation peak in the frequency noise spectrum generates lobes in the wings of the laser lineshape. These lobes appear spaced by integer multiples of the relaxation oscillation frequency from line centre **[35]**. However, since the relaxation oscillation occurs at frequencies large compared to typical linewidths, the Lorenztian approximation remains valid near line centre.

Excess low frequency noise tends to broaden the line near its centre, and in the limit that 1/f noise dominates, the laser line shape becomes approximately Gaussian **[41]**. Excess low frequency FM noise can occur due to side mode suppression ratios (SMSR) lower than about 20 dB in Fabry-Perot lasers, or 30 dB for DFB lasers **[28, p207]**. 1/f noise has been shown to be practically power independent, so at very high power levels linewidth can be dominated by 1/f noise and independent of power **[7]**. These mechanisms are most likely responsible for linewidth floor and linewidth rebroadening which occurs in most lasers at high output power **[32]**.

2.5 Optical Feedback Effects

One of the chief advantages of employing optical feedback is that linewidth narrowing can occur. This potential advantage becomes detrimental in the case of parasitic optical feedback, when unintentional reflections to

the laser cause changes in FM noise characteristics. A theoretical description of feedback effects on linewidth allows an estimation of the optical isolation required to ensure negligible optical feedback effects, an important consideration when designing a linewidth measurement system. It also provides an estimate of the effects of the SXC on the natural linewidth of the solitary laser.

Figure 2.5 illustrates a laser subject to feedback from a simple reflector. The derivation of linewidth in the presence of optical feedback proceeds as described in the previous two sections, except that a time delayed term corresponding to the external reflection is included. When the effective reflectivity of the external mirror is assumed to be small, only one round trip in the external cavity need be considered, and the rate equations may be linearized. In this case, the linewidth is [25]

$$\Delta\nu_{fb} = \frac{\Delta\nu}{\left(1+\kappa\tau\sqrt{1+\alpha^2}\cos(\Phi)\right)^2} \qquad (2.21)$$

where τ is the external cavity round trip time, κ is the feedback coupling rate given by

$$\kappa = \frac{(1-R_1)\sqrt{R_{ext}}}{\sqrt{R_1}\tau_l} \qquad (2.22)$$

where τ_l is the laser round trip time, and Φ is given by
The mode frequency ω_o depends on the feedback as well, and

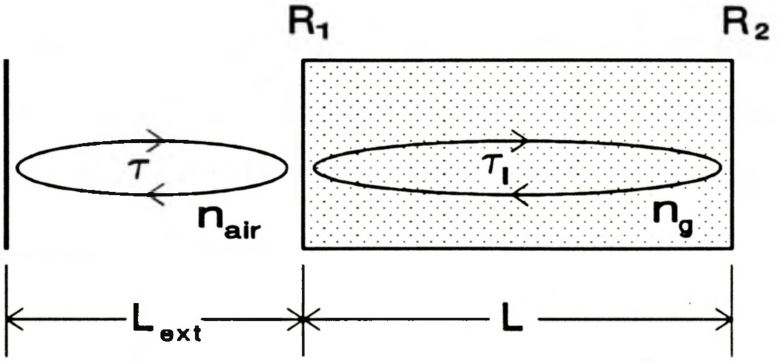

Figure 2.5 Schematic of a laser with external optical feedback

$$\Phi = \tan^{-1}\alpha + \omega_o\tau \qquad (2.23)$$

must be determined from the open form equation

$$\omega_o = \omega_{nf} - \kappa\sqrt{1+\alpha^2}\sin(\tan^{-1}\alpha + \omega_o\tau) \qquad (2.24)$$

with ω_{nf} representing the mode frequency with no feedback present. Frequency tuning is discussed in greater detail in Chapter 5.

The external cavity effect is included via parameters R_{ext} and τ. Note that depending on the sign of $\cos(\Phi)$ the linewidth can be enhanced or reduced by external feedback. With long external cavities (large τ) the linewidth change can be large even with a very small reflectivity.

The tolerable amount of parasitic feedback for a linewidth measurement instrument can be estimated using

(2.21). Assuming the reflection to occur 2 metres† from the laser, $R_{ext} \simeq 1x10^{-11}$ for a maximum linewidth change of 10%, using typical values of $R_1 = 0.32$, $\tau_l = 7$ psec, and $\alpha = 6$. This may represent an overestimation of the isolation requirement, since the derivation of (2.21) includes an assumption that the round trip transit time in the external cavity be much smaller than the coherence time of the laser, whereas they are of the same order of magnitude for a cavity length of 2 metres. In **[42]** linewidth change of 30% was observed with feedback corresponding to $R_{ext} = 1x10^{-8}$ for 1.5 μm emitting distributed feedback lasers subject to a reflection 40 centimetres from the laser. Obviously a large degree of optical isolation is required to eliminate external cavity effects on linewidth measurements.

The effect of a short external cavity on the linewidth can also be estimated. This has been done in Chapter 5, where the theoretical linewidth change was found to be a few percent. This means that linewidth measured on a laser with a short external cavity is indicative of the natural linewidth of the solitary laser.

---

† This corresponds to the distance to the Fabry-Perot Interferometer - see Chapter 3.

2.6 Summary

The theoretical background for studying FM noise in semiconductor lasers has been reviewed. FM noise was shown to originate predominantly from spontaneous emission. The coupling of spontaneous emission to FM noise occurs by two mechanisms, via direct phase modulation of the laser field, and indirectly by refractive index fluctuations induced by laser response to intensity fluctuations. The latter process is characterized by α, the linewidth enhancement factor.

The relationship between frequency noise and linewidth was given. Assuming white FM noise, gave a Lorentzian line shape with a linewidth proportional to the magnitude of FM noise. The linewidth is inversely proportional to the laser output power and depends on a number of laser parameters such as laser length, facet reflectivity, linewidth enhancement factor, and internal loss.

The linewidth can be strongly affected by optical feedback. Length of the external cavity and strength of reflection are the important parameters. The feedback strength required to significantly affect the linewidth was estimated at $10^{-8} > R_{ext} > 10^{-11}$ for a cavity length of 2 metres. The SXC effect on the linewidth, however, is only a few percent.

CHAPTER 3 EXPERIMENTAL TECHNIQUE

3.1 Introduction

This chapter describes the experimental technique developed for measuring frequency noise and frequency tuning in SXC configured laser diodes. A description of the optical and electronic apparatus in the context of frequency noise measurement is given in Section 3.2. A discussion of the frequency response of the Fabry-Perot interferometer is contained in Section 3.3. The method of calibrating the instrument to obtain frequency noise spectra is discussed in Section 3.4. Section 3.5 is concerned with techniques for identifying and eliminating unintentional optical feedback. Section 3.6 discusses limitations imposed by other noise sources on FM noise measurement. Section 3.7 provides a summary of this chapter.

3.2 Description of Apparatus

Figure 3.1 is a schematic of the optical apparatus. The lasers under test were InGaAsP semiconductor Fabry-Perot lasers operating at wavelengths of 1300 to 1400 nanometres. Such lasers exhibit a multimode spectrum, and so a SXC (short external cavity) was used to obtain single mode oscillation. A complete description of the SXC module is given in **[43]**.

The lasers were bonded active region up on standard chip carriers. The carriers were fixed to copper heat sinks using thermal conductive epoxy. Temperature of the heatsink was controlled by a thermoelectric cooler. The heatsink and thermoelectric cooler were mounted on an aluminum bar which was fastened to the SXC module. Electrical contacts to the laser were made with gold wire bonds from the chip carrier pads to copper pads. The copper pads had soldered wire contacts which connected to the laser driver circuit. This configuration was found to be robust, versatile and compact.

The short external cavities were formed using a small planar or spherical reflector mounted on a piezoelectric transducer (PZT). The planar mirrors were gold coated diamond heatsinks. The spherical mirrors were polished aluminum with a surface formed by impression of a precision ball bearing of 380 μm diameter. The external reflectors were aligned to give cavity lengths of about 150 μm. A positioner with 3 axes

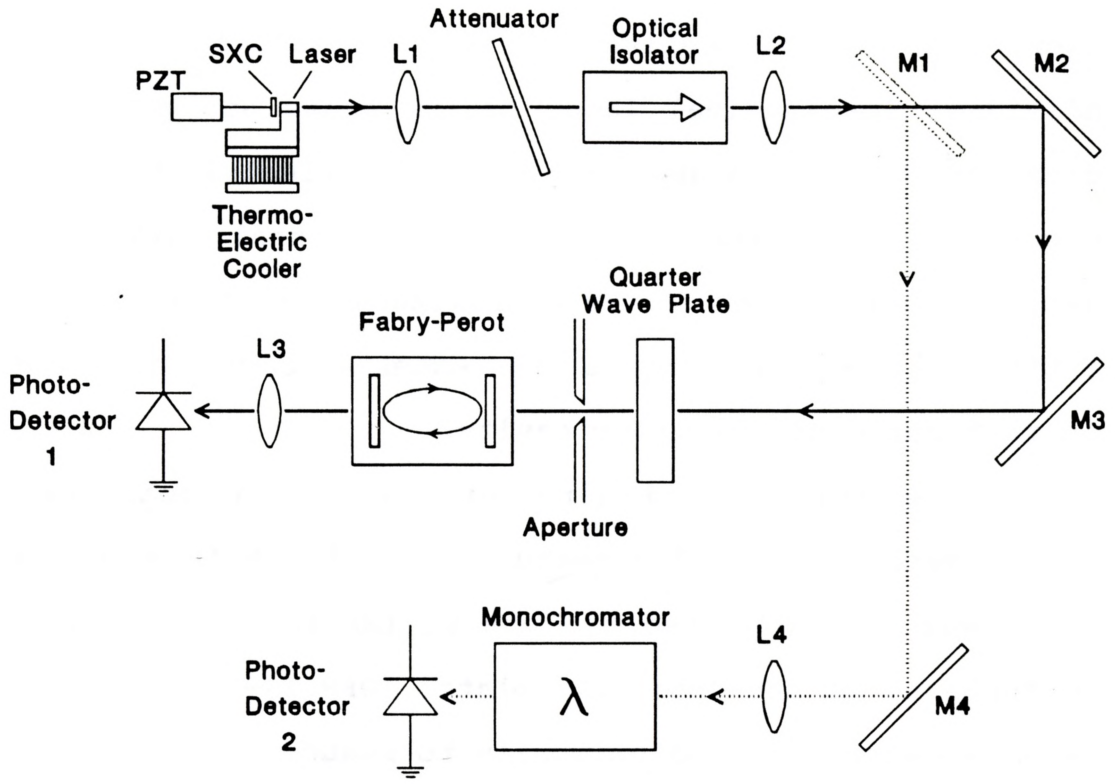

Figure 3.1 Optical Apparatus

translational and 3 axes rotational adjustment was used to adjust the position of the external reflector. Once aligned, the PZT was locked in the SXC module with setscrews, allowing the positioner to be removed. This arrangement proved very stable in terms of both long term alignment drift and isolation from vibrations.

The SXC lasers gave single mode operation with side modes suppression ratios (SMSR) ranging from 30 to 4000†. The

† SMSR is defined as the ratio of main mode intensity to the mode intensity of the strongest side mode.

SMSR varied with alignment, optical power level, type of laser, and type of reflector [44]. Selection of about 8 individual longitudinal laser cavity modes was possible by adjusting the voltage applied to the piezoelectric transducer, which fine tuned the length of the external cavity. The number of modes obtained was approximately given by the ratio of the free spectral range of the external cavity to the free spectral range of the laser cavity.

The thick solid line in Figure 3.1 outlines the optical path for FM noise measurement. Light from the laser under test was collected by lens L1 (Melles-Griot 06GLC003) and focussed at the optical isolator (OFR IR-1 or OFR IR-2). The attenuator was used primarily to reduce optical feedback from the first surface of the optical isolator. Lenses L1 and L2 (1:1 achromat objective, 80 mm EFL) formed a beam collimator/expander. The divergence of the beam had to be small to obtain high finesse from the interferometer.

The interferometer (Burleigh RC 140) employed dielectric-coated planar mirrors with 97% reflectivity. Fine control of cavity length was provided by PZTs driven by a high voltage ramp generator (Burleigh RC-43). In scanning mode the cavity length was ramped over three transmission fringes of the interferometer. The ramp generator also had external inputs which were used for modulation and stabilization of the cavity length, as described below.

In order to get the high finesse fringes required for efficient FM detection, tilt of the interferometer had to be small. This made optical isolation a critical requirement. The combination of attenuator, optical isolator, and quarter wave plate provided the isolation. While the optical isolator and the attenuators were commercial optical components, the quarter wave plate was constructed from a 1/4 inch section of acrylic, compressively stressed and mounted in a rotation stage. The stress-induced birefringence caused optical retardation proportional to the amount of stress applied. Optical isolation is discussed in more detail in Section 3.5.

The dashed line in Figure 3.1 follows the optical path with the removable mirror M1 installed. The collimated beam was focussed onto the input slit of the monochromator with lens L3 (simple biconvex, FL ≈ 11 cm). The monochromator (0.5 m. Jarrell-Ash) was equipped with a galvanometric scanning mirror, which when driven by a ramp generator (General Scanning Inc. CX-660) covered a wavelength range of about 30 nanometres. The monochromator was used for characterizing the laser mode spectra before installation of the SXC, for aligning the SXC mirror, for measuring SMSR and longitudinal mode spacing, for measuring mode partition noise (Section 3.6), and for laser mode identification during FM noise measurements.

Figure 3.2 shows the electronics connections used

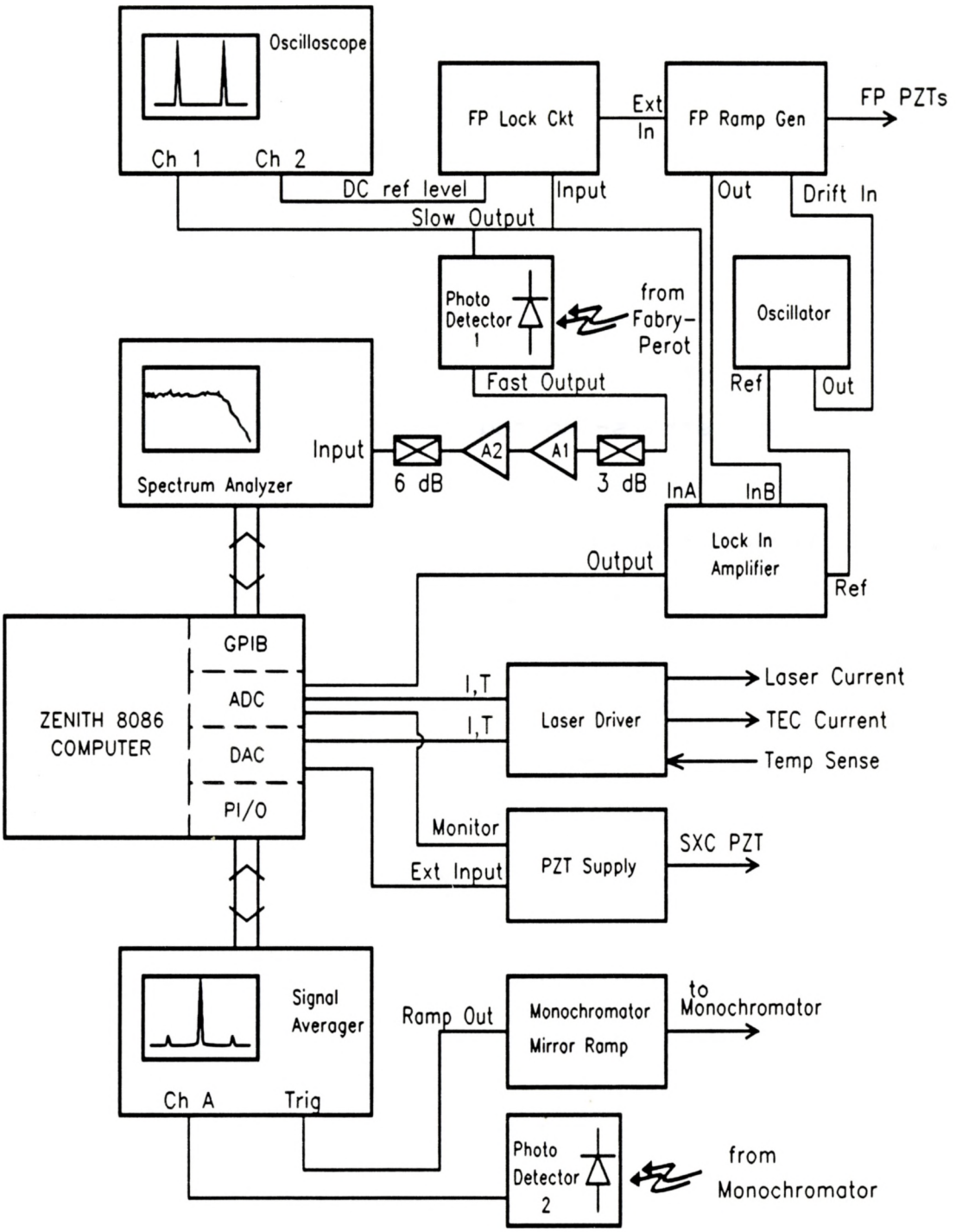

Figure 3.2 Electronics and data acquisition configuration

during frequency noise measurement. Schematics for photodetector 1 and the Fabry-Perot lock circuit are contained in the Appendix .

The laser driver was a slightly modified version of a standard laser driver developed by D.T. Cassidy. It provided a stable, low noise current source for the laser diodes. The gain of the current output circuit was rolled off at about 10 kHz for FM noise measurements to reduce laser current noise. Bandwidth-limiting capacitors were installed in sockets and were easily removed to facilitate frequency modulation above 10 kHz. With the capacitors removed the laser driver response bandwidth was about 1 MHz.

The temperature of the laser was controlled using a thermoelectric cooler driven by a proportional integral differential (PID) feedback control loop. The sensing element was a thermistor. Integral thermistors on the chip carrier were used when possible, otherwise a thermistor was mounted in the copper heat sink. The gain and time constant of the control circuit could be tailored to give optimal control of temperature. In practice it proved more convenient to tune the circuit to give slightly overdamped response. This way the temperature control did not require readjustment each time a different laser was installed. For all measurements in this thesis, the temperature was set to 25°C.

The FM noise spectrum was recorded with an RF spectrum

analyzer (HP 8557A, with HP853A display unit). The fast stage of photodetector 1 consisted of an Epitaxx ETX-300 300 μm InGaAsP detector terminated in 50Ω and amplified by an Avantek MSA-0886 monolithic microwave integrated circuit. Care was taken to employ high-speed, low-noise fabrication techniques. The circuit was constructed on a 50Ω stripline using low inductance chip capacitors for power supply bypassing and AC coupling.

Electrical reflections due to slight impedance mismatches caused partial standing-waves to form in the coaxial cable. This gave artificial undulations in the noise spectrum. This problem was eliminated by using 50Ω in-line attenuators at the interconnection points and at the spectrum analyzer input. Use of attenuators reduced the signal such that the baseline noise level was due to the spectrum analyzer, effectively limiting sensitivity. Amplifiers A1 (Avantek GPD 461) and A2 (Avantek GPD 462) were added to increase the signal such that the baseline was the thermal noise at the detector.

During measurement of frequency noise, the Fabry-Perot length was biased such that the average frequency of the laser was at the maximum slope position of an interferometer transmission fringe. This position was maintained by the Fabry-Perot lock circuit, a slow feedback loop controlling the piezoelectric transducers attached to the Fabry-Perot mirrors.

Locking the interferometer to the laser frequency gave immunity to drift in laser frequency and interferometer spacing. The transfer function of this feedback loop was adjusted to give stable response to transients, zero steady state error, and minimal feedthrough of line noise and modulation signals.

Figure 3.3 illustrates how a Fabry-Perot transmission fringe was employed to convert frequency modulation to intensity modulation. This is essentially the same technique used to estimate linewidth in lead-salt laser diodes in **[45]**. With the average laser frequency maintained at the maximum slope position of the fringe, any relative change of laser frequency caused an intensity modulation at the interferometer output. In this fashion random frequency fluctuations of the laser caused corresponding intensity noise at the output of the interferometer. The detector converted this to an electrical signal, which was Fourier decomposed by the RF spectrum analyzer. This signal, once corrected for detector frequency response and normalized by the fringe slope, yielded the frequency noise spectrum. Greater detail on the use of the Fabry-Perot interferometer as an optical frequency discriminator is provided in Section 3.3.

Calibration of the spectrum analyzer signal required measurement of the Fabry-Perot fringe slope. A small amplitude 500 Hz modulation was applied to the length of the

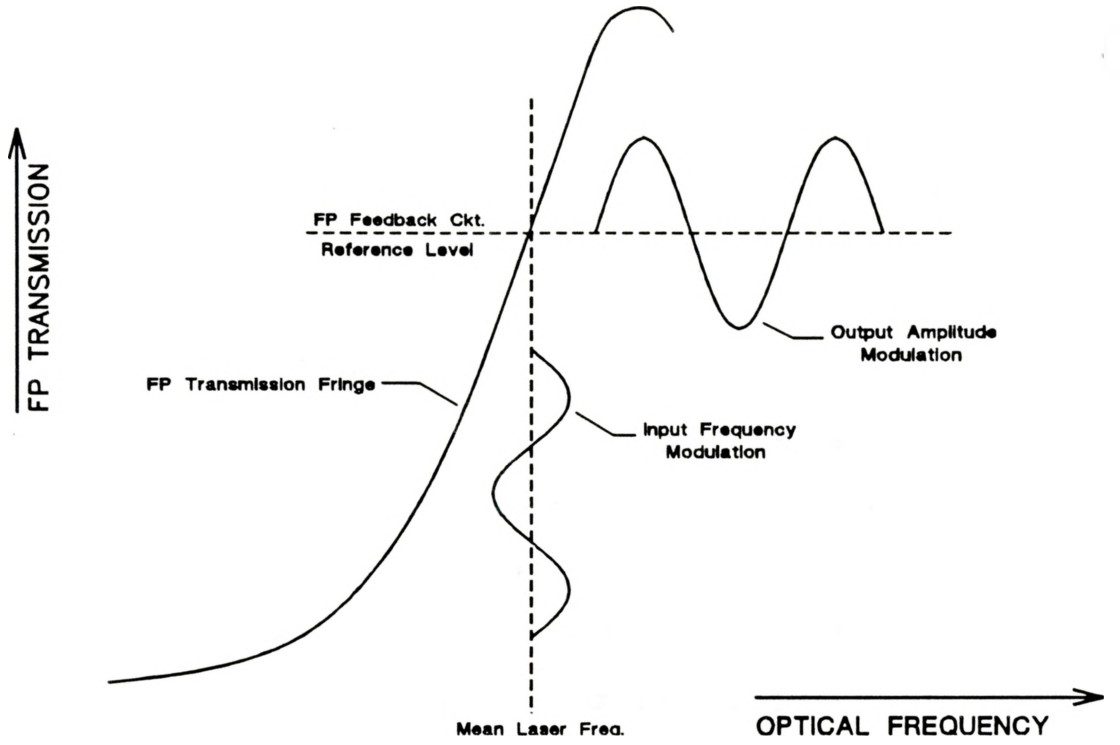

Figure 3.3 Fabry-Perot fringe used to convert frequency modulation to intensity modulation

Fabry Perot by connecting an oscillator to one of the Fabry-Perot ramp generator inputs. The sinusiodal modulation of the fringe about the mean laser frequency resulted in intensity modulation at photodetector 1. This was measured using a lock-in amplifier to determine the fringe slope. The use of small amplitude modulation left the Fabry-Perot biased in a linear region of the transmission fringe, allowing the slope and frequency noise measurements to be executed concurrently. This arrangement was particularly convenient since it was insensitive to variations in alignment, it did not require

knowledge of the exact bias point, and a separate measurement on the fringe was not required. Calibration details are supplied in Section 3.4.

3.3 Frequency Response of a Fabry-Perot Interferometer

The Fabry-Perot interferometer (FPI) was the integral FM discriminator component of the instrument. The FPI is thoroughly discussed in most general optics textbooks. However, a FPI is usually used as a tunable optical filter, so theoretical expressions are generally derived with the assumption that the input light is an unmodulated coherent field. Due to the slightly unorthodox application of the FPI in this thesis, it is necessary to consider the FPI in terms of its response to modulated optical fields.

Although Figure 3.3 provides a simple picture of how FM slope detection occurs, it should be used with caution. The physical picture represented in Figure 3.3 is valid only for modulation frequencies sufficiently low such that the interferometer output adiabatically tracks the modulated wave. The FPI transmission fringe is formed by the superposition of an infinite series of coherent, time-delayed waves generated by multiple reflections within the cavity. The FPI has a characteristic time constant related to the number of reflections required for a wave packet to decay to an

insignificant level and the time between successive reflections. If frequency modulation causes an appreciable phase shift in a time interval small compared to the FPI time constant, the interference is incomplete. The FWHM of the fringe is inversely proportional to this time constant, decreasing with increasing reflectivity and with increasing cavity length. From this argument it is apparent that the frequency response of a FPI is related to the spectral width of the transmission fringe.

Analysis of the impulse response of a FPI has been completed in **[46,47]** to determine its response to short duration laser pulses. The frequency response of the FPI as an optical frequency discriminator has been calculated in **[48]**, where the multiple reflections of a frequency modulated optical wave were summed by computer program, working solely in the time domain. The response was found under certain conditions to be similar to that of a low pass RC circuit, with a bandwidth related to the FWHM of the Fabry-Perot fringe.

In this section , the frequency response of the FPI optical frequency discriminator is considered in the frequency domain. The motivation is to obtain a clear, intuitive picture of the Fabry-Perot frequency response a treatment similar to the transfer function method commonly used with electrical circuits. This approach will be used to

investigate the inherent compromise between sensitivity and bandwidth. The frequency domain analysis has the additional benefit of being much more computationally efficient than the time domain calculations described in **[48]**.

In accord with the experimental situation, the Fabry-Perot is assumed to be comprised of two partially transmissive planar mirrors, similar to the Fabry-Perot laser of Figure 2.1. The response of a FPI is derived by considering the superposition of an infinite series of waves formed by multiple reflections occurring in the Fabry-Perot cavity. Electric field response is then given by **[49, p171]**

$$F(\nu) = t^2 \sum_{k=0}^{\infty} r^{2k} e^{j\frac{4\pi\nu kd}{c}} \qquad \textbf{(3.1)}$$

where

t = E field transmission coefficient of each mirror
r = E field reflection coefficient of each mirror
ν = optical frequency
k = order of reflection
d = spacing between mirrors
c = speed of light (refractive index of 1 assumed)

To keep the notation compact, this is rewritten

$$F(S) = t^2 \sum_{k=0}^{\infty} R^k e^{jkS} \qquad \textbf{(3.2)}$$

where

$$R = r^2 \tag{3.3}$$

$$S = \frac{4\pi d}{c}(\nu - \nu_{res}) \tag{3.4}$$

$$\nu_{res} = m\frac{c}{2d} \tag{3.5}$$

m is an integer. R is the mirror reflectivity, ν_{res} is the resonance frequency of the FPI, and S is normalized frequency. S represents the detuning from resonance in units of free spectral range. With R < 1, the infinite series (3.2) converges to

$$F(S) = \frac{t^2}{1 - Re^{jS}} \tag{3.6}$$

In polar form (3.6) becomes

$$|F(S)| = \frac{t^2}{\sqrt{1 - 2R\cos(S) + R^2}} \tag{3.7}$$

$$\sphericalangle F(S) = \tan^{-1}\left(\frac{R\sin(S)}{R\cos(S) - 1}\right) \tag{3.8}$$

Notice that (3.7) squared gives the intensity transfer function, which is the well-known Airy function. The Fabry-

Perot transfer function with R = 0.97 is plotted in Figure 3.4 over one free spectral range. The tranfer function is periodic, repeating as the optical frequency cycles through one free spectral range.

Analysis of the response to an FM modulated wave is lengthy and complicated for the general case. Instead of treating the general case, small-index tone modulation will be considered. Using the small-index limit restricts the number of significant sidebands to two, the upper and lower bands nearest the carrier. Tone modulation refers to the case where the modulation signal is a simple sinusoid. Connection to the laser FM noise is made by picturing the FM noise as a superposition of random tone modulations over a continuous spectrum.

AM and FM tone modulation spectra and phasor representations are reviewed in Figure 3.5. A_{-1}, A_0, A_{+1} denote the phasors of the lower side band, carrier, and upper side band respectively. The carrier frequency is f_c; f_m is the modulation frequency. AM tone modulation is characterized by side bands of equal amplitude and zero phase relative to carrier. In the phasor representation, the frame of reference is that of the carrier phasor. The side bands then rotate about the stationary carrier phasor at the modulation frequency and in opposite senses. The resultant of the side band phasors has sinusoidally varying amplitude and is always

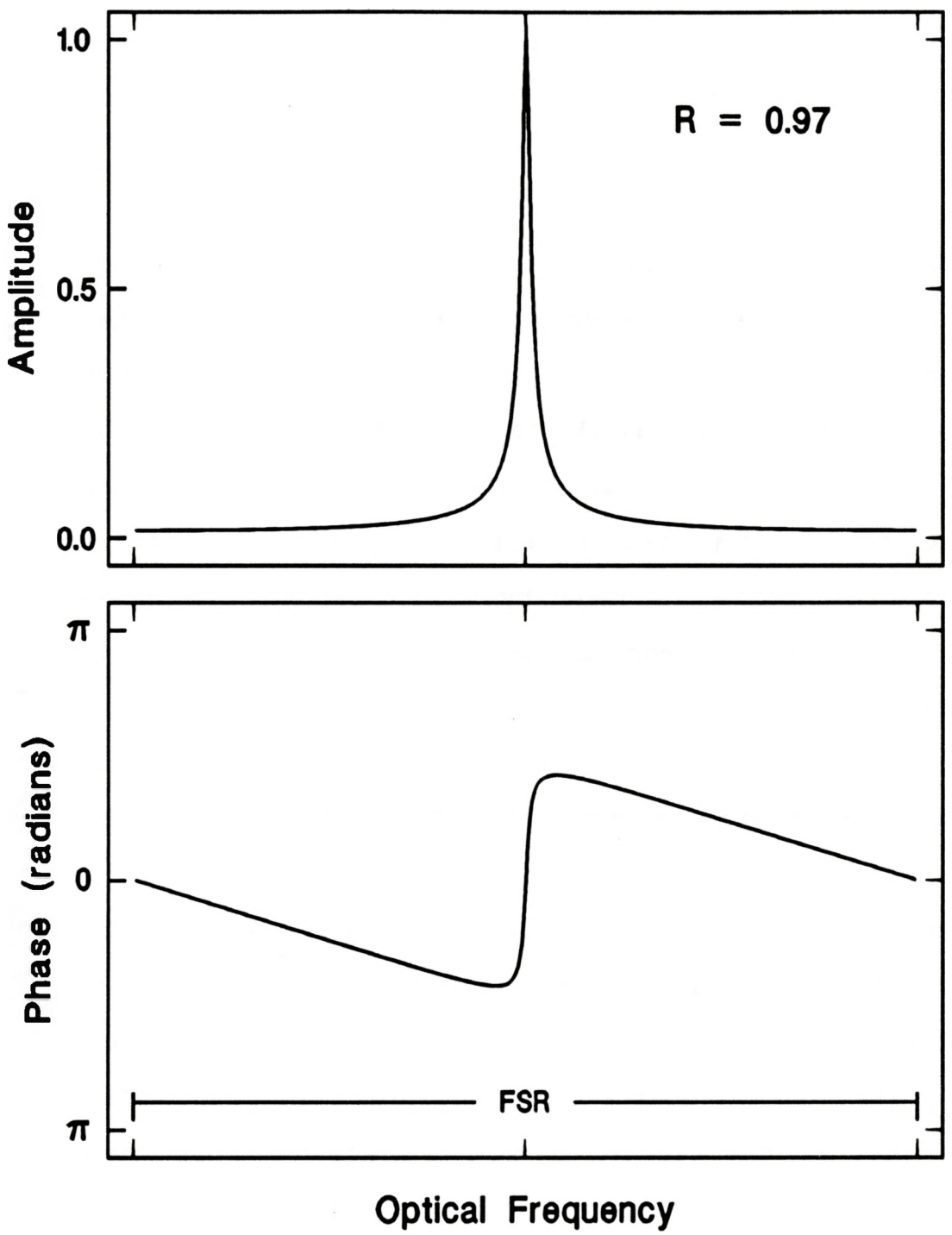

Figure 3.4 Transfer function of a Fabry-Perot interferometer

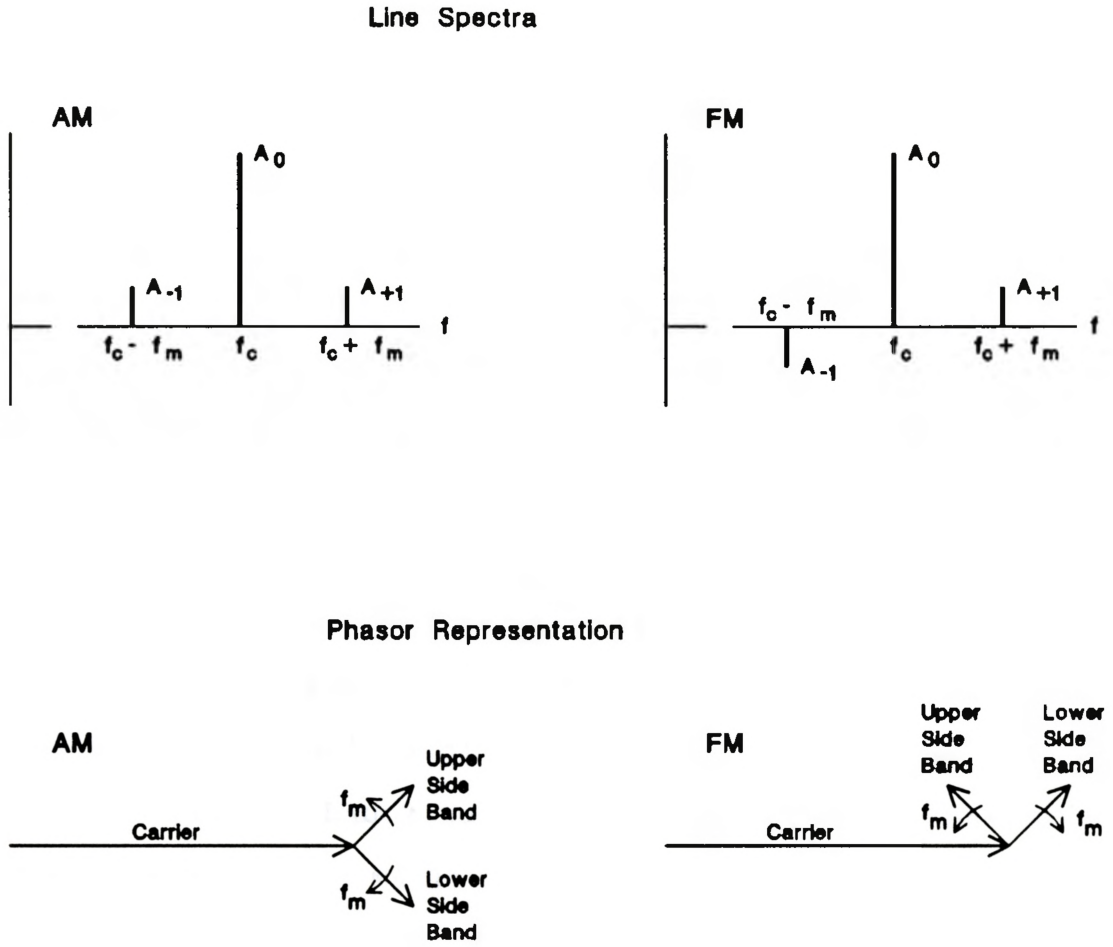

Figure 3.5 Comparison of FM and AM tone modulation

parallel to the carrier, thereby impressing amplitude modulation on the carrier.

The FM line spectrum (small-index) is very similar to the AM case. The upper and lower side bands again have equal amplitude, but as pictured the upper side band has zero phase relative to the carrier, while the lower side band has a relative phase of 180°. In the phasor representation the side band phasors again undergo opposite sense rotation about the

carrier, but the relative phase difference gives a side band resultant always perpendicular to the carrier. The result is a phasor rotating sinusoidally about the carrier frequency, representative of a field with time varying instantaneous frequency.

The circular arc traced out by the resultant phasor of a pure FM field has been approximated by the tangent to this arc, which is generated by the upper and lower sidebands. Exact description of a pure FM field requires an infinite number of side bands. When the maximum phase deviation is small the tangent approximation is good and only the lowest order side bands need be considered. This is simply another way of decribing the small-index approximation. More detail on AM and FM tone modulation can be found in [33].

Using this simple picture of FM and AM, the effect of a FPI on an incident FM optical field will be derived. The FPI transforms the incident FM field to a combination of AM and FM. The photodetector following the FPI is sensitive to intensity but not frequency, so the output amplitude modulation is the signal portion of the output wave.

The line spectrum of the output wave is given by

$$A_i' = A_i \, F(S_i) \quad ; \quad i = -1, 0, +1 \tag{3.9}$$

with A_i denoting the components of the input line spectrum and the corresponding output components given by A_i'. The

normalized frequencies S_i corresponding to each spectral component are given by

$$S_i = \frac{4\pi d}{c}\left[(\nu_o + i f_m) - \nu_{res}\right] \qquad (3.10)$$

where ν_o is the mean laser frequency (carrier frequency). The A_i' are complex quantities, since F(S) is complex. On output, the upper and lower sidebands are no longer of the same amplitude, nor is there a simple relationship between the phase of the spectral components.

Reverting to the phasor representation, the equation of motion describing the resultant of the side band phasors is

$$Resultant = A'_{+1} e^{+j2\pi f_m t} + A'_{-1} e^{-j2\pi f_m t} \qquad (3.11)$$

The component parallel to the output carrier phasor is

$$AM\ Output = \Re\left[\left(A'_{+1} e^{+j2\pi f_m t} + A'_{-1} e^{-j2\pi f_m t}\right) e^{-j\psi_o}\right] \qquad (3.12)$$

where

$$\psi_o = \sphericalangle F(S_0) \qquad (3.13)$$

is the angle of the output carrier component. All that remains is to calculate the time at which the amplitude contribution is greatest. Setting the time derivative of (3.12) to zero gives

$$t_{max} = \frac{1}{2\pi f_m} \tan^{-1}\left(\frac{\Im\left[e^{-j\Psi_o}(A_{-1} - A_{+1})\right]}{\Re\left[e^{-j\Psi_o}(A_{-1} - A_{+1})\right]} \right) \qquad \textbf{(3.14)}$$

The amplitude modulation is given by substituting t_{max} for t in (3.12).

The frequency response of the Fabry-Perot can be visualized by picturing the effect of the transfer function on the side bands. As the modulation frequency increases, the sidebands move away from the carrier frequency. At sufficiently high modulation frequencies, the FM spectrum width exceeds the linear region near the carrier frequency. If the carrier frequency occurs at the maximum slope of the Fabry-Perot fringe, the response falls off with increasing modulation frequency as the sidebands move into lower slope regions.

The frequency response of the FPI as an FM discriminator was calculated using (3.14), (3.12), and (3.6) for carrier frequency at several positions relative to the Fabry-Perot resonance frequency, reflectivities ranging from 0.93 to 0.98, and FPI cavity lengths from 0.18 cm to 1.66 cm. Comparison to calculations using the brute force approach of **[48]** revealed identical frequency response curves, confirming the validity of the frequency domain analysis. The computer

time required for the frequency domain analysis was over two orders of magnitude smaller than the time involved with the corresponding time domain analysis.

A comparison was also made between the theoretical and measured frequency response of the FPI. The results are shown in Figure 3.6. The Fabry-Perot tranmission fringe was measured with a cavity length of 0.6 cm and the interferometer in scanning mode. The portion to the right of fringe centre was fitted with an Airy function. Measured and fitted fringes are shown in the upper graph in Figure 3.6. The fit was excellent on the right hand side, but poor on the left. The asymmetry in the measured fringe was common to all lasers measured. The output laser beam actually consisted of the superposition of light from the front laser facet and light reflected from the SXC mirror. The far field of the SXC laser thus exhibited strong interference effects **[50]**. It is believed that this caused the asymmetry in the measured fringes. The asymmetry did not cause any deleterious effects.

Laser output was used as an FM modulated optical wave with an almost white FM noise spectrum. The average laser frequency was set to various positions on the fringe, labelled A-E in Figure 3.6, and the resulting noise spectra were recorded. The theoretical curves were calculated using the transfer function corresponding to the fitted fringe. Note that the curves are plotted normalized to low frequency

response, and that point A has greater absolute FM detection sensitivity than point E. Comparison of the theoretical and measured results shows reasonable agreement. The primary difference lies in the slope in the cut off region. The theoretical curves predict an 8 dB/octave roll off, whereas the measured slope was 4 dB/octave. A similar measurement was made on the left slope of the Fabry-Perot fringe, giving a 14 dB/octave slope. Note that the theoretical slope is approximately equal to the mean of the measured values using the left and right portions of the Fabry-Perot fringe. The difference between theory and measurement was attributed to the interference fringes in the input beam.

These investigations revealed that the FPI slope detection method is limited by a compromise between sensitivity and bandwidth. Increasing slope of the fringe increases FM to AM conversion, but decreases the frequency range over which the frequency response is constant.

In practice it was determined that a FPI cavity length of about 0.5 cm was appropriate when using the rising edge of the Fabry-Perot fringe with the interferometer aligned as close to on-axis as feedback restrictions allowed. This gave flat response to 200 MHz and sufficient sensitivity for most purposes. For measurements on low linewidth lasers, longer FPI cavity lengths were used to obtain greater sensitivity, but in these cases the bandwidth was less than 200 MHz.

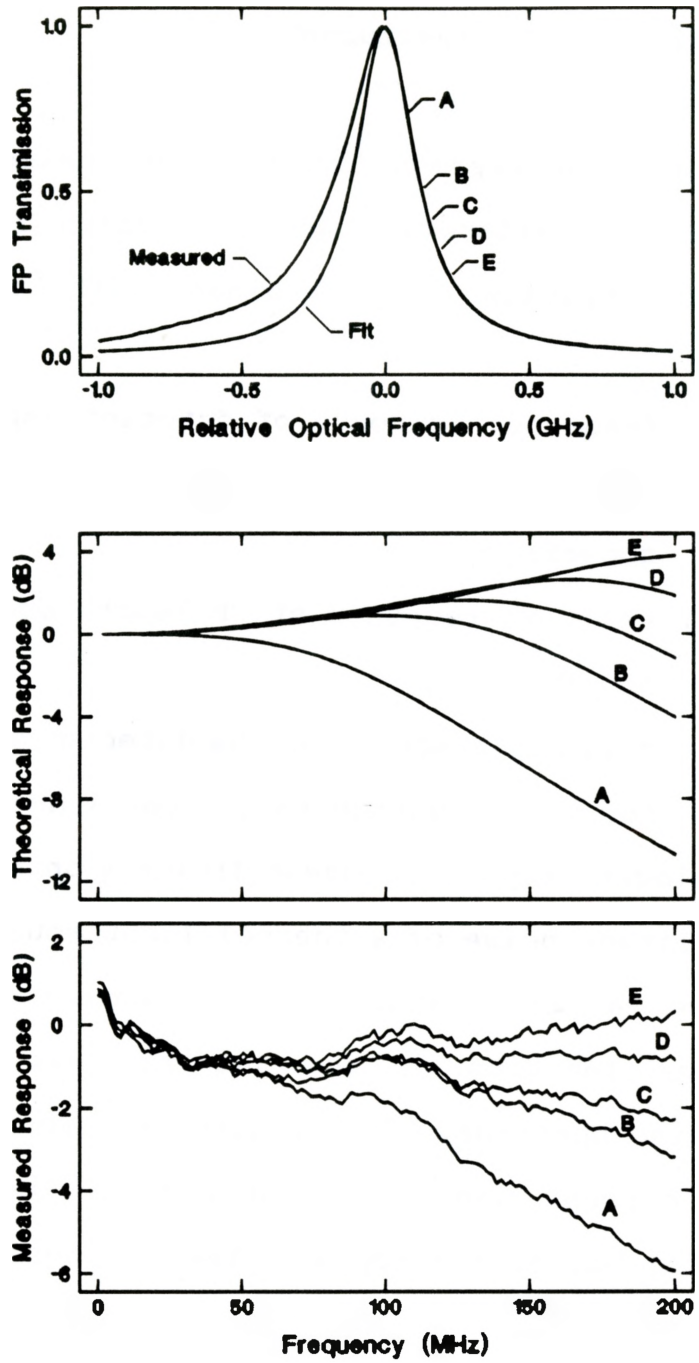

Figure 3.6 Normalized frequency reponse of the FPI showing the measured and fitted fringes, and the theoretical and measured frequency response at points A through E.

3.4 Calibration of the Instrument

Accurate and reproducible frequency noise measurements required careful calibration and correction for systematic errors. Calibration was obtained with the following measurements:

i) frequency response of detector/amplifiers

ii) Fabry-Perot piezo voltage/optical frequency conversion

iii) relative response of FP length modulation at 500 Hz

The frequency response of the detector was obtained in two stages. For the frequency range from 1 MHz to 350 MHz, a tungsten-halogen lamp was focussed directly onto photodetector 1. The amplitude noise of a thermal light source has a white spectrum over a large bandwidth, and hence the magnitude of the transfer function of the detector was given by the measured noise spectrum. For frequencies from 1 kHz to 1 MHz the laser current was modulated and the detector output measured with an oscilloscope. The response of the laser driver was checked using another detector with a flat response over this frequency range.

The 3 dB point of the photodetector response was about 150 MHz, and the ripple in response was less than 0.3 dB. The

frequency response data was used to correct raw data for the detector frequency response. The validity of the frequency response correction was evident by the flat laser frequency noise spectra obtained after frequency response correction - see Chapter 4 - in agreement with the prediction of Chapter 2.

As mentioned in the previous section, the slope of the Fabry-Perot transmission fringe was an essential parameter in calculating an absolute level for the frequency noise spectrum. To find this, the frequency modulation corresponding to the cavity length modulation had to be determined. Interferometer transmission fringes were recorded simultaneously with the ramp voltage applied to the Fabry-Perot PZTs while the interferometer was in scanning mode. Data from such a measurement is plotted in Figure 3.7. Since the free spectral range of the interferometer was known, the piezo voltage to frequency conversion of the interferometer was obtained. By measuring the piezo voltage modulation impressed during slope measurement and using the piezo voltage to frequency conversion, the corresponding frequency dither of the interferometer was found.

The piezo voltage to frequency conversion was measured at low frequency corresponding a 500 millisecond scan period, whereas the Fabry-Perot was modulated at 500 Hz during slope measurement. The relative response of cavity length modulation versus frequency was measured. The response at 500

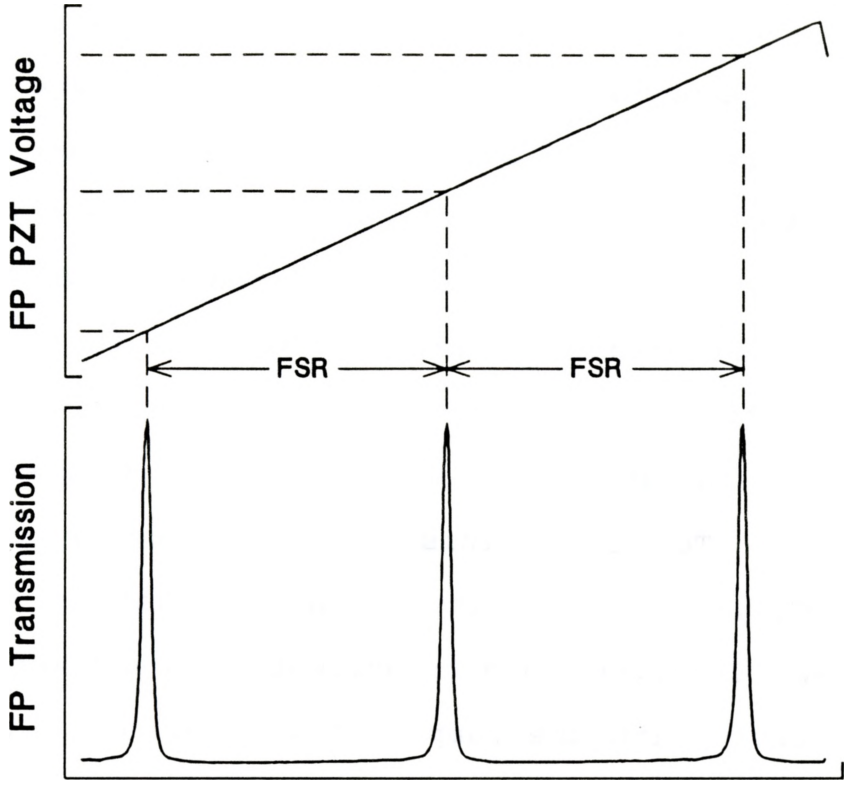

Figure 3.7 Fabry-Perot PZT voltage to frequency calibration

Hz was found to be 1.14 ± 0.03 times higher than at low frequency. This was taken into account in calibrating the measured slope. The frequency response of piezoelectric transducers was relatively complex due primarily to mechanical resonances. The choice of 500 Hz as dither frequency avoided resonances which occured at frequencies 1.1 kHz and higher. Modulation frequencies lower than 500 Hz required longer lock-in amplifier time constants and were more prone to line frequency interference and 1/f noise. Low modulation frequencies also caused more feedthrough of modulation in the Fabry-Perot lock circuit.

The following systematic errors were identified and quantified:

i) Offset of the FPI cavity length scale

ii) Nonlinearity in the spectrum analyzer

iii) Filter switching bandwidth in the spectrum analyzer

The uncertainty in reading the Fabry-Perot cavity length scale was approximately ± 0.05 mm. There was an offset in the cavity length scale which became obvious at small mirror spacings. The length of the Fabry-Perot cavity was calibrated using the longitudinal modes of a laser as spectral lines with a known frequency spacing. Using the monochromator, the laser mode spacing was measured over several modes. The Fabry-Perot was set to a cavity length with a free spectral range less than the free spectral range of the laser. The free spectral range of the laser is given by (2.1). By comparison of the separation of interferometer modes with the separation of laser modes, the free spectral range of the Fabry-Perot was determined. The length of the Fabry-Perot cavity was then determined from (2.1) with n_g = 1.0. The difference between this and the scale reading gave the length offset. Accuracy was improved by averaging measurements over all the modes used to determine mode spacing. In this fashion the length offset was determined to be 1.36 ± 0.04 mm.

The spectrum analyzer was calibrated according to the procedure outlined in its manual. Calibration assured that a full-scale signal was accurate to ± 1 dB. Signals less than full-scale suffer additional error due to nonlinearity in the post-mixer amplifier. The maximum nonlinearity was specified as ± 3% of full scale. Assuming signal levels of about 1/3 full scale, a signal level typically encountered during FM noise measurements, a 3% of full scale error implies a relative error of 9% in the spectrum analyzer display. The FM noise is proportional to the square of the spectrum analyzer signal, so the corresponding relative error in FM noise is 18%, an unacceptably high error.

The nonlinearity error was particularly troublesome because it impacted reproducibility. Measurements of a fixed laser noise level made under nonidentical conditions, e.g. different reference levels at the spectrum analyzer, caused the measured noise level to differ due to the nonlinearity error. This relative error in measurements was more detrimental than absolute calibration errors. The nonlinearity was measured and a correction was applied to the data. The nonlinearity was characterized by applying a 2 MHz electrical signal from an oscillator. The spectrum analyzer signal was compared with the amplitude measured with an oscilloscope. A cubic polynomial was fit to the linearity deviation and was used to correct spectrum analyzer raw data.

The residual nonlinearity error in the FM noise was estimated to be about 3%, due mainly to the error in the oscilloscope measurement. The correction was proven effective by comparing measurements of a fixed level noise signal at different spectrum analyzer reference levels. Data corrected for nonlinearity was insensitive to reference level changes, whereas uncorrected data was not.

The absolute signal level of FM noise was proportional to the spectrum analyzer filter bandwidth. To normalize FM noise to unit bandwidth, knowledge of the true filter bandwidth was required. The error in filter bandwidth in the spectrum analyzer was specified as ± 20%. Actual filter bandwidth was determined by measuring the relative change in a fixed noise level as the filter bandwidth was changed. The measured filter bandwidths rather than the nominal values were used for normalizing the spectrum. This procedure yielded consistent measurements independent of the filter bandwidth.

3.5 Observed Optical Feedback Effects

As discussed in Chapter 2, the frequency noise of semiconductor lasers is particularly sensitive to optical feedback. For accurate measurement of the inherent FM noise of the laser, unintentional feedback must be reduced to a very low level.

Free space optics has advantages over optical fibre in minimizing feedback effects. Optical fibres exhibit reflection from cleaved ends, and although these reflectivity may be relatively small, the long delay time associated with fibre lengths of about 1 km typical of a delay type linewidth measurement system can result in strong feedback effects. Even Rayleigh backscatter from optical fibres can have a large effect on laser linewidth **[28, p284]**.

Feedback from most planar optic surfaces was reduced to negligible levels by a tilt misalignment relative to the optical axis. Unfortunately it was impossible to tilt the Fabry-Perot interferometer enough to eliminate feedback effects without losing a great amount of FM detection sensitivity. Increasing tilt in the interferometer resulted in reduced finesse and throughput, giving transmission fringes with poor frequency discrimination. Feedback effects were instead supressed by a slight tilt misalignment of the interferometer in conjunction with the use of optical isolation components.

The simplest form of optical isolation component is an attenuator, or neutral density filter. Light reflected from any point after the attenuator must complete two passes of the attenuator before being coupled into the laser. An attenuator is convenient to use because it is alignment and wavelength insensitive. The major drawback is that the transmitted light

suffers attenuation as well.

The OFR IR-1 optical isolator was a Faraday rotator with input and output polarizers. The input polarizer was oriented to pass the plane-polarized laser beam, while the output polarizer was at an angle of about 45° relative to the input polarizer. The polarization of light propagating through the isolator in the forward direction was rotated approximately 45° and passed by the output polarizer. On return the reflected light was rotated another 45° and arrived perpendicular to the input polarizer, and was strongly attenuated. Isolation was specified at -46 dB at the design wavelength of 1.3 μm. Use at other wavelengths was possible by rotating the output polarizer slightly. In this case the one-pass rotation was no longer 45°, but the polarizers could still be arranged to have reflected light extinguished by the first polarizer with only a small decrease in throughput. Use outside the specified wavelength range also resulted in increased back reflections from the coated optic surfaces which were designed for 1.3 μm wavelength. This problem was counteracted by tilting the isolator slightly and by using an attenuator as shown in Figure 3.1. In theory it is possible to increase isolation by using several isolators in tandem. In practice, reflections from the isolator first surface become the limiting factor.

Quarter wave plates may also be used as optical

isolation components. Two passes through a properly oriented quarter wave plate rotates the polarization direction by 90° **[51, p249]**. In the experimental setup, the output polarizer of the optical isolator acted as an input isolator for the quarter wave plate and extinguished reflections from the Fabry-Perot interferometer. The quarter wave plate was placed after the two mirrors M1, M2 so the polarization effects of non-normal metallic reflection were minimized. The isolation provided by quarter wave plates is typically 30 dB or less depending on the configuration. There is no advantage to using several quarter wave plates in series.

The quarter wave plate shown in Figure 3.1 was a section of 1/4" thick acrylic with stress induced birefringence. The stress was applied by compressing the acrylic in its holder. Applied stress was perpendicular to the optical axis. Tuning for quarter wave retardation at different wavelengths was achieved by varying the amount of stress. As used, the quarter wave plate was zero order†. Zero order quarter wave plates are less sensitive to wavelength and temperature variation than similar multiple order plates.

Large amounts of optical feedback from the Fabry Perot

---

† Zero order quarter wave plates have a retardation of $\pi/4$, while multiple order plates exhibit retardation of $(m+1/4)\pi$, where m is an integer.

were easily identified by examination of the transmission fringes of a laser mode while the interferometer was in scanning mode. With large feedback, the laser frequency alternately locked to different longitudinal modes of the complex external cavity formed by the laser and the interferometer. This occurred in a chaotic fashion and resulted in a complex fringe shape. An example is given in Figure 3.8. Curve A was obtained with the interferometer aligned almost on-axis and the isolation components removed, while Curve B shows the smoother, more reproducible fringe shape resulting when the optical isolator was added.

At moderate feedback levels the Fabry Perot fringes appeared smooth as with Figure 3.8 Curve B, but examination of the frequency noise spectrum revealed peaks at frequencies f given by

$$f = m\frac{c}{2L_o} \quad ; \quad m = 1, 2, \ldots \qquad \textbf{(3.15)}$$

i.e, multiples of the frequency corresponding to the round trip time in the external cavity. L_o is the length of the external cavity, and c is the speed of light in air.

Examples of laser frequency noise with feedback level as parameter are given in Figure 3.9. In this case the feedback was from the front surface of an optical isolator

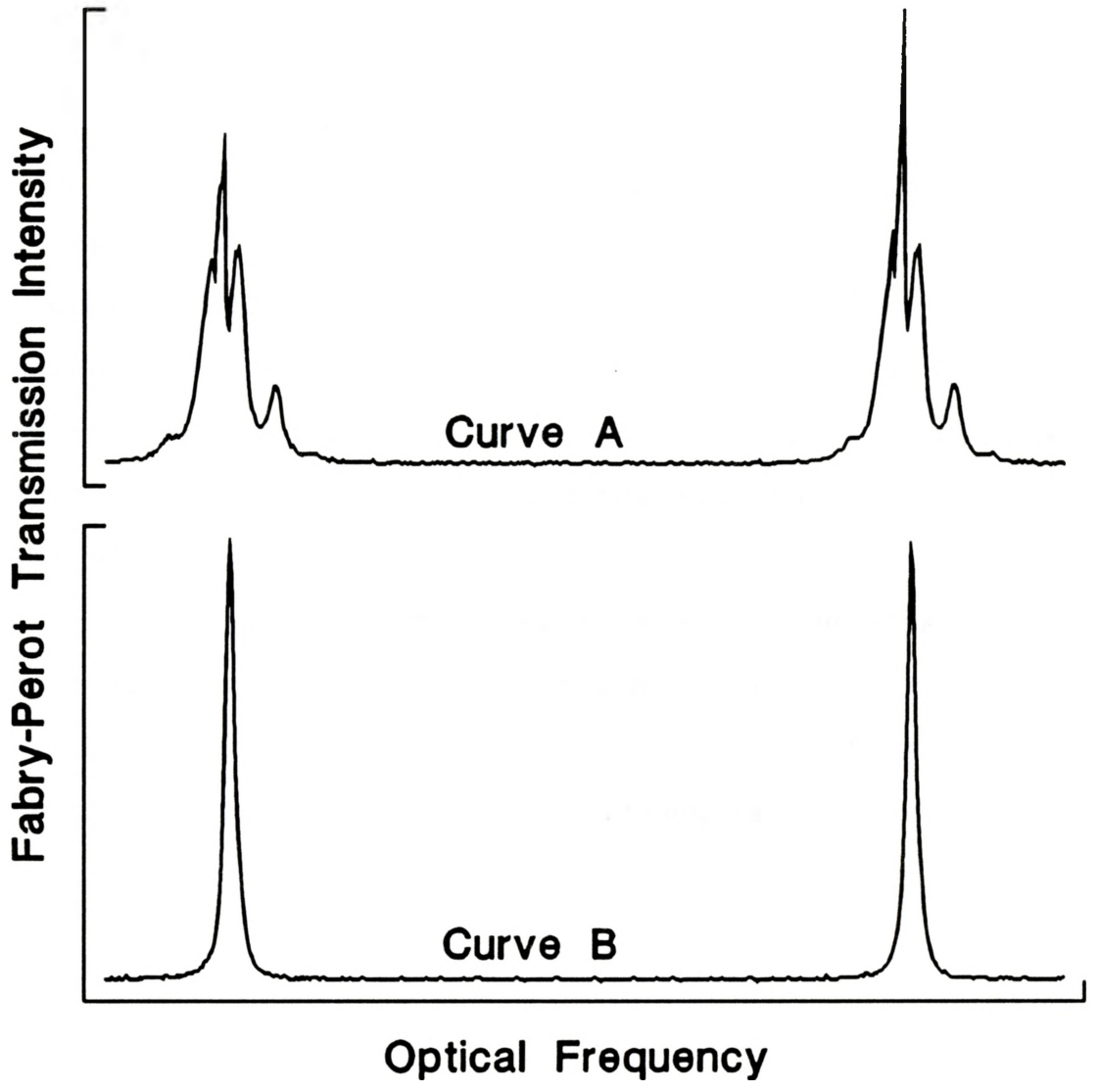

Figure 3.8 Fabry-Perot Fringes : Curve A - Large Feedback Curve B - Moderate Feedback

located 160 cm from the laser, which gave a characteristic external cavity frequency of 94 MHz. The level of feedback was controlled by tilting the isolator and adding attenuators. The absolute value of feedback was not determined. Relatively large feedback levels resulted in sharp noise peaks which

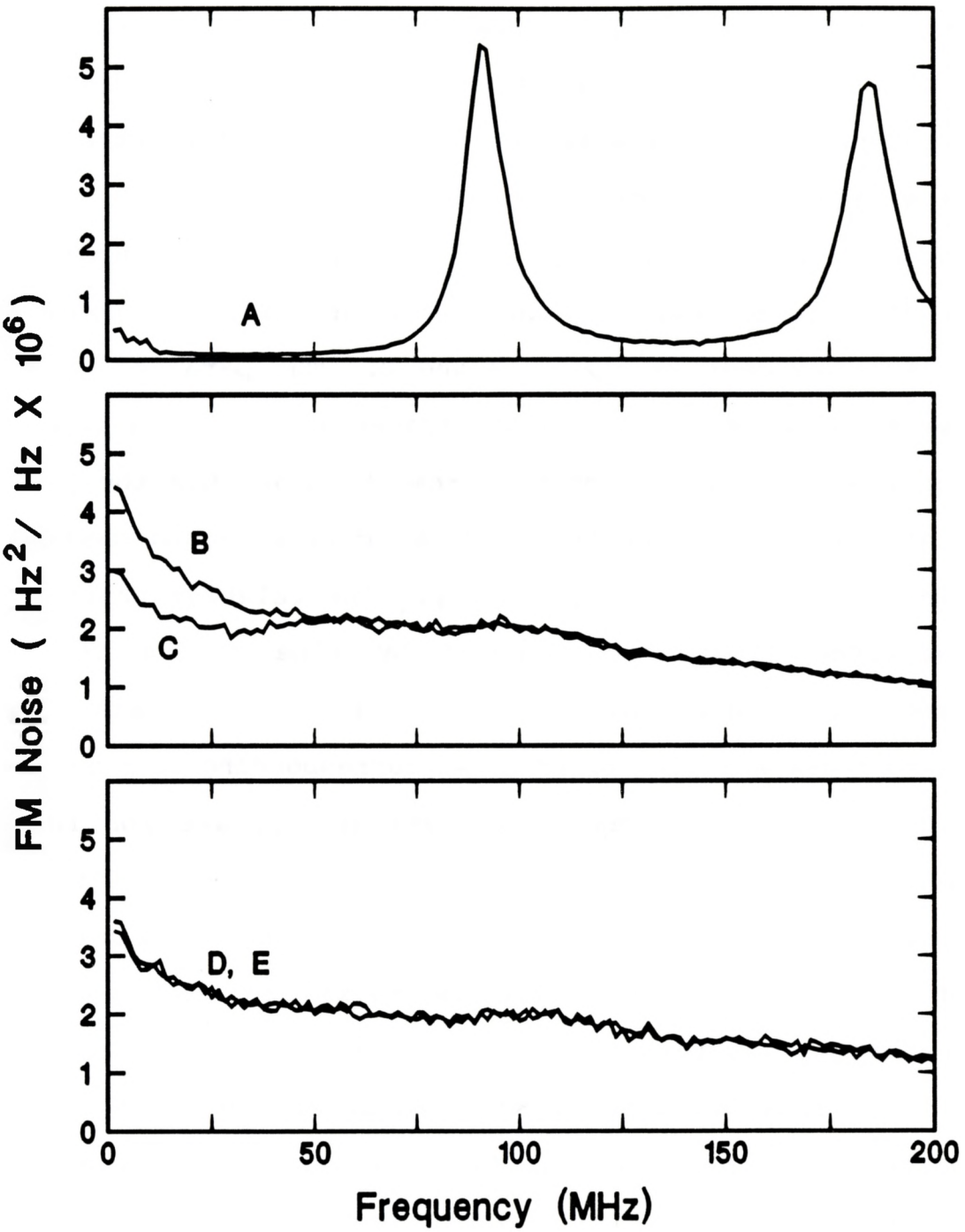

Figure 3.9 FM Noise spectra at different levels of optical feedback

appeared at the external cavity frequency (3.10) and low noise at other frequencies, as shown by Curve A in Figure 3.9.

Since linewidth is determined primarily by the low frequency part of the spectrum, this curve demonstrates that significant linewidth narrowing was occurring. As the feedback level decreased, the noise peak became broader and moved to lower frequency until it became difficult to discern. This is evident in Curves B and C. The parasitic external cavity effects were still significantly affecting linewidth. Curve B and C represent measurements made when the phase of light reflected from the external cavity caused maximum and minimum linewidth, respectively. The relative phase of the reflected light was adjusted by fine tuning the laser frequency with a minor adjustment of the SXC length. Curves D and E are examples of FM noise corresponding to B and C, but with feedback reduced to a level appropriate for FM noise measurements. Here the FM noise spectrum exhibited no apparent feedback effects, as demonstrated by the coincidence of curves D and E. The FM noise obtained under such conditions was taken to be that of the solitary laser.

This characteristic response of the shape of the FM noise spectrum to optical feedback was used to compare the feedback reduction for several isolation components. The Fabry-Perot was used as the external reflector, aligned to give maximum feedback. The isolation components were

introduced in the optical path between the laser and the interferometer.

Two commercial Faraday rotator optical isolators and the acrylic quarter wave plate were tested individually and with attenuators. Comparison of noise spectra was made with a benchmark series obtained using only attenuators. The isolation provided by the three components could be estimated using this comparison since the isolation of the attenuators was known. Table 3.1 shows the results. The relatively large uncertainty originates with changes in Fabry-Perot alignment between measurements.

TABLE 3.1 - Estimated Isolation

Component	Vendor	Part #	Isolation
Isolator 1	Newport	ISO-1315	40 - 45 dB
Isolator 2	Optikon	OFR IR-1	40 - 45 dB
Quarter Wave Plate	-	-	20 - 25 dB

It should be noted that the quarter wave plate was tested without the benefit of a polarizer. In this case the transverse electric (TE) output field of the laser returned to the laser as a transverse magnetic (TM) field rather than being extinguished. It is not certain what effect reinjected

light of this polarization had on the laser, but it is reasonable to expect that the isolation provided by the quarter wave plate would be improved by the addition of a polarizer. As used for FM noise measurement, the quarter wave plate utilized the output polarizer the optical isolator.

The insertion loss for the optical isolators was less than 1 dB at 1.3 μm and 1.4 μm wavelength. At 1.3 μm the quarter waveplate was also caused less than 1 dB attenuation. At 1.4 μm, the insertion loss of the quarter wave plate was $\approx$ 3 dB due to absorption in the acrylic.

An interesting effect was discovered when the quarter wave plate was tested. The frequency noise spectrum exhibited twice as many noise peaks as expected from the external cavity length, as shown in Figure 3.10. The data were obtained with the quarter wave plate and a 7 dB attenuator, but no polarizors. This spectral signature indicated an effective cavity length of twice the actual external cavity length. This can be explained by comparing the polarization of reinjected light under single pass and double pass conditions in the external cavity. Light which made a single pass in the external cavity was primarily TM and coupled weakly to the laser mode. Light which completed a double round trip was rotated from TE to TM and back to TE and hence coupled strongly to the laser mode. Of course, the attenuation incurred in a double round trip was larger than with a single

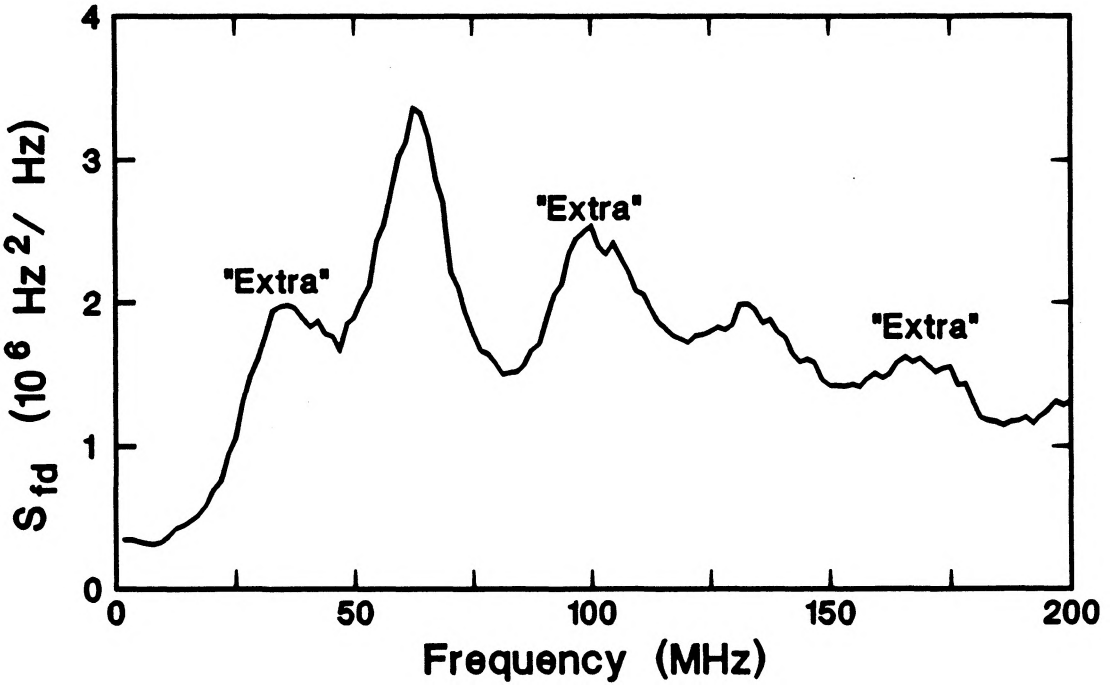

Figure 3.10 FM Noise spectrum with quarter wave plate, illustrating "Extra" peaks indicative of two passes in the external cavity

round trip. This demonstrated that the stressed acrylic was truly effective as a quarter wave plate.

For feedback originating less than about 50 cm from the laser, the peak in the frequency noise could not be observed directly since the spectrum analyzer bandwidth was 350 MHz. In this case the feedback was identified by ramping the laser frequency using temperature or current control of the laser. Feedback was manifest as an oscillating FM noise level versus laser frequency.

The collimating lens L1 of Figure 3.1 was a critical component since it was located in front of the isolation

components. Tests of different lenses were carried out to determine the best lens configuration to minimize first-optic feedback. The laser frequency was ramped by increasing the bias current. Figure 3.11 presents the results of these measurements, where the integrated FM noise is plotted against relative laser frequency. Curve A shows the large undulations in the frequency noise resulting when the KPX079 plano-convex lens was used with the planar side facing the laser. The period of the undulations corresponds to the free spectral range of a 3.5 cm external cavity, in agreement with the measured 3.6 cm external cavity length from the laser to the lens. The feedback was not decreased significantly even with a lens tilt of $\approx 10^{o}$.

Curve B demostrates that the KPX079 lens with the convex surface toward the laser exhibited much smaller feedback effects. Unfortunately this configuration suffered from severe spherical aberration which resulted in reduced sharpness of inteferometer fringes and poor optical power coupling to the detector. A better solution was found with lens 06GLC003, a commercial multielement laser diode collimator. Curve C indicates that it contributed negligible feedback. The working distance was approximately one fifth that of KPX079 which helped to reduce feedback effects. This lens also had the best imaging properties, and was used in all subsequent measurements. Both lenses were antireflection

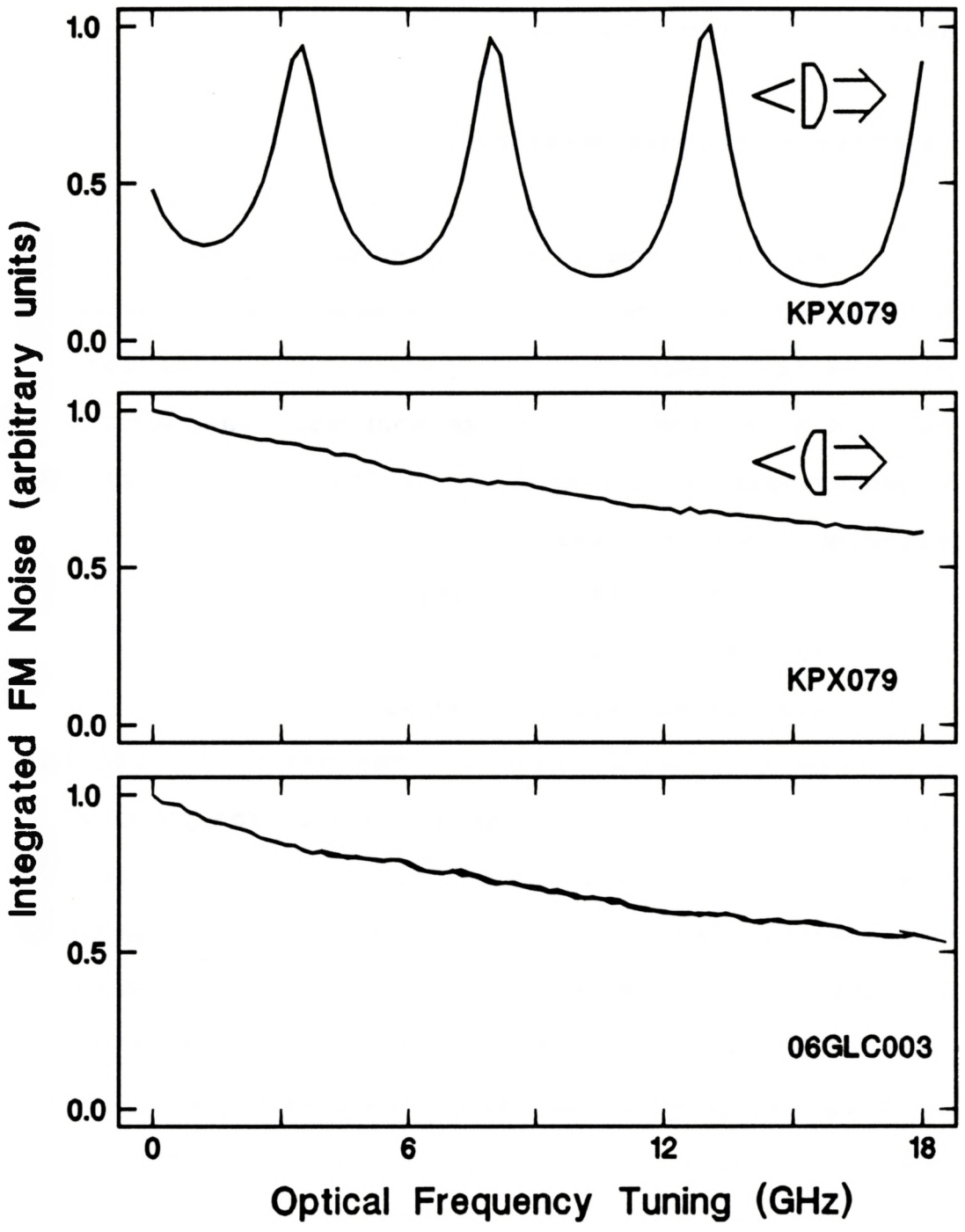

Figure 3.11 Feedback effects from different lenses. Large undulations in FM noise indicate large feedback effects.

coated for use at 1.3 μm, which was the wavelength of the laser used in these tests.

3.6 Effects Of Other Noise Sources

Any measurement is limited to some extent by noise. This is certainly the case for the measurements conducted for this thesis, since it is difficult to distinguish between laser FM noise and other noise sources. The sensitivity of frequency noise measurement was limited by the presence of the following types of noise:

i) dark detector noise

ii) shot noise

iii) laser amplitude noise

Dark detector noise was the baseline noise measured with no light incident on the detector. The physical origin lies in the thermal noise of the amplifiers and in photodetector dark current shot noise. In practice the former was dominant. This noise was strictly uncorrelated with other types of noise. The dark detector noise was subtracted from the total measured noise, since the power spectrum of summed independent noise signals equals the sum of the individual power spectra. In this way dark detector noise could be treated like a baseline level.

Shot noise is a direct consequence of the granular

nature of photons and electrons. Photocurrent generation occurs as a series of impulses rather than as a continuous process. Shot noise becomes dominant in the limit of low signal levels. The photocurrent shot noise can be related to the DC photocurrent by **[52]**

$$C_{rms} = \sqrt{2\,e\,C_{DC}\,B} \qquad \textbf{(3.16)}$$

where C_{rms} is the noise current in bandwidth B, C_{DC} is the DC photocurrent, and e is the elementary electronic charge. The minimum DC optical signal at the photodetector typical operation was approximately 5 μW. This corresponded to a shot noise level of about -90 dBm in a 1 MHz bandwidth at the spectrum analyzer. The baseline noise discussed above was about -65 dBm and hence shot noise was neglible.

Consideration of laser amplitude noise is more complicated. The slope FM discrimination described by Figure 3.3 is referred to as unbalanced FM detection, so termed because it is also sensitive to amplitude modulation. The level of AM noise in the measured noise spectrum may be estimated if the approximate amplitude noise level in the laser beam is known.

Amplitude noise in semiconductor lasers is largely suppressed by gain compensation, a point briefly discussed in Chapter 2. The gain feedback mechanism is effective in maintaining the total laser intensity near its steady state

value. A laser with non-negligible side modes has larger intensity noise of individual modes than for the total output. This occurs because the modal intensities are negatively correlated; a temporary increase in the intensity of one mode causes a decrease in other modes and vice versa. The phenomenon is termed mode partition noise and is discussed in much greater detail in **[28, Ch 7]**. Use of the interferometer in FM noise measurements effectively filters out the side modes of the laser, so the mode partition noise can be significant.

Nearly single mode lasers such as SXC lasers have mode partition noise which is strongly dependent on the side mode intensity. Measurements of mode partition noise in a 1.3 μm gain-guided laser with a planar-mirror SXC were conducted by placing photodetector 1 at the output slit of the monochromator. The SXC length was adjusted to vary the side mode suppression ratio (SMSR) and the relative intensity noise (RIN) spectrum at each value was obtained by Fourier decomposing the detector output with the spectrum analyzer. The RIN is defined as **[53]**

$$RIN = \frac{S_I(f)}{I^2} \qquad \textbf{(3.17)}$$

where $S_I(f)$ is the intensity noise spectral density and I is the average intensity.

Some results are shown in Figure 3.12. For these

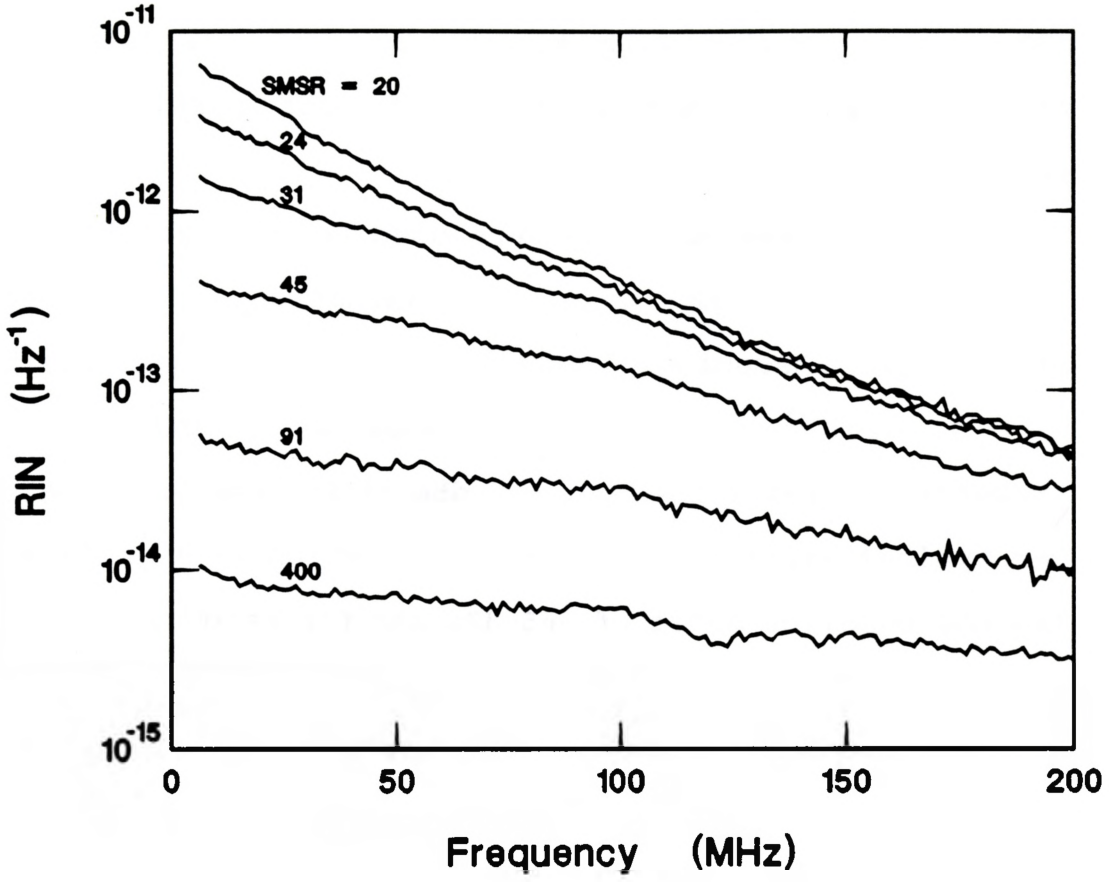

Figure 3.12 RIN noise in a gain-guided SXC laser at different side mode intensities.

particular measurements the dominant side mode was on the long wavelength side and adjacent to the main mode. The mode partition noise was generally slightly lower when the dominant side mode was on the short wavelength side.

The RIN level rose dramatically with increasing side mode intensity, with the low frequency portion of the spectrum increasing more rapidly than the high frequency part. This fact was used to identify amplitude noise contamination in

subsequent FM noise measurements. Significant side modes (SMSR < 100) coupled with excess noise at low frequencies generally indicated the presence of mode partition noise effects.

The RIN measurements were used to estimate the order of magnitude of AM noise contamination in FM noise measurements. Assuming a SMSR ≈ 100 gave an upper limit of RIN = 1×10^{-13}. With laser power of 5 mW/facet this represented a signal of about -75 dBm at the spectrum analyzer under typical experimental conditions, which is significantly below the baseline noise of -65 dBm and far below a typical FM noise level of > -55 dBm. Direct amplitude noise measurement was determined to be negligible for SMSR > 100. It should be realized that by a similar analysis the contaminant amplitude noise would roughly equal the FM noise level at SMSR ≈ 20.

Even if mode partition noise does not get measured, it can have an impact on the frequency noise measurement by affecting the FM noise in the laser. Measurements of linewidth and FM noise of a SXC laser has demonstrated a strong dependence on SMSR **[23]**. The mode partition noise appears to couple to the frequency noise, since the side mode induced frequency noise has the same spectral shape as the mode partition noise. The enhanced frequency noise occurs for SMSR < 100 in a Fabry-Perot type laser **[23]**. The FM noise dependence on side modes was generally avoided by ensuring

that measurements were taken with SMSR > 100.

3.7 Summary

In this chapter, the experimental technique developed to obtain FM noise spectra of SXC semiconductor lasers has been outlined. The apparatus has been reviewed, with particular attention paid to analyzing the frequency response of the Fabry-Perot interferometer when used as an FM demodulator. The compromise between high sensitivity of FM to AM conversion and large bandwidth was studied theoretically and experimentally. An appropriate configuration for obtaining flat response over a 200 MHz bandwidth was given.

The calibrations and corrections required to give absolute FM noise spectra have been described. The absolute accuracy of the calibration was about ± 30%, with the error largely due to the 1 dB accuracy of the spectrum analyzer calibration. The absolute accuracy doesn't affect comparison of measurements which have been made on the same instrument. Since measurements were be made primarily to compare and contrast different lasers, the relatively large absolute error is not considered important. Relative errors were reduced by correcting for nonlinearity and filter bandwidth switching errors occuring in the spectrum analyzer. Estimation of relative error magnitude is deferred to Chapter 4.

A comprehensive survey of optical feedback effects was given. It was shown that feedback could be reduced to a suitable level to allow meaningful measurements to be made. The optical feedback isolation of two commercial optical isolators and a quarter wave plate was estimated. The optical isolators were within specification, while the crudely constructed quarter wave plate proved surprisingly effective. Three lens configurations were tested for feedback effects. A commercial multielement laser diode collimator excelled, giving good imaging quality while avoiding optical feedback.

Effects of noise other than FM laser noise on the measurement were considered. The thermal noise of the first amplifier was shown to give a baseline which could be subtracted from the signal, but which affected the ultimate sensitivity of the instrument. Mode partition noise was found to be significant for side mode intensity greater than about one percent of the main mode intensity. It could be evident in two ways: directly, due to lack of AM discrimination inherent in the measurement technique, and indirectly, from coupling of mode partition noise into FM noise.

These investigations validate the use of a Fabry-Perot interferometer FM demodulator for measuring laser FM noise, and help define the limitations of the instrument. Results of such FM noise measurements are presented in the following chapter.

CHAPTER 4 FM NOISE AND LINEWIDTH MEASUREMENTS

4.1 Introduction

This chapter presents results of FM noise measurements on SXC semiconductor diode lasers. Examples of frequency noise spectra are given in Section 4.2, and the conversion to equivalent linewidth is demonstrated. Measurements of linewidth as a function of optical power are examined in Section 4.3. The dependence of linewidth on the mode selected by the SXC is investigated in Section 4.4. Section 4.5 provides a summary of the important points of this chapter.

4.2 FM Noise Spectra and Equivalent Linewidth

FM noise spectra of 3 index-guided bulk lasers and 9 quantum well lasers have been measured using the experimental technique described in Chapter 3. Direct comparison of individual FM noise spectra is somewhat cumbersome. An attempt to plot a family of FM noise spectra against another parameter, e.g. laser output or mode number, would result in a cluttered representation that is difficult to interpret. It is thus worth finding another form of data representation.

The FM noise spectrum shape was found to be generally invariant versus optical power for a given laser. The only notable exceptions occurred when side modes were contributing significantly to the noise spectrum. Comparison of the FM noise spectrum shape of different lasers demonstrated no significant differences.

Considering the constancy of spectral shape of the FM noise, it is worth exploiting the relationship between frequency noise and linewidth (2.16) to convert the data to equivalent linewidths. This has been done for the bulk of the data presented in this chapter. The linewidth representation has an additional benefit in that it is more readily compared to results published by others.

Figure 4.1 contains examples of FM noise spectra for 1651-5, a 250 μm PBH[†] bulk laser, with a planar mirror SXC. The shape of these curves is representative of all lasers measured, i.e., predominantly white, with enhanced noise below about 25 MHz. The extra noise at low frequency was ascribed to thermal enhancement as qualitatively described in Chapter 2. This conclusion was supported by the fact that it scaled inversely with optical power and did not have a 1/f shape. The FM noise spectrum obviously decreased with increasing optical power, but it is not immediately apparent from the

---

[†] Planar Buried Heterostructure

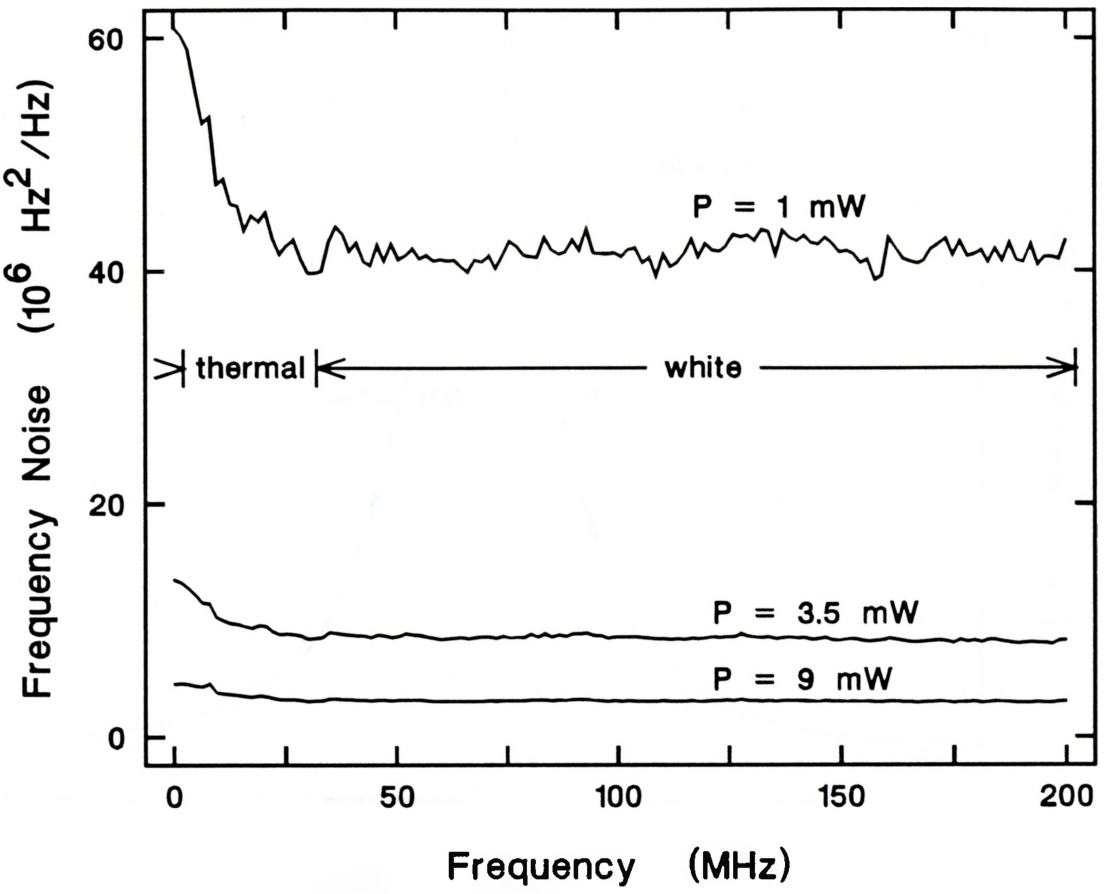

Figure 4.1 FM Noise of PBH laser 1651-5 with a planar SXC measured at three optical power levels

figure whether or not an inverse relationship was strictly obeyed. This will become clearer with the linewidth representation in Section 4.3.

The normalized spectral density of the electric field will be referred to as field spectral density or line shape. The line shape calculated from the P = 3.5 mW curve of Figure 4.1 is given in Figure 4.2. The solid line shows the calculated field spectral density, while the dashed line is a

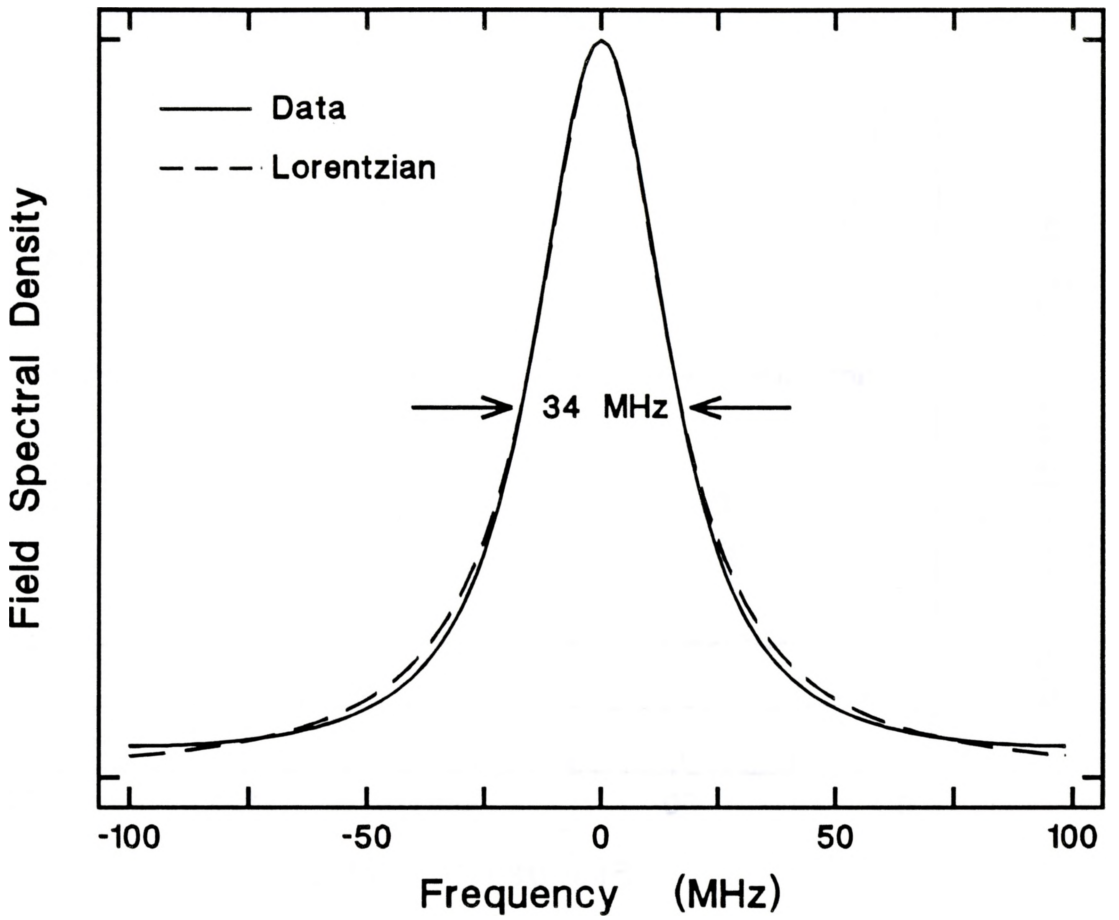

Figure 4.2 Solid curve - calculated line shape using FM noise data at P=3.5mW of Figure 4.1, Broken curve - Lorentzian with same FWHM as the solid curve.

Lorentzian curve having the same 34 MHz linewidth. Obviously the lineshape calculated from the measured FM noise was well described by the Lorentzian shape. This was true for each laser. The only exceptions occurred when side modes were large; side mode enhanced noise gave calculated line shapes with a tendency to look more Gaussian in nature. This was one method of identifying side mode influence.

A data acquisition computer program calculated the linewidth from the FM noise data using numerical integration and a Fast Fourier Transform (FFT) algorithm on a 128 point grid. The frequency span of the FFT was adjusted so the discrete nature of the transform did not affect the results. This could be ensured by verifying that the autocorrelation (which was displayed during the calculation) and field spectral densities were of roughly equivalent width in terms of their respective quantization units. For a 128 point grid, a good rule of thumb was to make the frequency span of the FFT 5 to 10 times the linewidth. The calculated linewidth was recorded along with the full FM noise spectrum for each measurement. In addition, the program also calculated the equivalent linewidth based on the low frequency and high frequency FM noise levels. This facilitated identification of enhanced noise at low frequencies, which usually signalled side mode effects or feedback effects.

4.3 Linewidth Versus Inverse Power

Due to the theoretical inverse relationship between linewidth and output optical power, a plot of measured linewidth versus inverse optical power is expected to be a straight line. The linewidth of a laser is thus conveniently characterized by the slope of this line, which is usually

termed the "linewidth-power product" and measured in units of MHz-mW. With a SXC laser, there is an additional degree of freedom; the linewidth can also be measured at different longitudinal modes of the laser. This section describes measurements of linewidth versus output power on a fixed mode. The variation of linewidth with mode is deferred to Section 4.4.

The previous section described how linewidth was calculated from the measured FM noise spectra. It was also necessary to known the single facet output power at the laser bias current for each measurement.

LI† curves were measured for each laser with a large-area germanium detector placed immediately before the front laser facet. Under computer control, the laser current was ramped by the digital-analog converter, while the laser current and detector voltage were measured using the analog-digital card. The LI measurement was used to determine the single facet output power as a function of laser current, but the situation was complicated by inadvertent measurement of back facet light reflected from the SXC mirror. Reflected light was transmitted both over top of the laser and through the substrate [50]. The amount of reflected light from the SXC was alignment dependent, and so the LI curve with the SXC

---

† Light output versus laser current (I)

could not be used by itself to determine the output power of the laser.

Planar mirror SXC lasers had external reflectivity $\approx 5 \times 10^{-4}$ (Chapter 5). At this level, the threshold reduction and change in differential quantum efficiency due to the increased reflectivity at the back facet are negligible. The small change in threshold was confirmed by measuring LI curves with and without the planar SXC. The threshold reduction was found to be less than 0.2 mA. For all measurements using a planar SXC, the LI curves measured without the SXC were used to determine the single facet output power at a given current level. The output power was corrected for the spontaneous emission in the LI curve measurement, as described below.

With spherical SXC elements the external reflectivity was considerably higher, and threshold reductions as great as 6 mA were obtained. In this case the LI curve without the SXC could not be simply used as it was with a planar mirror SXC. Instead, the LI curves with and without the SXC were measured, giving the threshold reduction. The output power versus current was taken from the LI curve measured without the SXC, with the current offset by the threshold reduction. The change in external differential quantum efficiency due to the SXC was estimated at 6% for a spherical SXC based on an external reflectivity of 1×10^{-2}. Since an attempt was made to make the amount of feedback commensurate for all the spherical

SXC lasers by ensuring the threshold reduction was roughly 2 mA for each laser, the variation in laser power due to underestimated differential quantum efficiency should be less than 6% when comparisons are made between lasers.

The LI curves were also corrected for the spontaneous emission extrapolated to threshold, since the optical power implied in the inverse linewidth-power relationship is the power in the lasing mode. Figure 4.3 shows a typical LI measurement on a 500 μm quantum well laser with and without the spherical mirror. The difference in the slope of the two curves was due to measuring back facet light reflected from the SXC. The inset shows the change in threshold and the spontaneous emission at threshold, given by A and B, respectively.

The purpose of SXC was to obtain single mode operation of the lasers without affecting the linewidth appreciably. For this reason the spherical mirror was not aligned to give maximum feedback, but instead was defocussed slightly while maintaining SMSR > 100. To be consistent, each spherical SXC alignment was such that the threshold reduction was about 2 milliamperes. Linewidth versus optical power was measured at the longest wavelength mode with SMSR > 100 at about 1 mW optical power. The long wavelength side was chosen since the gain peak tunes toward longer wavelength with increasing current.

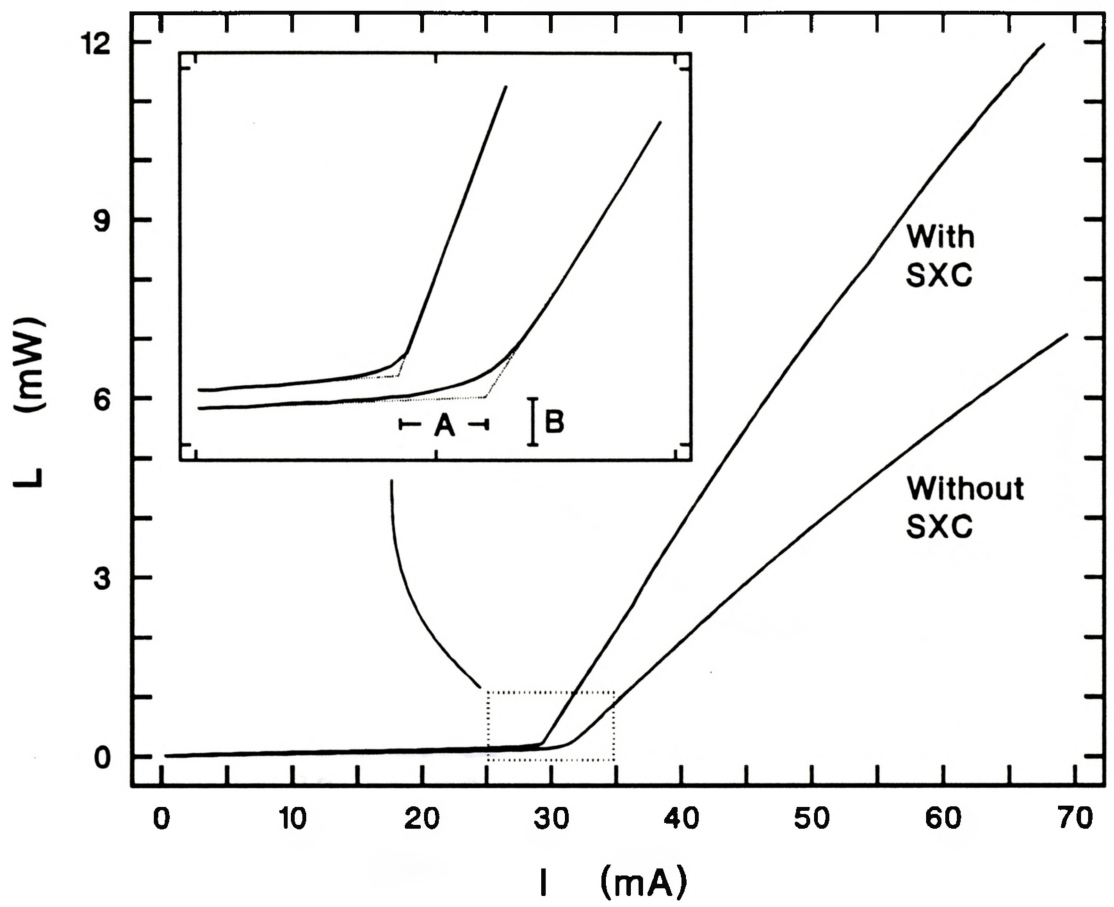

Figure 4.3 LI curves measured with and without a spherical SXC. A = threshold current reduction, B = amount of spontaneous emission.

Linewidth versus inverse optical power for ABC056, an 250 μm ABC† laser, with a planar SXC is shown in Figure 4.4. The data set represented by open circles was taken using an ND 0.6 attenuator, while the open triangles represent data taken one day later using an ND 0.9 attenuator, demonstrating insensitivity to variations in optical power at the detector,

† Arrowhead Buried Crescent

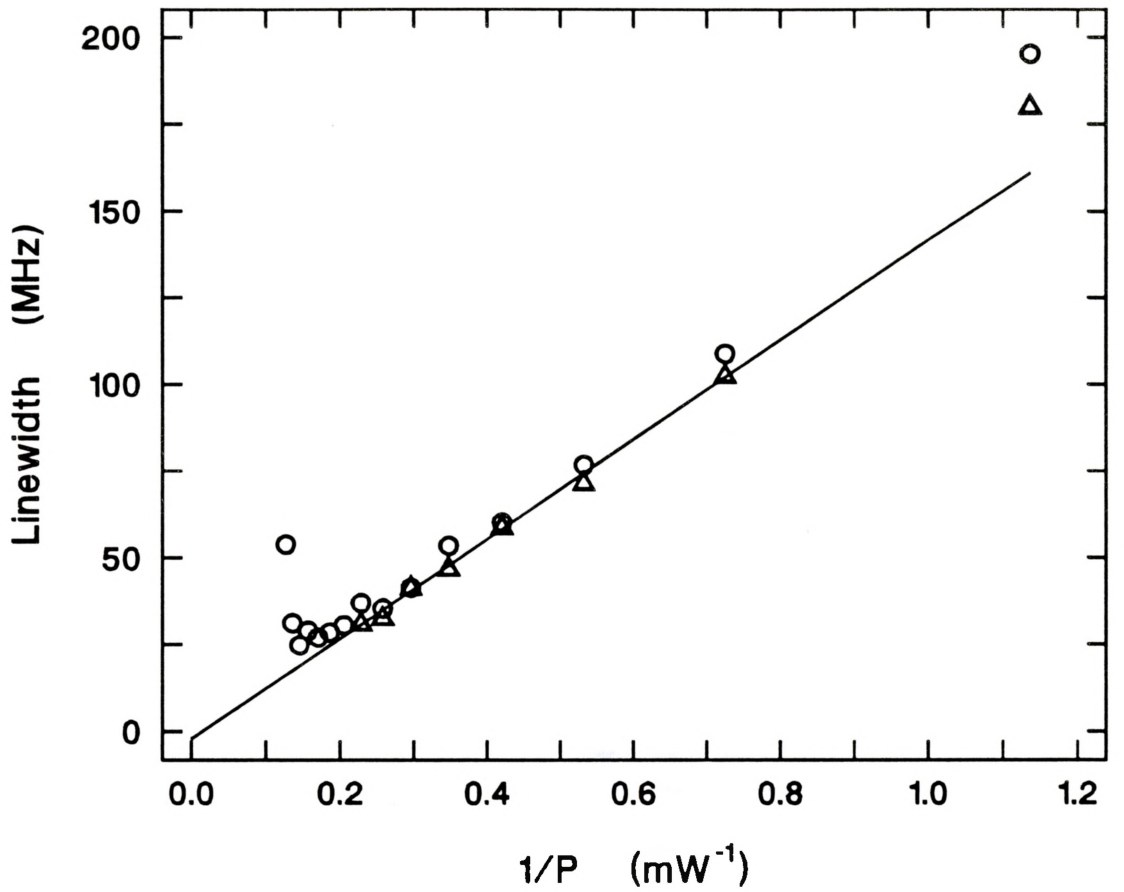

Figure 4.4 Linewidth versus inverse power for 250 μm laser ABC056 with a planar SXC. Line is a fit to the triangle data for 1/P < 1.0.

as well as giving an indication of the measurement reproducibility. For this example, an optical isolator designed for use at 1.5 μm wavelength was used, whereas the laser emission wavelength was 1.3 μm. The scatter in the data was attributed to feedback from the isolator front optic. The increase in linewidth at high power correlated with increased side mode intensity, with the side mode suppression ratio decreasing to 90 at the highest power level. This is an

example of the so-called linewidth-broadening. From this and other data, it was found that the SMSR > 100 rule of thumb did not ensure that side modes would have a negligible effect at high output power. The solid line, which was generated by linear regression analysis of the triangle data for $1/P < 1.0$, represents a linewidth-power product of 144 ± 4 Mhz-mW with an infinite-power intercept of -2 ± 2 MHz . A similar analysis on the open circle data yielded a slope of 149 ± 6 MHz-mW with an intercept of 1 ± 3 MHz. The quoted uncertainties are standard error estimates generated during regression analysis.

Linewidth was measured at a few power levels for a similar laser, ABC052, with a planar SXC. This measurement occurred prior to completion of calibrations described in Chapter 3. Post-calibration correction of this data gave agreement within 15% of the data of Figure 4.4.

Linewidth versus inverse optical power for a 250 μm PBH laser, 1651-5, with a planar SXC is shown in Figure 4.5. The straight linear fit to the data gave a slope of 111 ± 1 MHz-mW with an intercept of 1 ± 0.6 MHz. The small degree of data scatter about the linear fit indicates that feedback effects were small. Note that there was no indication of linewidth floor or rebroadening in this case even with optical power of almost 10 mW. The SMSR was 1500 at the highest power data point. Frequency tuning measurements reported in Chapter 5 indicated that the amount of SXC

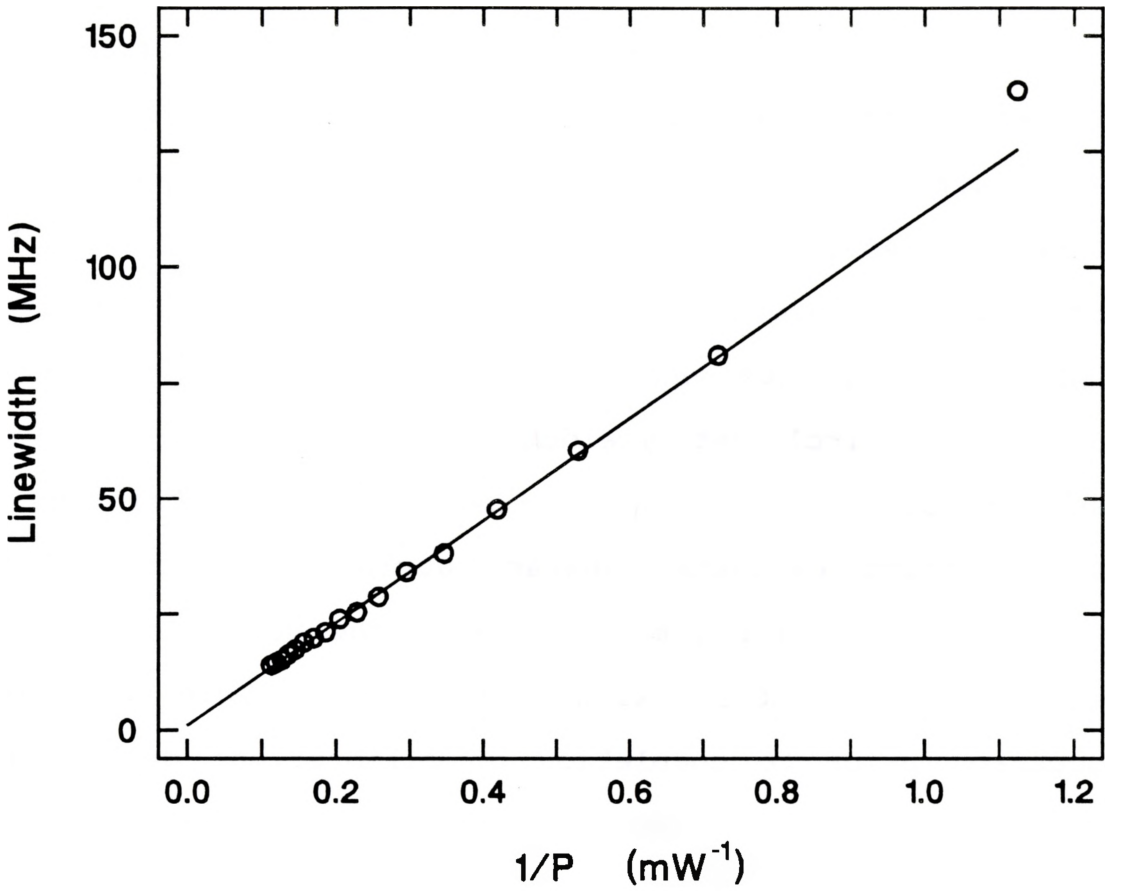

Figure 4.5 Linewidth versus inverse power for 250 μm PBH 1651-5 with a planar SXC. Line is a fit to the data for $1/P < 1.0$.

feedback was relatively high for this laser, which explains the high SMSR.

Figure 4.6 shows linewidth versus inverse power for two 250 μm strained (1.5% compressive) layer quantum well lasers, R1-394-23 and R1-394-26, **[54]** in planar SXC configuration. Measurements are represented by open circles for R1-394-23 and by open triangles for R1-394-26. The straight line represents a fit to the circle data, which

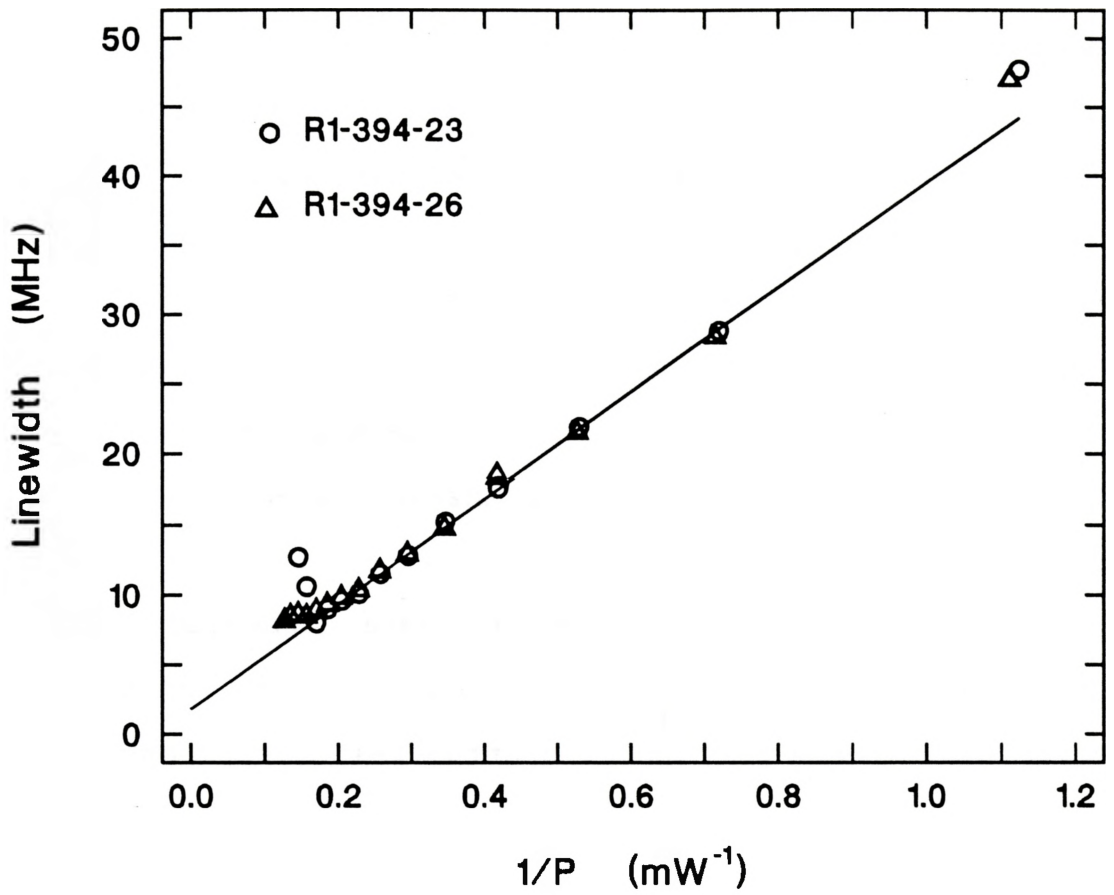

Figure 4.6 Linewidth versus inverse power for two 250 μm 5-quantum well lasers with 1.5% compressive strain. Line is a fit to circle data over the linear region.

yielded a slope of 37.7 ± 0.4 MHz-mW with an intercept of 1.8 ± 0.2 MHz. A similar fit to the triangle data gave a slope of 36.8 ± 0.9 MHz-mW with intercept 2.5 ± 0.4 MHz. From 1 to 5 mW the measurements for the two lasers match closely. Above 5 mW the side mode suppression ratio fell below 150 for the circle data, but was still above 300 for the triangle data. Again it appeared that side mode linewidth broadening effects occurred for SMSR > 100 at high power.

Linewidth versus inverse optical power for three 500 μm strained layer three quantum well lasers is shown in Figure 4.7. Due to the longer laser cavity, use of a spherical SXC was necessary to consistently achieve SMSR > 100. The linewidth-power product for the unstrained laser R1-400-161 was determined to be 28.2 ± 0.6 MHz-mW, with infinite power intercept of 0.7 ± 0.7 MHz. The corresponding results were 21.7 ± 0.4 MHz-mW and 0.5 ± 0.3 MHz for the compressive strain laser R1-399-164 and 20.5 ± 0.2 MHz-mW and -0.8 ± 0.2 MHz for the tensile strain laser R1-397-204.

The large deviation of data observed with the unstrained laser at 1/P between 0.2 and 0.3 mW^{-1} can be readily explained. These particular quantum well lasers operate in a wavelength range containing many strong H_2O absorption lines. Such an absorption line is similar to the Fabry-Perot transmission fringe in that it converts frequency noise to intensity noise when the laser frequency is at a sloping region of the absorption. In the case where the water line slope is in the same direction as the FPI fringe slope, the effective slope is higher than the FPI fringe slope and the experimentally determined linewidth is higher than the actual linewidth. The opposite situation, when the slope of the water line is counter to the Fabry-Perot slope, causes the experimentally determined linewidth to underestimate the actual value. Both of these situations occurred with the

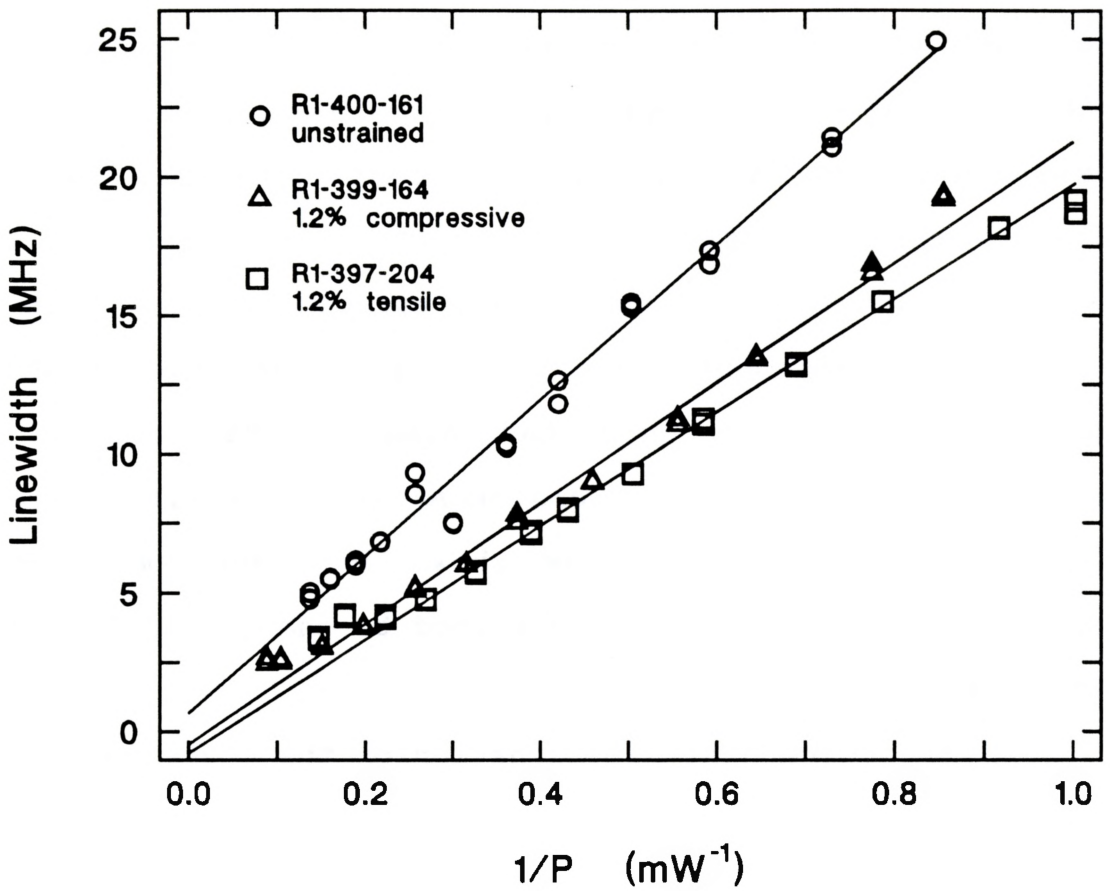

Figure 4.7 Linewidth versus inverse power for three 500 μm 3-quantum well lasers with spherical SXC's. Strain composition of each laser is indicated.

unstrained laser in Figure 4.7.

Another example of this effect is given in the following section. The water absorption lines thus introduce uncertainty in the measured linewidth, but only for lasers emitting near 1.4 μm. Strong absorption lines are easily detected by the large attenuation in the optical throughput, so it is possible to simply avoid making measurements at these wavelengths.

The results given in Figure 4.7 are very interesting in light of a predicted reduction of linewidth enhancement factor by the use of compressively strained layers in quantum well lasers [19] and measurements confirming this for both tensile and compressive strain [39,40]. As shown by (2.19), the linewidth is dependent on many parameters other than the linewidth enhancement factor; in particular, the threshold gain and waveguide loss may also be reduced by the introduction of strain. This means that the difference in linewidth between lasers as shown in Figure 4.7 cannot automatically be completely ascribed to changes in linewidth enhancement factor.

An independent determination of the other parameters in (2.19) for each laser is certainly beyond the scope of this thesis. Even without full knowledge of the other parameters in (2.19), it is believed that α reduction is the dominant strain dependent linewidth reduction mechanism. It is interesting to note that the linewidth versus strain did not follow the same trend as threshold current versus strain.

The linewidth versus inverse power plots indicate the measured linewidth at low optical power invariably falls above the linear fit. The reason for this is not presently known. The theoretical linear linewidth - inverse power relationship only holds "well above" threshold. It may be that this assumption breaks down at optical power of 1 mW and less.

At high optical power, the linewidth was seen to either rebroaden or saturate for most lasers. Rebroadening generally coincided with the onset of increasing side mode intensity. In some cases with the lower linewidth quantum well lasers, the linewidth saturated with no indication of increasing side modes. In these cases, examination of the FM noise spectra indicated a relative increase in the noise at low frequency, which could be due to 1/f noise. Confirmation of 1/f noise would require measurements made on a finer frequency scale.

A summary of linewith, threshold current, and wavelength for each laser measured is given in Table 4.1. The 250 μm lasers had linewidth of about 125 MHz and 37 MHz for the bulk and quantum well devices, respectively. Arbitrarily assuming the difference in linewidth to be entirely due to change in the linewidth enhancement factor, and estimating the bulk linewidth enhancement factor at 6 yields a estimated value from (2.19) of about 3.2 for the quantum well device. These values of α should be compared with estimates of α independently determined from frequency tuning in Chapter 5.

The 500 μm quantum well lasers had even smaller linewidth than the 250 μm quantum well devices. The difference was thought to be due primarily to a longer laser cavity. There were also differences in linewidth between lasers of different strain composition. The unstrained 500 μm

quantum well laser had higher linewidth than both tensile and compressive strain devices. To make another comparison, a linewidth reduction from 28 MHz-mW to 18 MHz-mW due only to change in the linewidth enhancement factor implies a change from an assumed $\alpha = 3$ to $\alpha = 2.3$ according to (2.19). An independent estimate of α for these lasers was not possible due to the failure of the present frequency tuning theory to model the spherical SXC results - see Chapter 5. Hopefully improvements in the frequency tuning analysis will allow such measurements to be made in the future.

TABLE 4.1 - Summary of Linewidth Data				
Laser Type	**Length (μm)**	**Threshold Current (mA)**	**Wavelength (μm)**	**LW-Power Product (MHz-mW)**
ABC052	250	15	1.3	120 ± 20†
ABC056	250	22	1.3	144 ± 4
PBH (1651-5)	250	26	1.3	111 ± 1
5-QW 1.5%(C) R1-394-23	250	20	1.39	37.7 ± 0.4
5-QW 1.5%(C) R1-394-26	250	18	1.39	36.8 ± 0.9
3-QW 0% R1-400-161	500	31.1	1.38	28.2 ± 0.6
3-QW 0% R1-400-162	500	30.0	1.38	28 ± 1
3-QW 1.2%(C) R1-399-164	500	21.8	1.39	21.7 ± 0.4
3-QW 1.2%(T) R1-397-204	500	45.8	1.41	20.5 ± 0.2
3-QW 1.2%(T) R1-397-201	500	43.9	1.41	14.8 ± 0.3††
3-QW 1.3%(T) R1-398-164	500	45.1	1.40	18.0 ± 0.5

† Linewidth estimated by applying calibration data after measurement

†† measured on mode nearer gain peak than others

4.4 Linewidth Variation with Laser Mode

The linewidth variation with output power was described in the previous section. The linewidth-power product resulting from such measurements was found to be useful in drawing comparisons between lasers. These measurements were usually taken on the longest wavelength mode at low optical power which had sufficiently high SMSR. This enabled a given mode to be measured while the gain spectrum tuned toward longer wavelength with increasing current, and also reduced any effects of modal linewidth variation on the comparison by introducing a consistent procedure for making the measurements. In this section, the modal linewidth variation will be isolated by presentation of several measurements of linewidth at different laser modes and at a fixed output power level.

Figure 4.8 displays the measured linewidth versus mode number for a 250 μm laser, ABC052. A planar SXC was used, with SXC length such that 6 laser modes could be selected. The upper graph was taken at 1 mW optical power; the lower was taken at 2 mW. At optical power greater than 3 mW this laser exhibited large side modes. The mode labelling on the horizontal axis is in order of increasing photon energy, or decreasing wavelength, with 0.85 nm wavelength change per mode interval. Note the trend of reduced linewidth at shorter

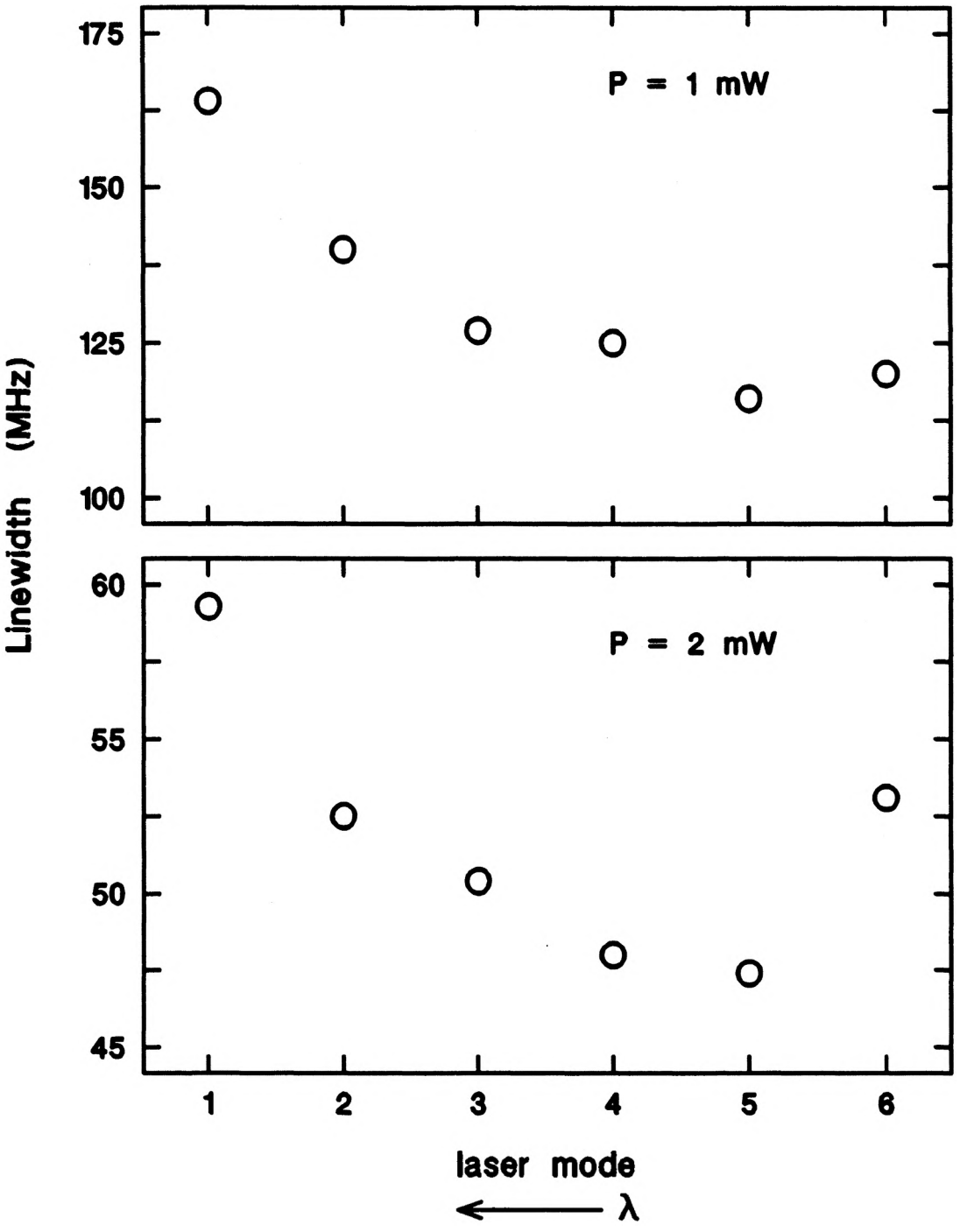

Figure 4.8 Linewidth versus mode at two optical power levels for ABC052 with a planar SXC.

wavelength. This trend was observed in all lasers for which these measurements were made. The maximum linewidth change relative to the first mode was 29% at 1 mW and 20% at 2 mW. The linewidth of the first and sixth modes are thought to have been broadened slightly by side modes.

Results for a ABC056 laser are plotted in Figure 4.9. Again a planar SXC was used, but it was aligned with a slightly shorter external cavity length, giving 7 selectable laser modes. This laser did not exhibit strong side modes on all the modes until optical power was increased above 5 mW. The modal linewidth dependence was taken at 1 mW, 3 mW, and 5 mW. At 5 mW the 7th mode could no longer be obtained, and the 6th mode had SMSR = 100 compared to SMSR ~ 180 for the other modes. At 3 mW the 7th mode had SMSR = 39 while the other modes had SMSR ~ 200. The 7th mode at 3 mW and the 6th mode at 5 mW were thought to be side mode broadened. Neglecting these modes, the relative linewidth change relative to the maximum was 36% at 1mW, 27% at 3 mW, and only 4% at 5mW. This indicates that the modal linewidth was power dependent, and tended to flatten at higher power. It is possible that the mechanism responsible for the increased side modes at high optical power is also responsible for the flattening of the linewidth variation with mode.

A 500 μm, 1.2% tensile strain 5-quantum well laser,

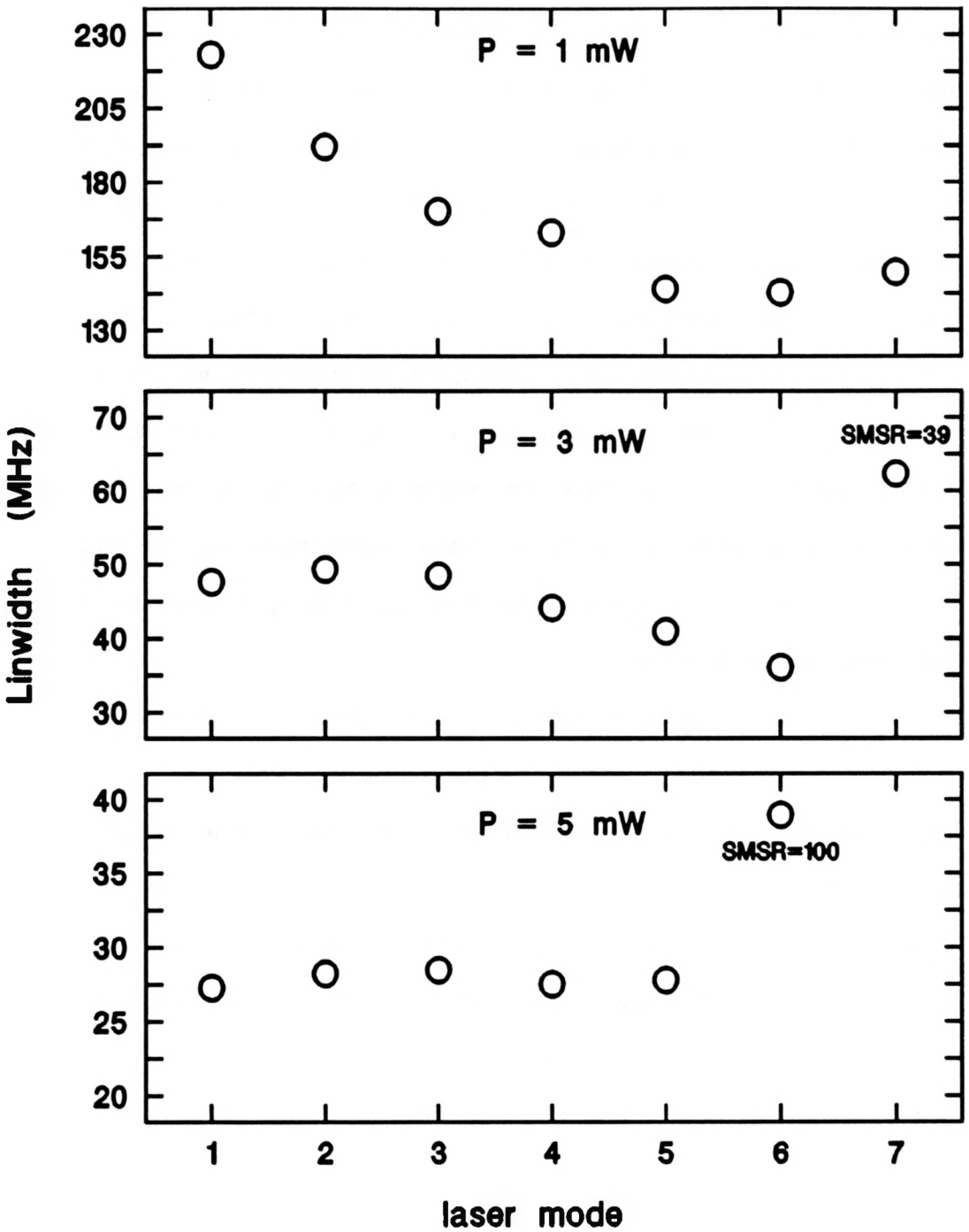

Figure 4.9 Linewidth versus mode at three optical power levels for ABC056 with a planar SXC.

R1-399-164, was also measured. As before, a spherical SXC was required with this type of laser. The cavity length was such that a total of 10 modes were available. Mode hops at either end of the SXC free spectral range tended to be irregular, so only modes near the centre of the gain peak were measured. Adjacent laser modes were successively selected in a regular fashion as the SXC was tuned over these central modes. Figure 4.10 shows the linewidth measured at several modes at optical power of 1 mW and 2.9 mW. For comparison with the previous two figures, it should be recognized that the wavelength interval corresponding to a laser mode spacing in Figure 4.10 is only 0.5 nm in this case due to the greater laser length and longer wavelength.

The variation in linewidth over 6 modes was 42% at 1 mW. Over 8 modes at 2.9 mW the change was 41%. Side modes were several hundred times smaller than the main mode and hence negligible for all measurements. The wavelength of mode 3 at P = 2.9 mW was near the peak of a strong H_2O absorption, which introduced additional error in the measured linewidth as discussed in the previous section.

At present, the origin of the linewidth variation with mode is not known. Identification of the dominant mechanism probably requires other, independent measurements. This falls outside the scope of this thesis, however, it is worth speculating about the candidate mechanisms.

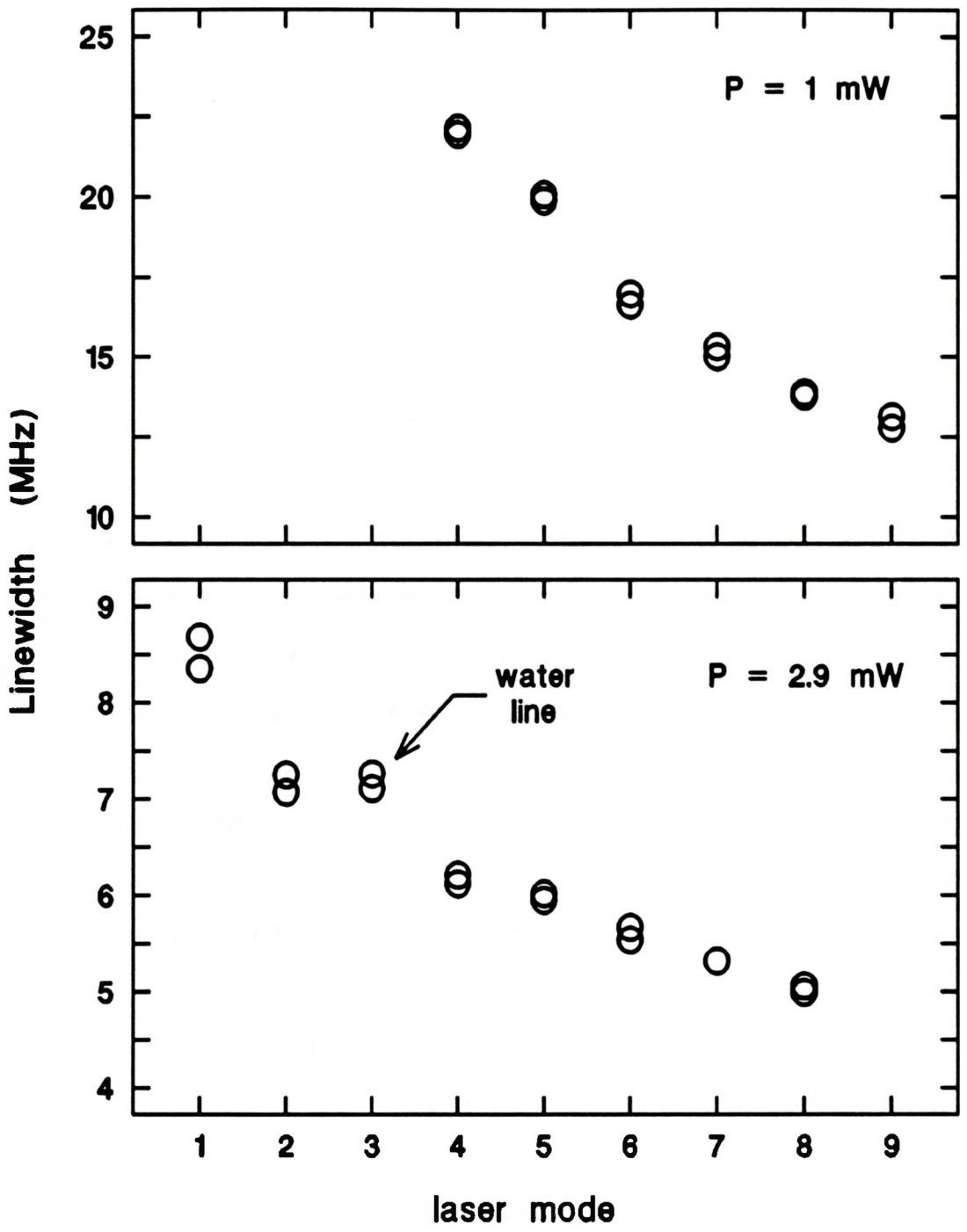

Figure 4.10 Linewidth versus mode at two optical power levels for R1-399-164 with a spherical SXC.

The linewidth enhancement factor is expected to be a function of wavelength. Experimental evidence for this was given in [55], where the dispersion in α was measured for a 1.5 μm wavelength InGaAsP laser. Using the data of [55] to make a rough estimate, the linewidth variation of α with wavelength gives an upper limit of about 10% over 6 modes of a 250 μm laser. This rough estimate is of the right order of magnitude and has the correct wavelength dependence, since α was found to be larger at longer wavelengths.

Another possibility is wavelength dependence of loss. Excluding facet output coupling which is wavelength insensitive, loss is composed of waveguide scattering loss and intervalence band absorption [32]. The scattering loss should vary as λ^{-4} assuming Rayleigh scattering, so it gives the opposite wavelength dependence to that required to explain the measured linewidth variation. The intervalence band absorption was found to increase with wavelength [32] and hence could give increased linewidth with wavelength. The loss disperion can be measured by looking for changes in external differential quantum efficiency. This was done in [44], where the inferred wavelength dependence of loss was found to have the correct behavior.

4.5 Summary

Linewidth measurements using the technique reported in Chapter 3 have been reviewed. The measurements provide the ultimate test of the utility of this approach to measuring linewidth. The inverse power relationship and Lorentzian lineshape predicted by theory were found to hold, confirming that the measurement results were indeed valid linewidth measurements.

The reproducibility was not the same for each laser measured. The limiting factor defeating reproducibility was thought to be residual parasitic feedback from either the front surface of the optical isolator or the collimating lens. Slight differences in alignment or a wavelength change with each new laser would result in a change in the amount of feedback and a concomitant change in the degree of reproducibility attained. In the worst cases, the reproducibility for an individual linewidth measurement was about 10% from day to day, while in the best cases it was less than 2%. Even with the worst case reproducibility in individual measurements, the linewidth-power product determination from linear regression was reproducible within about 5% since it tended to average out the data scatter. Repeat measurements conducted on the 500 μm quantum well devices with spherical SXC's after a complete realignment,

including removal and reinstallation of the SXC, gave linewidth-power products which agreed within 7%.

Linewidths as small as 2.5 MHz have been measured. Lasers with sufficiently narrow linewidth to experimentally determine the ultimate resolution of the present instrument were not available. It is felt that linewidths $\approx$ 200 kHz could easily be measured, and that improvements in optical throughput and a lower noise detector could further reduce the lower limit.

The linewidth measurements demonstrated a distinct reduction in the linewidth of quantum well lasers compared to commensurate length bulk devices. Longer cavity quantum well devices gave still lower linewidth, as expected. Both tensile and compressive strain appeared to reduce the linewidth, with tensile strain giving the lowest linewidth-power product.

Further measurements demonstrated a clear change in linewidth as the laser mode selected by the SXC was varied. Lower wavelength modes exhibited generally lower linewidth for both the planar and spherical SXC configurations. The dominant mechanism has not been isolated, but dispersion of the linewidth enhancement factor and of the waveguide loss have been identified as candidates.

CHAPTER 5 FREQUENCY TUNING MEASUREMENTS

5.1 Introduction

This chapter describes measurements on frequency tuning, which is the change in optical frequency caused by tuning the SXC cavity length. Such measurements yield information on the strength of feedback provided by the SXC and provide a means to estimate α, the linewidth enhancement factor.

The background required to interpret the frequency tuning curves is reviewed in Section 5.2. Experimental technique is described in Section 5.3, while measurement results are presented and discussed in Section 5.4. The chapter concludes with a summary in Section 5.5.

5.2 Frequency Tuning - Theory

The effects of an external reflector on the spectral output of laser diodes have been studied in **[10,24,25]** which form the basis of this section. These papers were primarily concerned with external cavities much longer than the laser cavity and neglected the effect of the gain spectrum shape.

Here a similar approach will be used to describe frequency tuning in SXC lasers. The spectral shape of the gain will be included where appropriate.

The effect of the external cavity is included by a time-delayed field component arising from the external reflection in a rate equation analysis. The reflectivity of the external cavity is assumed to be sufficiently small that multiple external reflections may be ignored. In this case, the change caused by the external cavity is described by [24]

$$\delta\nu = \nu_o - \nu_{nf} = -\frac{X\sqrt{1+\alpha^2}}{2\pi}\sin\left(2\pi\nu_o\tau_{ext} + \tan^{-1}(\alpha)\right) \qquad (5.1)$$

$$\frac{\Delta C_{th}}{\Delta C_{th,\max}} = -\cos\left(2\pi\nu_o\tau_{ext}\right) \qquad (5.2)$$

$$\Delta\nu = \frac{\Delta\nu_{nf}}{\left[1 + X\cos\left(2\pi\nu_o\tau_{ext} + \tan^{-1}(\alpha)\right)\right]^2} \qquad (5.3)$$

$$X = \frac{\tau_{ext}\left(1-R_2\right)}{\tau_1}\sqrt{\frac{R_3}{R_2}} \qquad (5.4)$$

where

ν_{nf} is the mode frequency with no feedback
ν_o is the mode frequency with feedback
$\delta\nu$ is the frequency tuning
X is the feedback parameter
α is the linewidth enhancement factor
τ_{ext} is the round trip time in the SXC
τ_l is the round trip time in the laser cavity
$\Delta\nu$ is the linewidth
$\Delta\nu_{nf}$ is the linewidth with no feedback
R_2 is the rear facet reflectivity
R_3 is the reflectivity of the external reflector
ΔC_{th} is the threshold current reduction
$\Delta C_{th,max}$ is the maximum threshold current reduction

Equation (5.1) describes the change in laser emission frequency caused by external feedback. The emission frequency depends on the length of the external cavity, the strength of the external reflection, and the linewidth enhancement factor. The length of the cavity also determines the relative threshold reduction via (5.2). For a given SXC length, the threshold reduction is different for each laser mode, and the laser oscillates at the mode with the greatest threshold reduction. As the SXC length is ramped, the emission frequency changes such that equation (5.1) is satisfied. With sufficient SXC length change, another laser mode becomes the most favourable and a mode hop occurs. Thus (5.1) describes the frequency tuning curve, while (5.2) defines the upper and lower bounds caused by mode hops.

The frequency tuning characteristics of a SXC laser were calculated using a computer program. An iterative

solution was necessary, since (5.1) cannot be put in a closed form. Frequency and threshold reduction were calculated at each of three adjacent laser modes as the length of the external cavity was varied. The endpoints of the central mode frequency tuning curve were determined by mode hops to the adjacent laser modes.

Examples of such calculations are shown in Figure 5.1. Here the variation of the curves with the linewidth enhancement factor is demonstrated by plotting optical frequency tuning versus length of the external cavity. The parameters used in generating these curves are typical of the experimental situation: laser length of 250 μm, effective refractive index of 4, wavelength of 1.3 μm, ratio of the optical length of the laser cavity to that of the SXC cavity of 6, facet reflectivity of 0.32, and SXC reflectivity of 5×10^{-4}. The dash-dot curve was obtained with α=0, the dashed curve with α=3, and the solid curve with α=6. The latter two values are thought to be typical values for InGaAsP quantum well and bulk lasers, respectively. Note the dramatic change in the character of the curve due to the linewidth enhancement factor. This particular sensitivity of the frequency tuning curves provides the means for estimating α from frequency tuning data.

Other parameters were also varied independently to determine their effect on frequency tuning. For Figure 5.2,

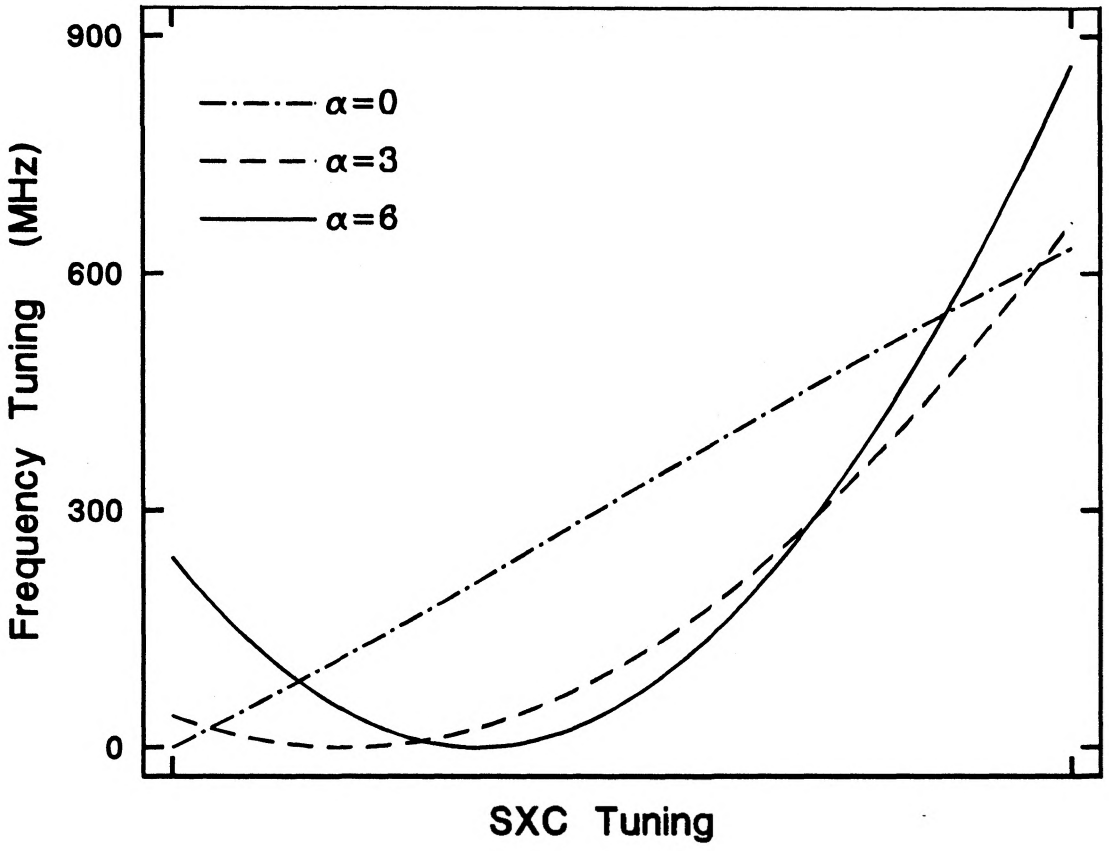

Figure 5.1 Theoretical frequency tuning - α dependence.

the ratio of cavity lengths was 6 and α=6 for all curves, while the SXC reflectivity was 5×10^{-4}, 2×10^{-3}, and 1×10^{-2} for the dash-dot, dashed, and solid lines respectively. The lowest reflectivity is representative of a planar-mirror SXC **[44]**, while the highest is roughly that obtained with a spherical mirror. Increasing reflectivity does not change the shape of the frequency tuning curve, but rather changes the magnitude of optical frequency deviation. The magnitude of frequency tuning is proportional to the square root of the SXC

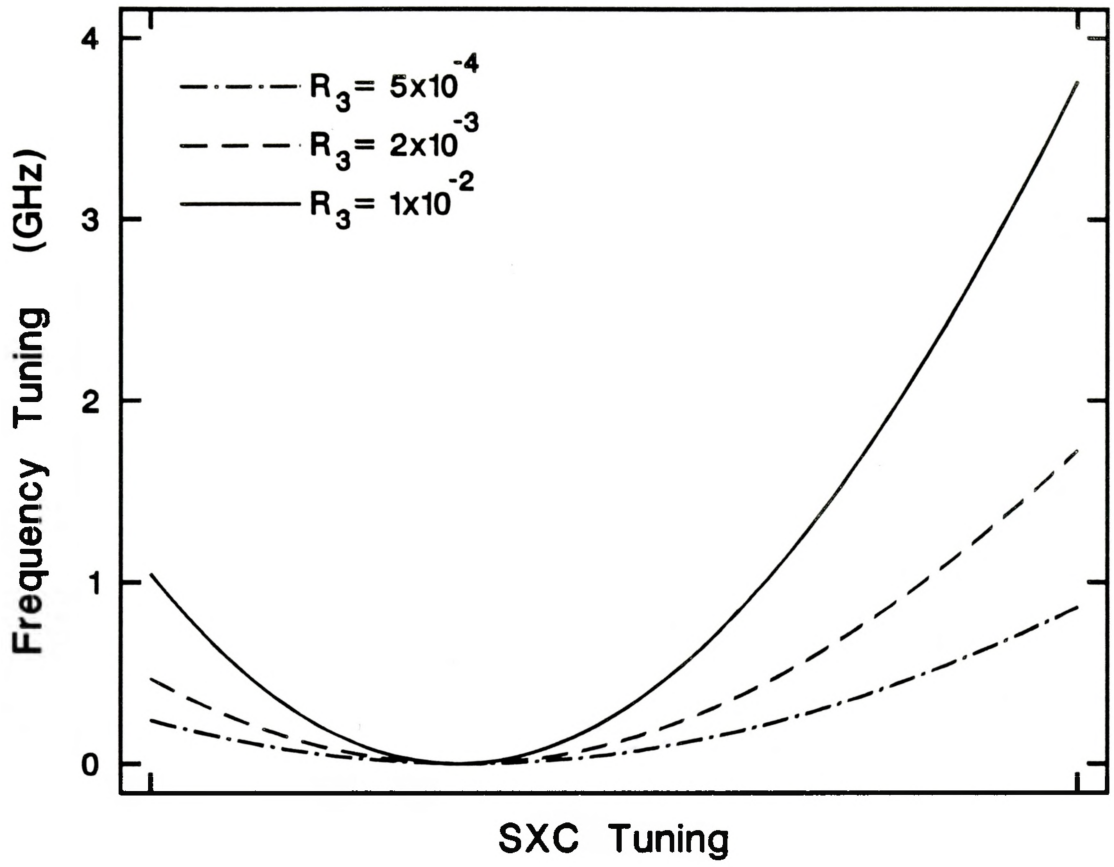

Figure 5.2 Theoretical frequency tuning - SXC reflectivity dependence.

reflectivity. The effect of the laser gain spectrum curvature and of multiple reflections in a spherical-mirror SXC each make the reflectivity dependence more complicated than represented in Figure 5.2. This is discussed further in Section 5.4.

The external cavity length dependence was determined using α=6 and SXC reflectivity of 5×10^{-4}. The dash-dot, dashed, and solid curves of Figure 5.3 were obtained with cavity length ratios of 6, 7, and 8, respectively. Note that

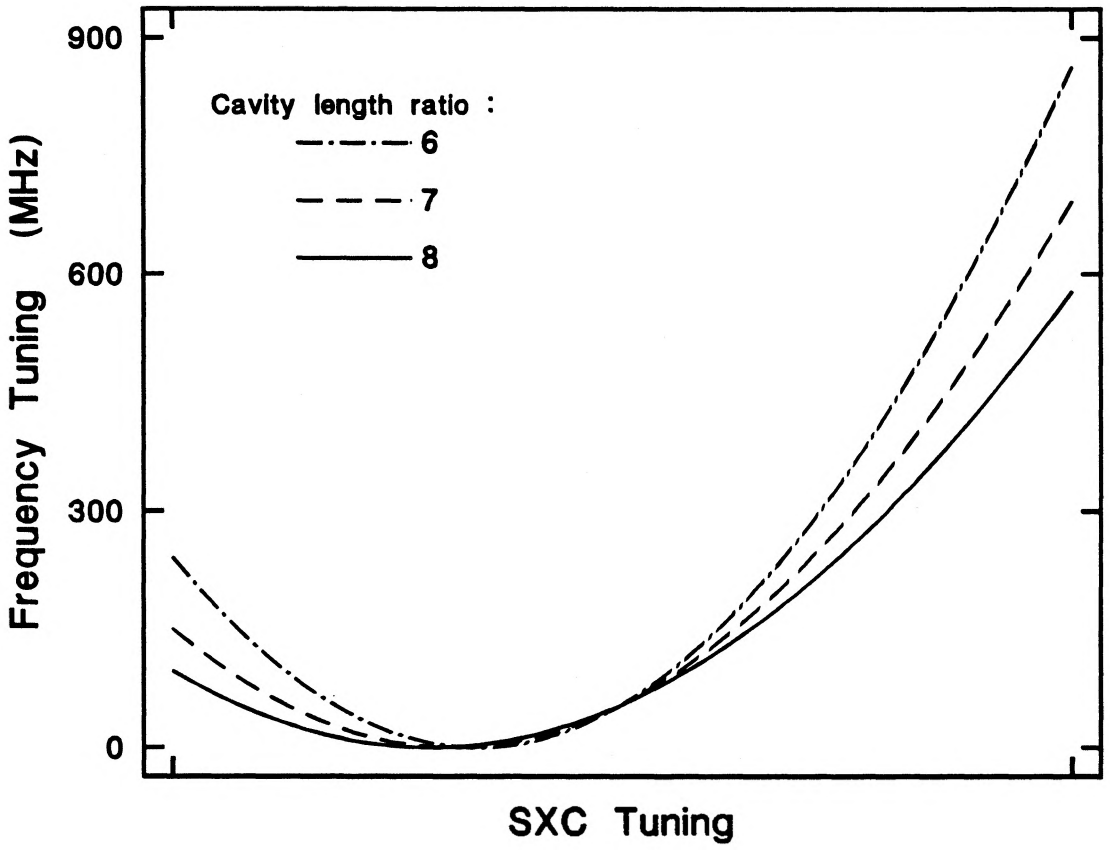

Figure 5.3 Theoretical frequency tuning - cavity length ratio dependence.

the changes in the curves are similar to changes caused by different values of α as shown in Figure 5.1. The uncertainty in detemining α from frequency tuning measurements therefore depends on the accuracy to which the external cavity length is known. Fortunately, the ratio of cavity lengths may be independently determined, since it is simply the ratio of external cavity FSR to laser mode FSR. A fit of the model to the data can be obtained using the measured value of cavity length ratio and adjusting the linewidth enhancement factor

and the external reflectivity.

Finally, the linewidth reduction from (5.3) is plotted versus cavity tuning in Figure 5.4. For the dashed line, the ratio of cavity lengths was 9, the SXC reflectivity was 1×10^{-2}, and the linewidth enhancement factor was 3, corresponding to a 500 μm quantum well laser with a spherical-mirror SXC. The dashed line had cavity length ratio of 6, SXC reflectivity of 5×10^{-4}, and α=6, as for a planar-mirror SXC with a bulk type 250 μm laser. These curves are useful in estimating the effect of the SXC configuration on the linewidth of the laser both in terms of linewidth reduction compared to a solitary laser, and in linewidth variation as the cavity length is tuned within a mode spacing. For these cases the predicted linewidth reduction due to addition of the SXC is only a few percent, and so the linewidth measurements reported in Chapter 4 represent the natural linewidths of the lasers. The change in linewidth with SXC cavity tuning is also seen to be small. If the linewidth had been strongly dependent on SXC tuning, it would have been difficult to obtain reproducible linewidth measurements. Notice that the SXC can actually give linewidth broadening over a small range of SXC tuning. Multiple passes in the SXC have not been considered here.

In Section 5.4 it will be shown that multiple reflections may indeed be important for a spherical mirror SXC, and thus the solid line in Figure 5.4 probably

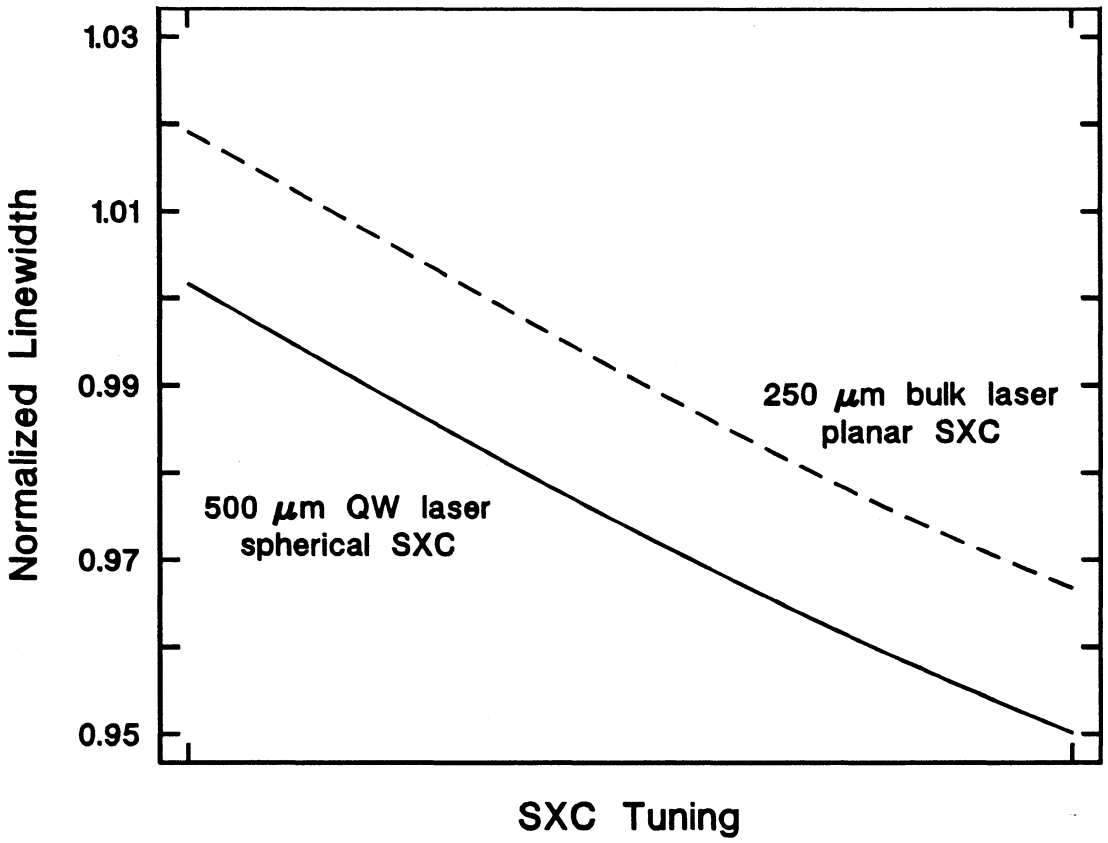

Figure 5.4 Effect of SXC on linewidth, normalized to solitary laser linewidth. Span of SXC tuning corresponds to tuning of one laser mode.

underestimates the true linewidth reduction and should be considered a first-order approximation.

5.2 Experimental Technique

Two techniques were developed to measure frequency tuning. Each has its relative merits, and the data presented contain examples of both. Method 1 involved locking the

Fabry-Perot interferometer transmission resonance to the laser frequency and tracking it as the length of the SXC was ramped. The optical path was as described by Figure 3.1, with mirror M1 removed. These measurements were much less sensitive to feedback compared to linewidth measurement.

The electronics connections were similar to Figure 3.2. The spectrum analyzer and monochromator were not used. A small modulation was applied to the Fabry-Perot mirror spacing just as with the linewidth measurement. The sinusoidal signal from the slow output of photodetector 1 was demodulated using a PAR Model 126 lock-in amplifier which had an integrate mode on its output stage. With the proper choice of phase reference at the lock-in amplifier, the output was an error signal corresponding to the deviation of the Fabry-Perot fringe from the peak value. This signal was fed back to the interferometer mirror spacing via the Fabry-Perot ramp generator external input. The Fabry-Perot thus remained locked to the laser frequency while the laser was frequency tuned by the SXC. The integrate mode of the lock-in was particularly useful because it allowed the Fabry-Perot to track the laser frequency over the full frequency range of the interferometer, about 3 free spectral ranges, with zero steady-state error. A voltage divider was inserted between the lock-in amplifier and the Fabry-Perot ramp generator to ensure that the maximum piezo voltage was not exceeded.

To carry out a measurement, the interferometer was locked as described above. The length of the SXC was then slowly ramped under computer control while the photodetector signal and the Fabry-Perot piezo voltage were measured with the ADC card. These measurements gave the optical power and the relative frequency, respectively. The frequency determination relied on the piezo voltage to optical frequency calibration described in Chapter 3. The SXC was generally ramped over several free spectral ranges of the external cavity. The piezoelectric transducer used in the SXC exhibited hysteresis in expansion versus applied voltage, which was measured by comparing mode hop intervals at different piezo voltages. The concomitant nonlinearity was minimized by only using data from the most linear region. In this case the nonlinearity was about 1% over one mode spacing, so a correction for nonlinearity was not necessary.

Method 1 gave good signal to noise ratio and was a relatively quick measurement, but in some cases the behavior at mode hops was not well characterized. At a mode hop, the Fabry-Perot could remain locked to a mode which was no longer the dominant one, and it could take too long to acquire a lock to a new mode when starting from a position between fringes where the slope and thus the error signal was very small. In some cases successive mode hops caused the FPI piezo voltage to increase or decrease monotonically until the locked fringes

walked off the range of the FPI and locking circuit. These problems could be reduced by adjusting the Fabry-Perot cavity length such that successive fringes tended not to walk off, and by detuning the interferometer to give low finesse and hence only a small region with little slope between fringes. Because of the poor finesse fringes, multiple modes at mode hops tended to overlap and smear the frequency tuning curves. One potential solution is to disengage the lock at mode hops and relock automatically at the fringe nearest the centre of the FPI tuning range. A simpler technique which overcomes these difficulties is discussed below.

With Method 2, the optical apparatus was again as in Figure 3.1, with electronics connections similar to Figure 3.2. Instead of being locked to the laser frequency, the FPI was put in scanning mode with a period of 100 or 200 milliseconds. The laser current was modulated at 50 kHz, causing an optical frequency modulation of the laser output. This was used to measure the slope of the Fabry-Perot fringe in a manner analogous to wavelength modulation spectroscopy. As the Fabry-Perot fringe swept through the laser mode, a lock-in amplifier demodulated the 50 kHz photodetector signal, giving the slope of the Fabry-Perot fringe. The time constant of the lock-in had to be 1 millisecond or less at 100 - 200 millisecond scan rates. The "S"-shaped derivative signal was digitized at the ADC card and processed by the computer, which

used a zero-crossing algorithm to find the peak of the Fabry-Perot fringe. Several scans were averaged between steps in the SXC ramp. The chief advantage of this technique was that the behavior at mode hops was clearly obtained, even with several modes oscillating simultaneously. The measurement required more time (1-3 hours) than Method 1, but it could be left unattended. In order to maximize measurement speed, special purpose assembler code was written to digitize the derivative signal in blocks corresponding to an entire scan. The acquisition rate was ultimately limited by the speed of the analog to digital converter on the ADC card. An optimizing Fortran compiler was used for the data processing code to further expedite measurements. Without such measures the data acquisition time would have been many times greater. Despite the generally poorer signal to noise ratio of Method 2, it was preferred over Method 1 for its clearer results near mode hops.

5.4 Frequency Tuning Measurements

The measured frequency tuning characteristics of a 250 μm ABC laser, ABC052, is shown in Figure 5.5. The SXC tuning axis is in the direction of decreasing external cavity length, and the modes are in order of decreasing wavelength. These data were obtained with Method 1 described above. Note that the frequency tuning curves were quite different for each mode. The cavity ratio and external reflectivity are mode independent, whereas the linewidth enhancement factor is expected to have some wavelength/mode dependence **[55]**. To replicate the measured frequency tuning curves, α would have to range from about 10 to 3, which is a much larger variation than expected and inconsistent with the modal dependence of linewidth reported in Chapter 4. In fact, the major contribution to the variation in frequency tuning between modes is not due to dispersion in α.

The shape of the gain spectrum has an effect on the location of mode hops with the SXC laser. Tuning toward the gain peak causes mode hops to occur earlier than if the gain spectrum were flat, while tuning away from the gain peak has the opposite effect. Equation (5.2) is thus valid only at the gain peak. Inclusion of the gain spectrum gives a new equation describing the mode-dependent threshold reduction

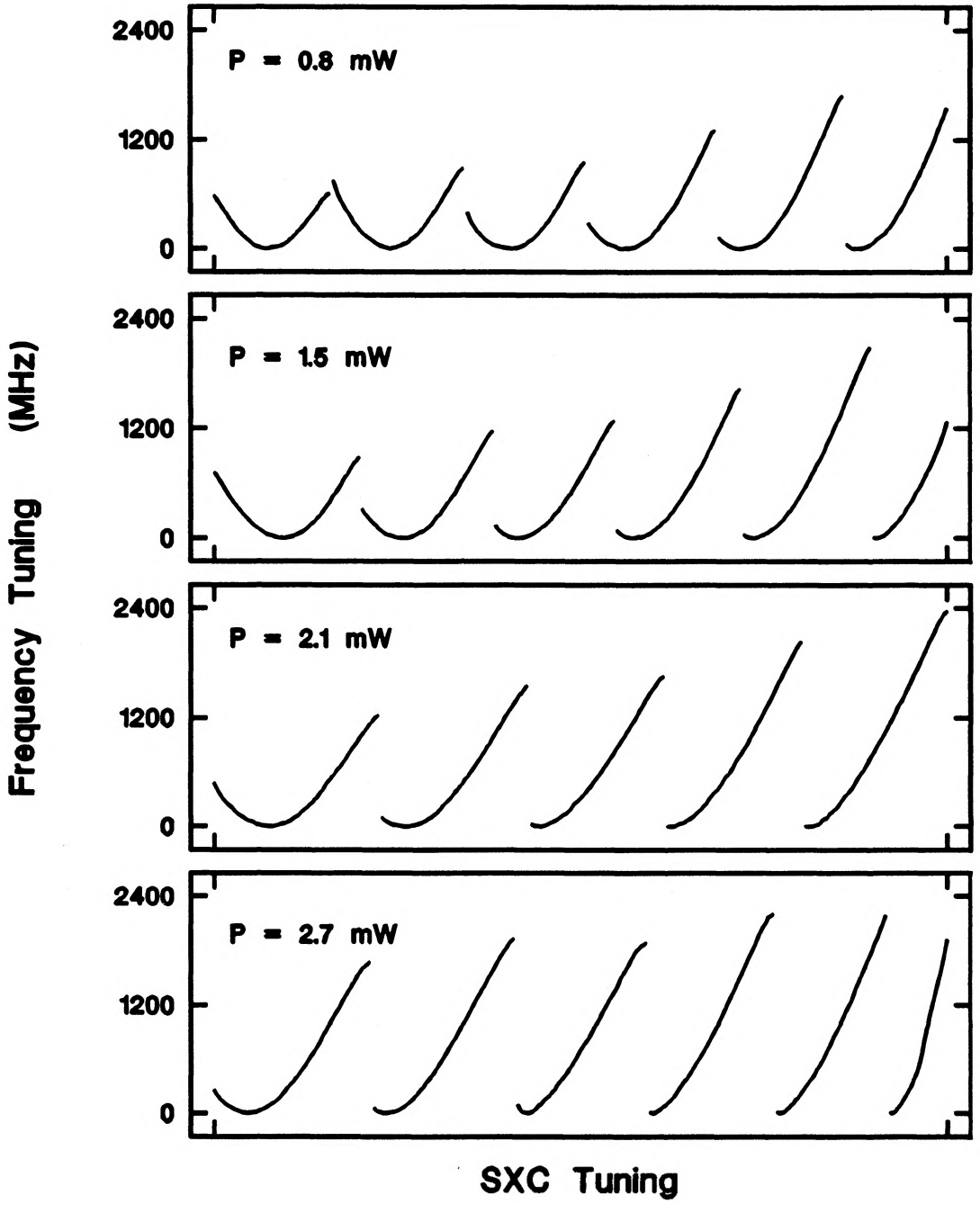

Figure 5.5 Experimental frequency tuning curves for ABC052 with a planar SXC. Each curve represents a laser mode. Modes are ordered with decreasing wavelength from left to right. SXC length decreases from left to right.

$$\frac{\Delta C_{th}(\nu_m)}{\Delta C_{th,\max}} = \frac{\gamma \tau_{ext}}{2X}\left[1 - \frac{1}{g(\nu_m)}\right] - \frac{\cos\left(2\pi \nu_m \tau_{ext}\right)}{g(\nu_m)} \qquad (5.5)$$

where

γ_m is the frequency of mode m, with feedback
γ is the loss in the laser, assumed wavelength independent
g is the normalized gain E field gain spectrum (g = 1 at gain peak)

Equation (5.5) was derived by assuming that gain equals loss at threshold, and that in the absence of gain saturation the gain is proportional to current. The below threshold normalized gain spectrum had already been measured for this ABC laser **[56]**. The absolute value of gain was not known, but was estimated from the external differential quantum efficiency **[28, p35]**. Assuming an internal quantum efficiency of about 0.8, the loss was 92 cm^{-1}.

Theoretical curves were generated using the measured gain spectrum, a cavity length ratio of 5.7 determined from the FSR of the SXC, estimated loss of 92 cm^{-1}, linewidth enhancement factor of 6, and SXC reflectivity of 5×10^{-4}. The result is shown in Figure 5.6, which clearly resembles the measured curves at low power in Figure 5.5. Figure 5.6 does not represent a fit to the data; the estimated parameters were not adjusted to match the data. The strong resemblence of the theoretical curves to the low power data clearly indicates the

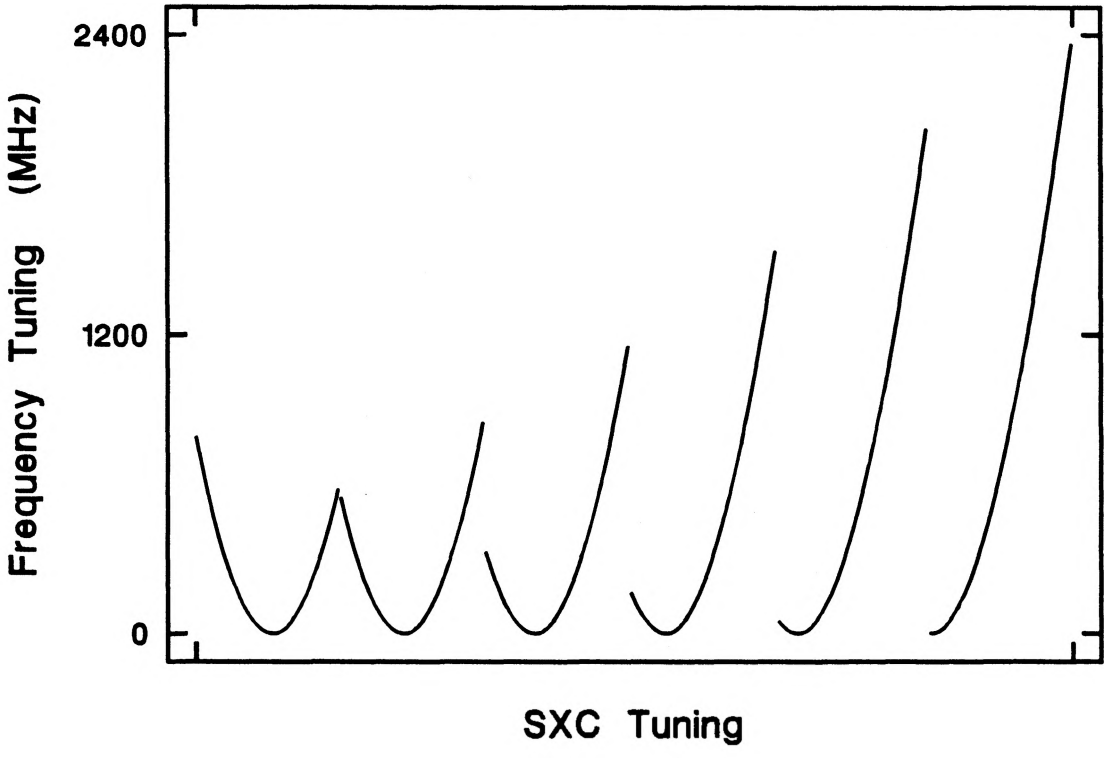

Figure 5.6 Theoretical frequency tuning including measured gain spectrum shape. Compare Figure 5.5.

role of the laser gain spectral shape in determining modal dependence of the frequency tuning curves.

A detailed fit of theory to experiment over all modes was not attempted, since introduction of the gain curve shape introduces a number of new parameters which must be measured independently or included as fitting parameters. The complexity of making such measurements on each laser is prohibitive, while the physical validity of extracting values from a fit dependent on so many parameters is dubious. A simpler and satisfactory alternative is to fit to the modes

nearest the gain peak where the gain spectrum curvature is minimal. Using modes on either side of the gain peak gives upper and lower bounds for the linewidth enhancement factor.

Figure 5.5 indicates that the frequency tuning curves were strongly dependent on the optical power. This behavior was exhibited by all lasers measured, although generally at higher output optical power. At present this behavior is not understood; the model represented by equations (5.1)-(5.3) indicates that the frequency tuning should be independent of optical power. A Fabry-Perot approach **[57]** might yield a more accurate model, although it is not immediately obvious that this would result in an optical power dependence in the frequency tuning.

Another possibility is that the effective gain spectrum shape is dependent on optical power. There is additional evidence for this argument; at elevated optical power the side modes in the SXC lasers rose dramatically, indicating that the effective side mode gain had risen relative to the gain of the main mode. The ABC laser of Figure 5.5 clearly showed strong side modes above 3 mW optical power per facet. Characterization of this behavior is currently underway **[58]** and will hopefully clarify the situation. For the purposes of this thesis the power dependence issue was avoided by considering measurements at output power at 1 mW per facet or less.

An example of estimating α from a fit to the frequency tuning results is shown in Figure 5.7. The data was obtained with 250 μm PBH laser 1651-5 with a planar-mirror SXC. The SXC was aligned to give 8 modes, and the measured cavity length ratio was 7.9. The solid curve indicates measured frequency tuning curves for modes 4 and 5, which bracket the gain peak. The SXC reflectivity and linewidth enhancement factor were adjusted to give the theoretical dashed curves. For the theoretical curves, SXC reflectivity was $4x10^{-3}$ for both modes, while α was 6.6 and 6.2 for modes 4 and 5, respectively. Adjusting α by $\pm$ 5% or SXC reflectivity by $\pm$ 10% gave a significant difference in the theoretical curves. Note that the reflectivity was considerably higher than for ABC052 laser. The difference was partly due to having the planar mirror closer to the back facet, but was probably also due to the difference in laser structure. The PBH laser's side mode suppression ratio was the highest obtained with a planar-mirror SXC, which also indicates a relatively high level of SXC feedback.

Frequency tuning for the two central modes of R1-394-26, a 250 μm 1.5% compressive strained layer 5-quantum well laser, are shown in Figure 5.8. The SXC reflector was planar. Again the solid curve represents measured data, while the broken curves are theoretical curves fitted to the experimental results. There were 6 tunable modes, and the

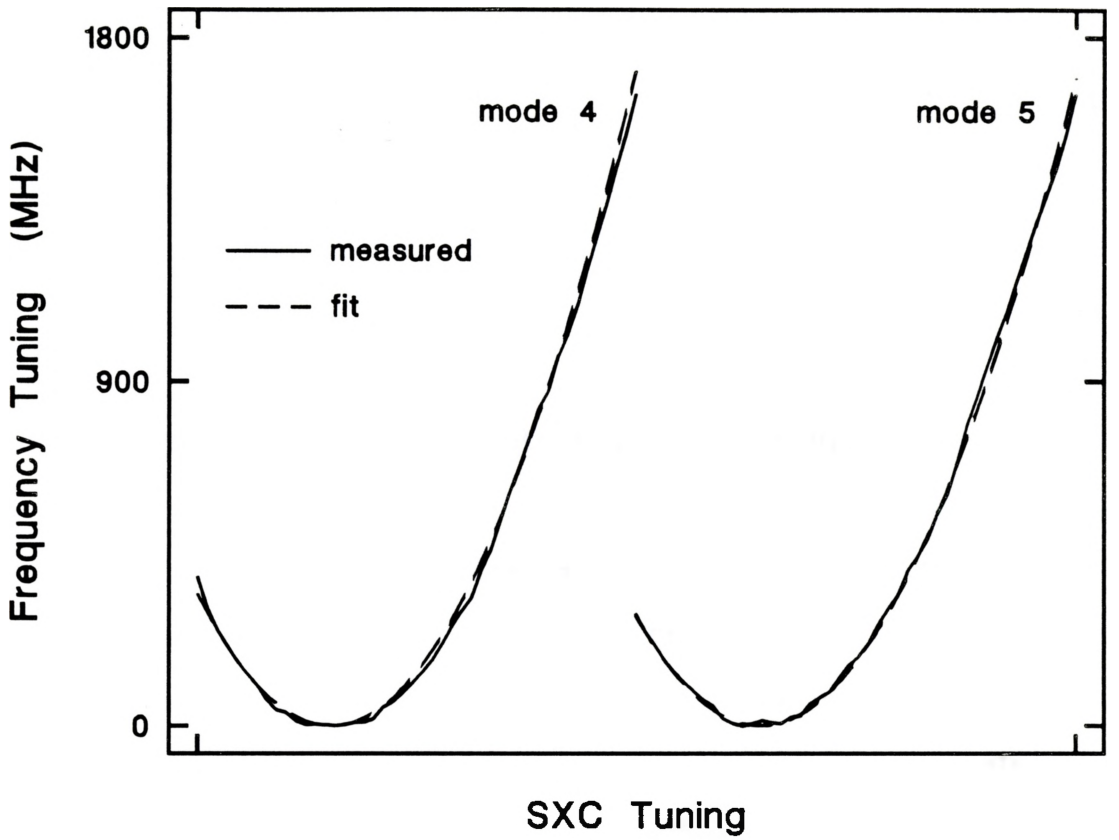

Figure 5.7 Frequency tuning of 1651-5, a 250 μm PBH laser, with a planar SXC.

measured cavity ratio was 5.7. Mode 3 was fit with reflectivity of 3×10^{-4} and α=3.2, while mode 4 required reflectivity of 3.5×10^{-4} and α=2.9. The measured values of α lie in the range of expected values for quantum well lasers.

A spherical mirror SXC was expected to be less sensitive to the gain spectrum curvature and to give larger frequency tuning compared to a planar SXC, and thus appeared to offer an improved frequency tuning measurement. Experimental results for R1-399-164, a 500 μm 1.2% compressive

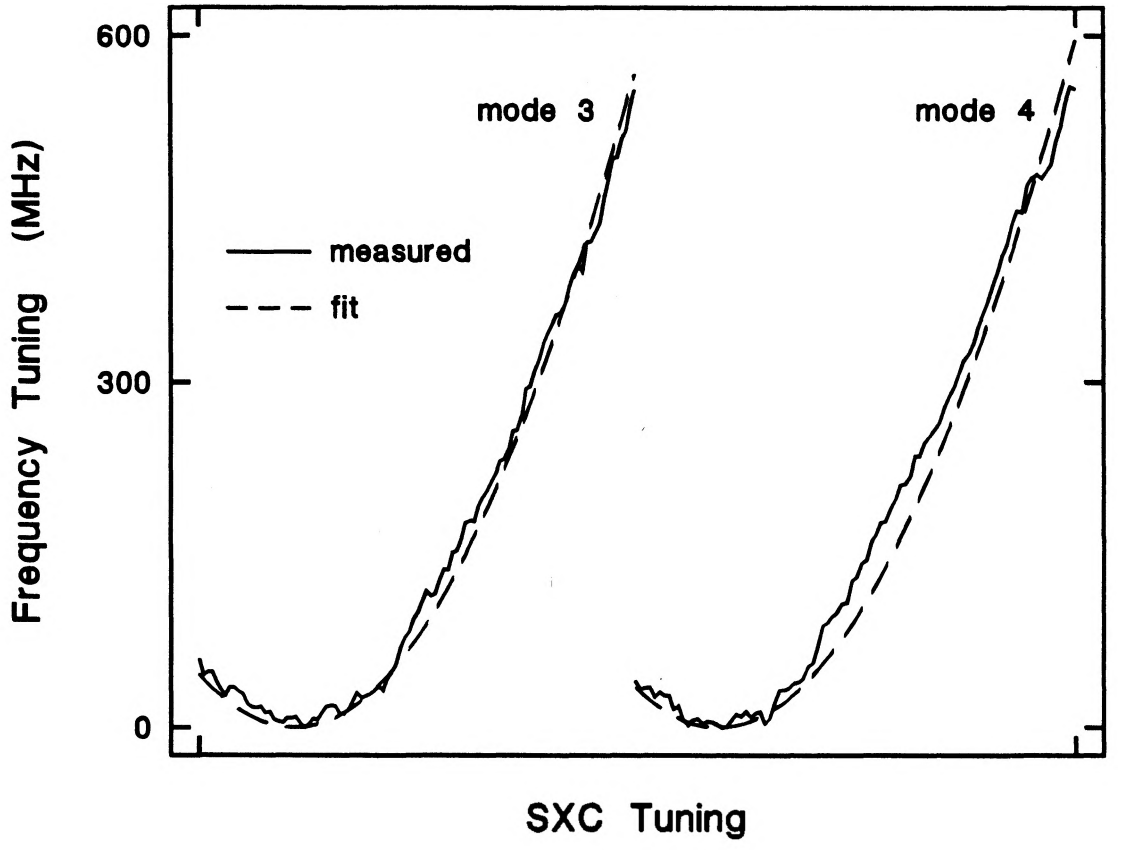

Figure 5.8 Frequency tuning of R1-394-26, a 250 μm 5-quantum well laser, with a planar SXC.

strained layer 3-quantum well laser with a spherical SXC are shown in Figure 5.9. As expected, the frequency tuning was less mode dependent, while the signal to noise ratio was improved by using a spherical reflector. The cavity length ratio was about 12, based on the ratio of SXC free spectral range to mode spacing. An attempted fit to the data using equations (5.1-5.3) and reasonable values of linewidth enhancement factor failed to generate matching theoretical curves.

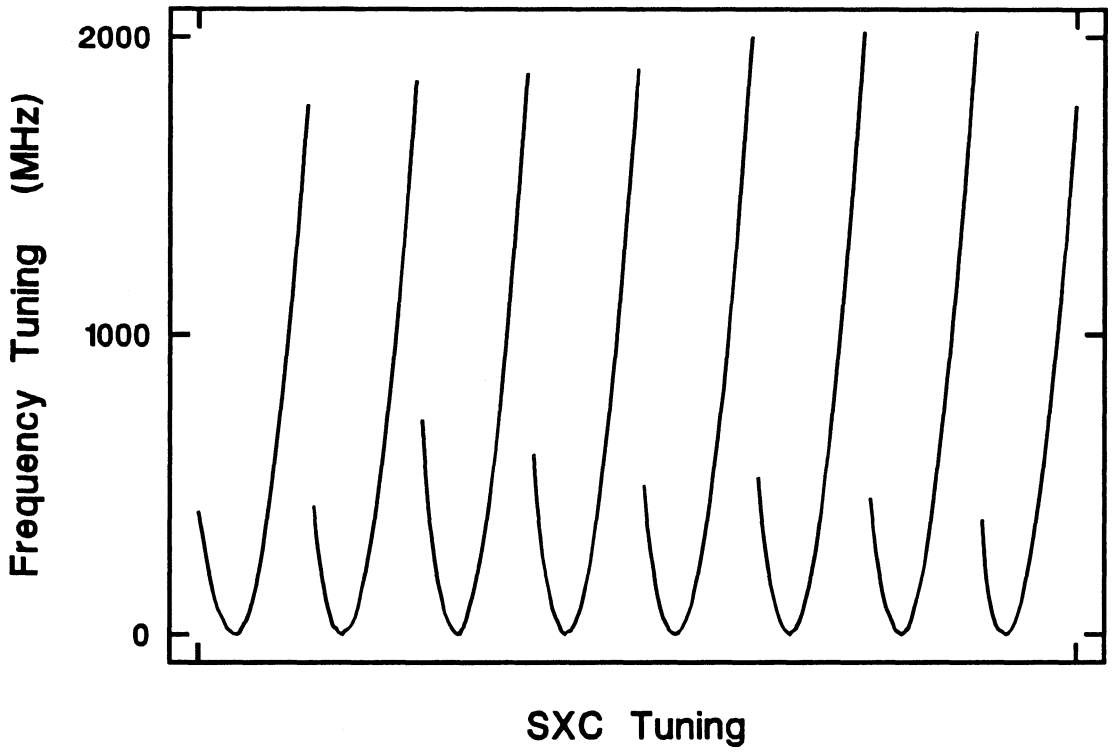

Figure 5.9 Frequency tuning curves for R1-399-164, a 500 μm, 3-quantum well laser, with a spherical SXC.

One possibility is that multiple reflections in the external cavity should be considered with a well-aligned spherical mirror SXC. Another possibility is that the linearization of the gain with carrier density breaks down with quantum well lasers and large feedback. Once again there appears to be a requirement for improvements in the theoretical model.

Measurements on two other 500 μm quantum well lasers yielded similar results.

5.5 Summary

Measurements on the frequency tuning characteristics of planar and spherical mirror SXC lasers have been reported. The theory required to model this behavior has been reviewed. Refinement to include the gain spectral shape explained variation in the appearance of the frequency tuning curves with laser mode. When limited to low optical power and low SXC reflectivity, this theory provided a good fit to the experimental data, and demonstrates that the frequency tuning curves can be used to extract information on the linewidth enhancement factor and the amount of SXC feedback.

The theory fails to account for the power dependence of the frequency tuning curves. It also appears to break down with the spherical mirror SXC configuration, perhaps due to the relatively large amount of feedback and a need to consider multiple reflections. It is hoped that a better model will account for these effects and allow α to be estimated using spherical SXC configurations.

Within the limitations discussed above, theoretical fits to experimental data have been presented, which gave α of 6.4 ± 0.2 for a PBH bulk laser and 3.1 ± 0.2 for a compressively strained quantum well laser. The error range indicates the upper and lower bound given by two modes bracketing the gain peak.

CHAPTER 6 SUMMARY

A system has been developed for directly measuring frequency noise in InGaAsP semiconductor lasers. From the frequency noise data, equivalent linewidth may be calculated. An advantage over more conventional heterodyne-type linewidth systems is that the approach taken here directly obtains the spectral shape of the frequency noise, which is more directly applicable to coherent communications applications. In addition, 1/f noise, side mode induced linewidth broadening, and external feedback are easily identified using this technique.

A considerable effort was expended in calibrating the system to give absolute linewidth values and flat frequency response for FM noise spectra. Absolute accuracy of linewidth measurements was estimated to be about ± 30%, limited by calibration tolerance with the spectrum analyzer used. Reproducibility of individual linewidth measurements was typically between 2% and 10%, and was attributed to residual optical feedback.

Other factors limiting system performance, namely amplitude noise throughput, unintentional external optical feedback, and Fabry-Perot interferometer frequency response

were investigated theoretically and experimentally. It was demonstrated that both amplitude noise throughput and external optical feedback could be reduced to satisfactory levels, and that the Fabry-Perot interferometer response could be tailored to meet the required measurement bandwidth.

The system was further tested by making measurements on eleven Fabry-Perot lasers used in a short external cavity configuration to obtain single mode oscillation. The frequency noise of all lasers was found to be predominantly white over the measurement bandwidth, with slightly enhanced noise at frequencies less than 25 MHz. The linewidth calculated from the FM noise was Lorentzian in shape and approximately inversely proportional to the output power of the laser. Deviations from a linear relationship between inverse power and linewidth occurred at low and high optical power levels. At high optical power, linewidth broadening correlated with growing side mode intensity.

Linewidth of conventional lasers of 250 μm length was found to be about 125 MHz-mW, compared to 37 MHz-mW for quantum well devices of similar length. Strained layer quantum well lasers of 500 μm length had linewidth in the range 18 MHz-mW to 28 MHz-mW with an apparent strain dependence. Both compressive and tensile strained lasers exhibited lower linewidth than unstrained lasers. An unexpectedly large variation in linewidth with mode of 20% to

40% over about 5 nanometres was also discovered.

The instrument was adapted to make measurements of laser optical frequency tuning with change in short external cavity length. Such measurements provided a novel means for estimating the linewidth enhancement factor and the reflectivity of the external cavity element. Refinement of theory to include the effect of the gain spectrum accounted for the change in frequency tuning with mode. The current model failed to account for power dependence of the frequency tuning curves and did not accurately depict the results obtained with quantum well lasers with spherical external reflectors. However, the theory did describe planar type external cavity laser frequency tuning. Linewidth enhancement factors of 6.4 ± 0.2 and 3.1 ± 0.2 for a bulk laser and a quantum well laser respectively were obtained by fitting a theoretical model to experimental results. These values are in agreement with commonly accepted values for such devices, and are in approximately the correct ratio to explain the change in linewidth between the devices.

There are many paths which could branch out from this work. Frequency noise measurements have been taken from a few hundred kilohertz to a few hundred Megahertz. A natural extention is to expand the measurement to lower or higher frequencies. Especially interesting is the behavior of FM noise around the relaxation oscillation frequency.

A variation in linewidth with mode in SXC lasers has been identified. More measurements are required to determine how this effect depends on dispersion of the linewidth enhancement factor and on the type of laser and reflector. Such measurements may provide a means of measuring the dispersion of the linewidth enhancement factor with the laser operating above threshold.

Side mode induced linewidth broadening has been identified at several points in this thesis, but has not been explicitly measured. Such measurements have been made in **[23]**, and a model incorporating nonlinear gain was used to explain the results. Since nonlinear gain and its origin is not well understood, it would seem useful to further investigate side mode effects on linewidth using a number of different lasers. The linewidth measurement technique developed in this thesis might need modification to increase amplitude noise rejection before such a survey could be made.

Finally, the frequency tuning measurement requires further investigation. Currently, the technique offers a promising method to obtain information on the linewidth enhancement factor and SXC reflectivity from a relatively straightforward measurement, with the laser operating above threshold. However, as previously stated, more sophisticated theoretical modelling is required to gain a more complete understanding of these curves.

APPENDIX CIRCUIT SCHEMATICS

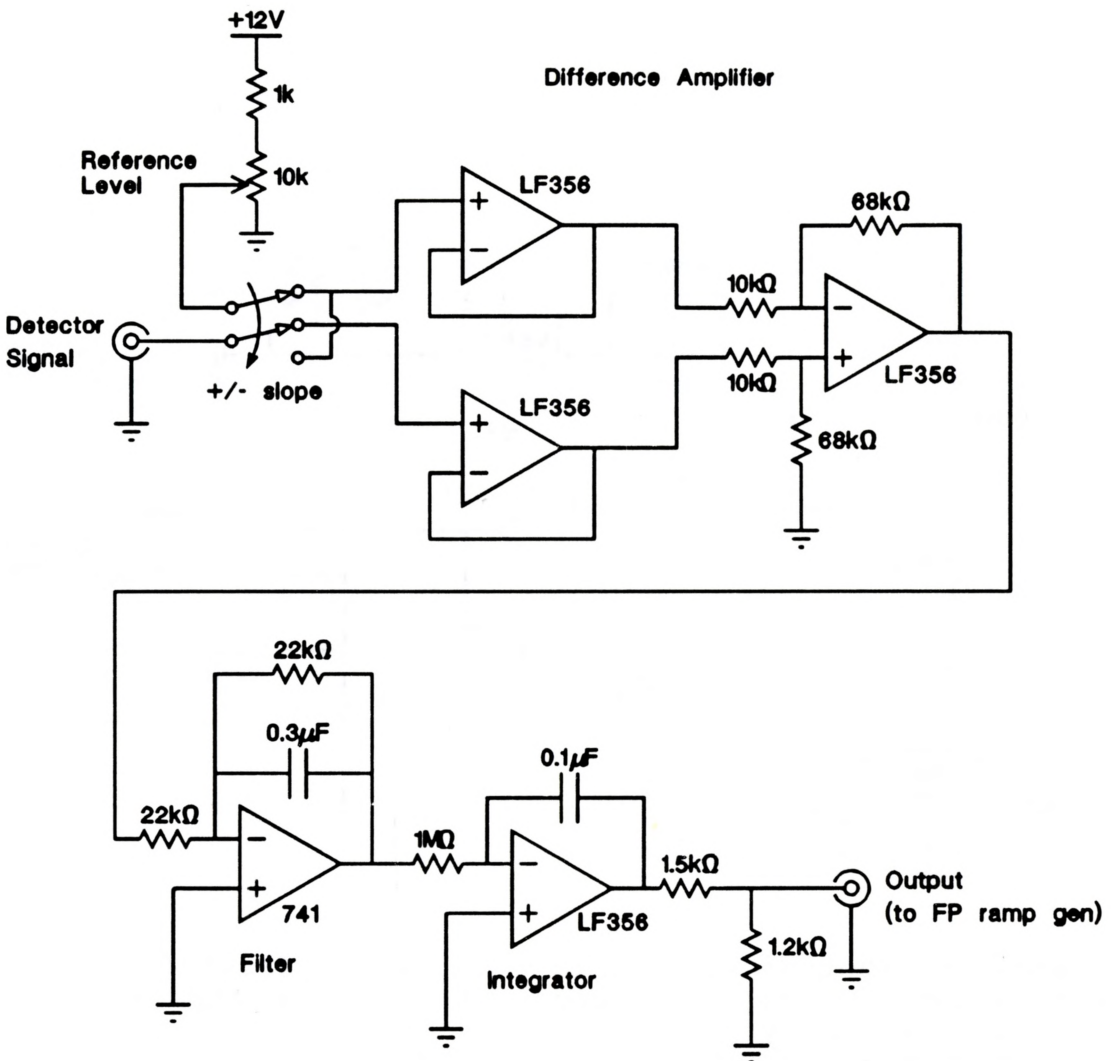

Figure A1 Circuit used to lock the Fabry-Perot interferemeter. Switch selects positive or negative slope of fringe. Reference level potentiometer selects height on fringe.

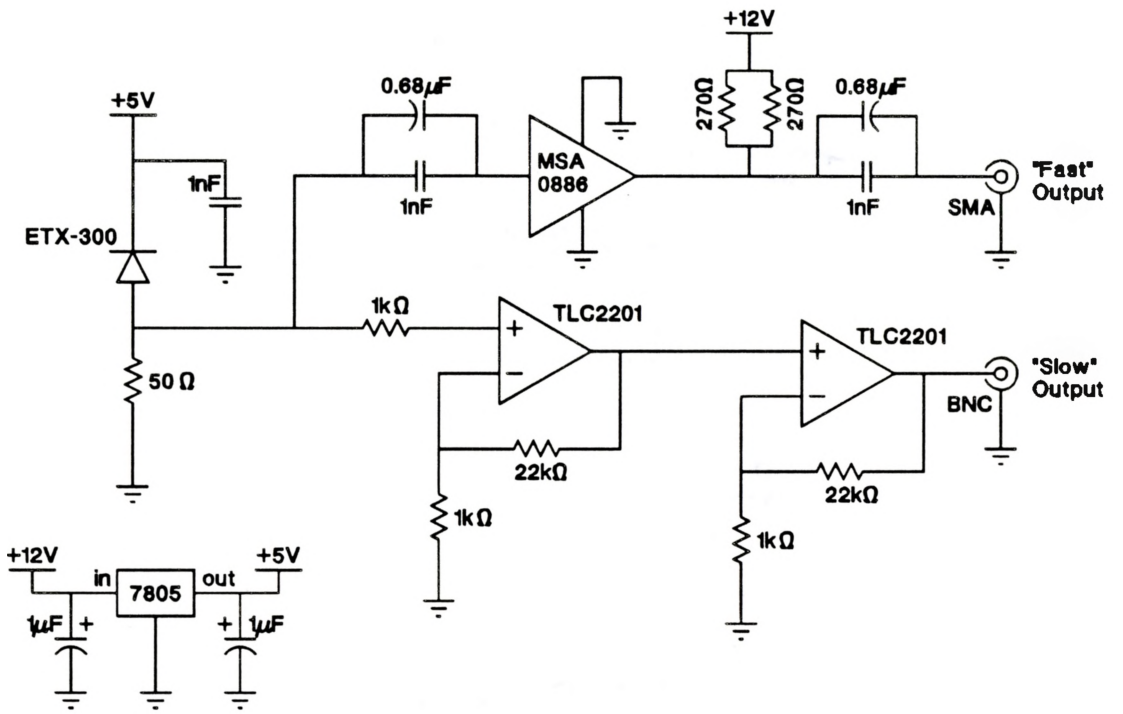

Figure A2 Photodetector 1 circuit, with "fast" (ac-coupled) and "slow" (dc-coupled) output stages. Op Amps operate on +5V, single supply.

REFERENCES

[1] C.H. Henry, "Theory of the Linewidth of Semiconductor Lasers", IEEE J. Quantum Electron., **QE-18**, pp 259-264, 1982

[2] B.F. Ventrudo, D.T. Cassidy, "Operating Characteristics of a Tunable Diode Laser Absorption Spectrometer using Short-External-Cavity and DFB Laser Diodes", Appl. Opt., **29** (33), pp 5007-5013, 1990 (and references therein)

[3] M. Ohtsu, K. Nakagawa, Chapter 5 in COHERENCE, AMPLIFICATION, AND QUANTUM EFFECTS IN SEMICONDUCTOR LASERS, Y. Yamamoto Ed., John Wiley & Sons Inc., 1991

[4] A. Dandridge, A.B. Tveten, R.O. Miles, T.G. Giallorenzi, "Laser Noise in Fiber-optic Interferometer Systems", Appl. Phys. Lett., **37** (6), pp 526-528, 1980

[5] A. Dandridge, A.B. Tveten, R.O. Miles, D.A. Jackson, T.G. Giallorenzi, "Single-mode Diode Laser Phase Noise", Appl. Phys. Lett., **38** (2), pp 77-78, 1981

[6] T.G. Hodgkinson, Chapter 6 in COHERENCE, AMPLIFICATION AND QUANTUM EFFECTS IN SEMICONDUCTOR LASERS, Y. Yamamoto Ed., John Wiley & Sons Inc., 1991

[7] K. Kikuchi, "Effects of 1/f-Type FM Noise on Semiconductor Laser Linewidth Residual in High-Power Limit", IEEE J. Quantum Electron. **QE-25** (4), pp 684-688

[8] M. W. Fleming, A. Mooradian, "Fundamental line broadening of single-mode (GaAl)as diode lasers", Appl. Phys. Lett., **38** (7), pp 511-513, 1981

[9] P.M. Asbeck, D.A. Cammack, J.J. Daniele, V. Klebanoff, "Lateral Mode Behavior in Narrow Stripe Lasers", IEEE J. Quantum Electron., **QE-15** (8), 1979

[10] R. Lang, K Kobayashi, "External Optical Feedback Effects on Semiconductor Injection Laser", IEEE J. Quantum Electron., **QE-16** (3), pp 347-355, 1980

[11] M. Osiński, "Linewidth Broadening Factor in Semiconductor Lasers-An Overview", IEEE J. Quantum Electron., **QE-23** (1), pp 9-28, 1987

[12] S. Banerjee, A.K. Srivastava, "Reduction in linewidth enhancement factor for $In_{02}Ga_{0.8}As/GaAs/Al_{0.5}Ga_{0.5}As$ strained quantum well lasers", Appl. Phys. Lett., **58** (20), pp 2198-2199, 1991

[13] T.P. Lee, S.G. Menocal, H. Matsumura, "Characteristics of Linewidth Narrowing of a 1.5 μm DFB Laser With a Short GRIN-Rod External Coupled Cavity", Electron. Lett., **21** (15), pp 655-656, 1985

[14] R. Wyatt, W.J. Devlin, "10 kHz Linewidth 1.5 μm InGaAsP External Cavity Laser With 55 nm Tuning Range", Electron. Lett., **19** (3), pp 110-112, 1983

[15] G.P. Barwood, P. Gill, W.R.C. Rowley, "An Optically Narrowed Diode Laser for Rb Saturation Spectroscopy", J. Mod. Optics, **37** (4), pp 749-758, 1990

[16] N.A. Olsson, C.H. Henry, R.F. Karazinov, H.J. Lee, B.H. Johnson, "Narrow Linewidth 1.5 μm Semiconductor Laser with a Resonant Optical Reflector", Appl. Phys, Lett., **51** (15), pp 1141-1142, 1987

[17] H.R. Telle, "Narrow Linewidth Laser Diodes with Broad Continuous Tuning Range", Appl. Phys. B, **49**, pp 217-226, 1989

[18] M. Ohtsu, N. Tabuchi, "Electrical Feedback and its Network Analysis for Linewidth Reduction of a Semiconductor Laser", J. Lightwave Tech. **LT-6** (3), pp 357-369, 1988

[19] T. Ohtoshi, N. Chinone, "Linewidth Enhancement Factor in Strained Quantum Well Lasers", IEEE Photonics Tech. Lett., **1** (6), pp 117-119, 1989

[20] T. Okoshi, K. Kicuchi, A. Nakayama, "Novel Measurement for High Resolution of Laser Output Spectrum", Electron. Lett, **16** (16), pp 630-631, 1980

[21] K. Iiyama, K. Hayashi, Y. Ida, S. Tabata, "Delayed Self-Homodyne Method Using Solitary Monomode Fibre for Laser Linewidth Measurements", Electron. Lett., **25** (23), pp 1589-1590, 1989

[22] M.O. Van Deventer, P. Spano, S.K. Nielsen, "Comparison Of DFB Laser Linewidth Techniques Results From Cost 215 Round Robin", Electron. Lett., **26** (24), pp 2018-2020, 1990

[23] U. Krüger, K. Petermann, "Dependence of the Linewidth of a Semiconductor Laser on the Mode Distribution", IEEE J. Quantum Electron., **QE-26** (12), pp 2058-2064, 1990

[24] E. Patzak, H. Olesen, A. Sugimura, S. Saito, T. Mukai, "Spectral Linewidth Reduction in Semiconductor Lasers by an External Cavity with Weak Optical Feedback", Electronics Lett., **19** (22), pp 938-940, 1983

[25] G.P. Agrawal, "Line Narrowing in a Single-Mode Injection Laser Due to External Optical Feedback", IEEE J. Quantum Electron., **QE-20** (5), pp 468-471, 1984

[26] M. Sargent III, M.O. Scully, W.E. Lamb Jr., Laser Physics, Chapter 4, Addison-Wesley, 1974

[27] G.P. Agrawal, N.K. Dutta, Long Wavelength Semiconductor Lasers, Chapter 5, Van Nostrand Reinhold Company, 1986

[28] K. Petermann, Laser Diode Modulation And Noise, Kluwer Academic, 1991

[29] L.D. Landau, E.M. Lifshitz, Electrodynamics of Continuous Media, Reading, MA: Addison-Wesley, 1960, sect. 63

[30] M. Lax, "Quantum Noise. X. Density Matrix Treatment of Field and Population-Difference Fluctuations", Phys. Rev., **157**, pp 213-231, 1967

[31] K.Y. Lau, A. Yariv, Chapter 2 in Semiconductors And Semimetals, Vol 22 Part B, Bell Telephone Laboratories, 1985

[32] C.H. Henry, Chapter 2 in COHERENCE, AMPLIFICATION, AND QUANTUM EFFECTS IN SEMICONDUCTOR LASERS, Y. Yamamoto Ed., John Wiley & Sons Inc., 1991

[33] A.B. Carlson, Communication Systems, 3rd Ed., McGraw-Hill, 1986

[34] R.J. Lang, K.J. Vahala, A. Yariv, "The Effect of Spatially Dependent Temperature and Carrier Fluctuations on Noise in Semiconductor Lasers", IEEE J. Quantum Electron., **QE-21** (5), pp 443-451, 1985

[35] C.H. Henry, "Theory of the Phase Noise and Power Spectrum of a Single Mode Injection Laser", IEEE J. Quantum Electron., **QE-19** (9), pp 1391-1397, 1983

[36] H.E. Rowe, Signals and Noise in Communication Systems, D. Van Nostrand Company, 1965

[37] L.S. Cutler, C.L. Searle, "Some Aspects of the Theory and Measurement of Frequency Fluctuations in Frequency Standards", Proc. of the IEEE, **54** (2), pp 136-154, 1966

[38] F.H. Peters, D.T. Cassidy, "Spectral Output of 1.3 μm InGaAsP Semiconductor Diode Lasers", IEE Proc. J **138** (3), pp 195-198, 1991

[39] C.A. Green, N.K. Dutta, W. Watson, "?", Appl. Phys. Lett., **50**, pp1409, 1987

[40] N.K. Dutta, H. Temkin, T. Tanbun-Ek, R. Logan, "Linewidth Enhancement Factor for InGaAs/InP Strained Quantum Well Lasers", **57** (14), pp 1390-1391, 1990

[41] L.B. Mercer, "1/f Frequency Noise Effects on Self-Heterodyne Linewidth Measurements", J. Lightwave Tech., **LT-9** (4), pp 485-493, 1991

[42] T.W. Tkach, A.R. Chraplyvy, "Regimes of Feedback Effects in 1.5-μm Distributed Feedback Laser", J. Lightwave Tech., **LT-4** (11), pp 1655-1661, 1986

[43] D.T. Cassidy, D.M. Bruce, B.F. Ventrudo, "Short-External-Cavity Module for Enhanced Single-Mode Tuning of InGaAsP and AlGaAs Semiconductor Diode Lasers", Rev. Sci. Instrum., **62** (10), pp 2385-2388, 1991

[44] L.J. Bonnell, Single Mode Tunable Short External Cavity Semiconductor Diode Lasers, M.Sc. Thesis, McMaster Eng. Physics Dept., 1989

[45] J. Reid, D.T. Cassidy, R.T. Menzies, "Linewidth Measurements of Tunable Diode Lasers Using Heterodyne and Etalon Techniques", Appl. Opt., **21** (21), pp 3961-3965, 1982

[46] C. Roychoudhuri, "Response Fabry-Perot Interferometers to Light Pulses of Very Short Duration", JOSA **65** (12), pp 1418-1426, 1975

[47] J. Helmcke, S.A. Lee, J.L. Hall, "Dye Laser Dpectrometer for Ultrahigh Spectral Resolution: Design and Performance", Appl. Opt., **21** (9), pp 1686-1694, 1982

[48] M. Ohtsu, N. Tabuchi, "Electrical Feedback and its Network Analysis for Linewidth Reduction of a Semiconductor Laser", J. Lightwave Tech., **6** (3), pp 357-369, 1988

[49] G. Hernandez, Fabry-Perot Interferometers, Cambridge University Press, 1986

[50] B.F. Ventrudo, Private Communications

[51] E. Hecht, A. Zajac, Optics, Addison-Wesley, 1974

[52] P. Horowitz, W. Hill, The Art of Electronics, Cambridge University Press, 1983, page 289

[53] J. Buus, Single Frequency Semiconductor Lasers, SPIE, 1991, page 54

[54] J.D. Evans, T. Makino, N. Puetz, J.G. Simmons, D.A. Thompson, "Strain-Induced Performance in Long-Wavelength, Multiple-Quantum-Well, Ridge-Waveguide Lasers with All Quaternary Active Regions", IEEE Photon. Technol. Lett., Vol. 4 (4), pp 299-301, 1992

[55] L.D. Westbrook, "Dispersion of Linewidth-Broadening Factor in 1.5μm Laser Diodes", Electron. Lett., **21** (22), pp 1018-1019, 1985

[56] J.E. Hayward, D.T. Cassidy, "Correlation of Spectral Output and Below-Threshold Gain Profile Modulation in 1.3 μm Semiconductor Diode Lasers", Appl. Phys. Lett **59** (10), pp 1150-1152, 1991

[57] D.T. Cassidy, "Comparison of Rate-Equation and Fabry-Perot Approaches to Modeling a Diode Laser", Appl. Optics, **22** (21), pp 3321-3326, 1983

[58] J.E. Hayward, Private communication.